ÇUKUROVA UNIVERSITY
INSTITUTE OF NATURAL AND APPLIED SCIENCES

MSc THESIS

Rahmi İlker KAYAALP

MODELLING AND ANALYSIS OF BIDIRECTIONAL DC-DC CONVERTER

DEPARTMENT OF ELECTRICAL AND ELECTRONICS ENGINEERING

ADANA, 2015

ÇUKUROVA UNIVERSITY
INSTITUTE OF NATURAL AND APPLIED SCIENCES

MODELLING AND ANALYSIS OF BIDIRECTIONAL DC-DC CONVERTER

Rahmi İlker KAYAALP

MSc THESIS

DEPARTMENT OF ELECTRICAL AND ELECTRONICS ENGINEERING

We certify that the thesis titled above was reviewed and approved for the award of degree of the Master of Science by the board of jury on 27/07/2015.

.....	.....	.....
Prof. Dr. Mehmet TÜMAY	Asst. Prof. Dr. Lütfü SARIBULUT	Asst. Prof. Dr. M. Uğraş CUMA
SUPERVISOR	MEMBER	MEMBER

This MSc Thesis is written at the Department of Institute of Natural And Applied Sciences of Çukurova University.
Registration Number:

Prof. Dr. Mustafa GÖK
Director
Institute of Natural and Applied Sciences

This thesis was supported by the Scientific Research Project Unit of Cukurova University for my thesis (Project Number: FYL-2014-3276).

ABSTRACT

MSc THESIS

MODELLING AND ANALYSIS OF BIDIRECTIONAL DC-DC CONVERTER

Rahmi İlker KAYAALP

ÇUKUROVA UNIVERSITY
INSTITUTE OF NATURAL AND APPLIED SCIENCES
DEPARTMENT OF ELECTRICAL AND ELECTRONICS ENGINEERING

Supervisor : Prof. Dr. Mehmet TÜMAY
Year : 2015, Pages 111
Jury : Prof. Dr. Mehmet TÜMAY
: Asst. Prof. Dr. Mehmet Uğraş CUMA
: Asst. Prof. Dr. Lütfü SARIBULUT

Bidirectional dc-dc converters are used a lot of industrial areas such as electric vehicles, uninterruptable power supplies, fuel cells, solar panel cells as energy sources are searched in order to improve the quality of power at the transmission and distribution lines and other areas. All of these industrial applications give importance on system loss, efficiency drop, shortening the life of circuit elements. Thus, it should be improved control systems in order to prevent power losses as far as possible and efficiency of bidirectional power flow is very important for high quality electrical energy. Owing to different types of control methods provide bidirectional power flow and each of these has different algorithm. Nowadays, these control methods are improved by increasing complexity of mathematical equations or exchanging better equipments. In the light of these works, comparing of common used control methods provides contribution to efficiency studies at bidirectional dc-dc converter literature. The main aim of this thesis work, applying different phase shift control methods on single phase isolated bidirectional full bridge dc-dc converter and comparing these control methods on efficiency way by reducing cost with or without using snubber capacitors.

In this thesis, Isolated Bidirectional DC-DC Converter topology is modelled and all controllers are written by FORTRAN programming language.

According to the results, it is observed that efficiency results of DPS and EPS are almost equal and higher than SPS without using snubber capacitors. This statement shows the discovered and innovative way of this thesis work.

Key words: Bidirectional DC-DC Converter, Phase Shift Control Methods, Efficiency, Comparison.

ÖZ

YÜKSEK LİSANS TEZİ

ÇİFT YÖNLÜ DOĞRU AKIM DÖNÜŞTÜRÜCÜSÜNÜN MODELLENMESİ VE ANALİZİ

Rahmi İlker KAYAALP

ÇUKUROVA ÜNİVERSİTESİ
FEN BİLİMLERİ ENSTİTÜSÜ
ELEKTRİK ELEKTRONİK MÜHENDİSLİĞİ ANABİLİM DALI

Danışman : Prof. Dr. Mehmet TÜMAY
Yıl: 2015, Sayfa 111
Jüri : Prof. Dr. Mehmet TÜMAY
: Yrd. Doç. Dr. Mehmet Uğraş CUMA
: Yrd. Doç. Dr. Lütfü SARIBULUT

Çift yönlü doğru akım dönüştürücüleri; elektrikli araçlar, kesintisiz güç kaynakları, yakıt hücreleri, güneş paneli hücreleri gibi iletim ve dağıtım hatlarında güç kalitesini iyileştirmek amacıyla kullanılmaktadır. Endüstriyel uygulamalarda sistem kayıpları, verimlilik düşüşü ve devre elemanlarının ömürleri giderek önemli hale gelmektedir. Bu yüzden güç kayıplarını olabildiğince önlemek için kontrol sistemlerinin geliştirilmesi gerekir ve bu bakımdan çift yönlü güç akışı, verimliliği yüksek kaliteli elektrik enerjisi için çok önemlidir. Farklı tipte kontrol metodları sayesinde çift yönlü güç akışı sağlanır ve bu kontrol metodlarının her biri farklı algoritmalara sahiptir. Son zamanlarda ise kontrol metodları, matematiksel denklemlerin kompleksliği artırılarak ya da sistemde kullanılan materyallerin yapıları değiştirilerek geliştirilmektedir. Bu çalışmalar doğrultusunda en sık kullanılan kontrol metodlarını karşılaştırmak, çift yönlü doğru akım dönüştürücüsünün verimlilik çalışmalarına katkı sağlayacaktır. Bu tez çalışmasının ana amacı farklı faz kaydırıcı kontrol metodlarının tek faz izoleli çift yönlü tam köprü doğru akım dönüştürücüsü üzerine uygulanması ve bu kontrol metodlarının şok giderici kapasitörler kullanılmadan maliyet düşürülerek verimlilik yönünden karşılaştırmaktır.

Bu tez çalışmasında izoleli çift yönlü doğru akım dönüştürücüsü topolojisi modellenmiş olup tüm kontrol metodları FORTRAN programlama diliyle yazılmıştır.

Elde edilen sonuçlara göre şok giderici kapasitörler olmadan DPS ve EPS kontrol metodlarının verimlilik sonuçları neredeyse eşit ve SPS kontrol metodundan yüksek olduğu tespit edilmiştir. Bu durum bu tez çalışmasının keşfedilmiş ve yenilikçi bir yönünü göstermektedir.

Anahtar Kelimeler: Çift Yönlü Doğru Akım Dönüştürücüsü, Faz Kaydırmalı Kontrol Metodları, Verimlilik, Karşılaştırma

ACKNOWLEDGEMENTS

The subject of this thesis was suggested by my supervisor, Prof. Dr. Mehmet TÜMAY to whom I would like to express my heartfelt thanks for his supervision, guidance, encouragements, extremely useful suggestions and continuous confidence in me throughout this thesis. It has been a great honor to have Prof. Dr. Mehmet TÜMAY as supervisor.

I am also grateful to Assoc. Prof. Dr. K. Çağatay BAYINDIR and Asst. Prof. Dr. Lütfü SARIBULUT for their help and support during my study. I appreciate all their contributions of time, ideas and funding to make my thesis.

I am also grateful to Asst. Prof. Dr. Mehmet Uğraş CUMA for his support and ideas. I am also grateful to the members of the Electrical and Electronics Engineering Department, Çukurova University.

I owe special thanks to Res. Asst. Tahsin KÖROĞLU, Res. Asst. Tuğçe DEMİRDELEN and other Research Assistants for their companionship and cooperation during my study.

I would like also to thank and acknowledge the financial supported by Scientific Research Project Unit of Çukurova University for my MSc thesis (Project Number: FYL-2014-3276).

Finally, I wish to express my deepest gratitude to my mother Nimet KAYAALP and my father Gökhan Tamer KAYAALP for their endless support, encouragement and patience.

Rahmi İlker KAYAALP

CONTENTS **PAGE**

LIST OF TABLES **PAGE**

LIST OF FIGURES **PAGE**

LIST OF SYMBOLS

η	: Efficiency
ΔI_L	: Inductor Current Ripple
ΔV_{in}	: Input Voltage Ripple
C	: Capacitor
C_1	: Input Capacitor
C_2	: Output Capacitor
C_{DC}	: DC Link Capacitor Value
C_{input}	: Input Capacitor
C_{output}	: Output Capacitor
D	: Duty Cycle
D_1	: Diode of Stage A
D_2	: Diode of Stage A
D_3	: Diode of Stage A
D_4	: Diode of Stage A
D_5	: Diode of Stage B
D_6	: Diode of Stage B
D_7	: Diode of Stage B
D_8	: Diode of Stage B
E_{offD}	: OFF Condition of Diode Switching Energy
E_{offT}	: OFF Condition of Transistor Switching Energy
E_{onD}	: ON Condition of Diode Switching Energy
E_{onT}	: ON Condition of Transistor Switching Energy
E_{refoff}	: OFF Condition of Reference Energy
E_{refon}	: ON Condition of Reference Energy
F	: Farad
f	: Fundamental Supply Frequency
f_{sw}	: Switching Frequency
F_{SW}	: Switching Frequency of Converter
I_{cap}	: Capacitor Current

I_{cav} : Capacitor Average Current

I_{Dav} : Average Diode Current

I_{dc1} : DC Link Input Current

I_{dc2} : DC Link Output Current

I_{Drms} : Root Mean Square Diode Current

I_{L1} : Input Inductor Current

I_{L2} : Output Inductor Current

I_{LOAD} : Load Current

I_{min} : Inductor Minimum Current

I_{out} : Desired Maximum Output Current

I_{peak} : Inductor Peak Current

I_{ref} : Reference Current

I_{RMS} : Inductor Root Mean Square Current

K_{ind} : Estimated Coefficient

L : Sum of Transformer Leakage Inductance

L_1 : Input Inductor

L_2 : Output Inductor

$L_{Auxiliary}$: Auxiliary Inductor

L_{Trans} : Transformer Leakage Inductance

N : Transformer Turn Ratio

P : Active Load Power

P_1 : Input Power

P_2 : Output Power

P_{CD} : Diode Conduction Losses

$P_{conduction}$: Conduction Losses

P_{CT} : Transistor Conduction Losses

$P_{semiconductor}$: Total of Conduction and Switching Losses

P_{sw} : Switching Losses

P_{swD} : Diode Switching Losses

P_{swT} : Transistor Switching Losses

$P_{totalloss}$: Total Power Loss

Q_1 : IGBT of Stage A

Q_2 : IGBT of Stage A

Q_3 : IGBT of Stage A

Q_4 : IGBT of Stage A

R : Resistance

r_C : Capacitor Internal Resistance

r_D : Diode Internal Resistance

S_1 : IGBT of Stage B

S_2 : IGBT of Stage B

S_3 : IGBT of Stage B

S_4 : IGBT of Stage B

T_S : Switching Period

T_{SW} : Switching Period

u_{CE0} : Collector Emitter Voltage of Transistor

u_{D0} : Diode Voltage

V_1 : Input Voltage

V_2 : Output Voltage

V_{cap} : Capacitor Voltage

V_{dc1} : DC Link Input Voltage

V_{dc2} : DC Link Output Voltage

V_{inmax} : Maximum Input Voltage

V_{inmin} : Minimum Input Voltage

V_{L1} : Voltage of Input Inductor

V_{out} : Desired Output Voltage

V_{ref} : Reference Voltage

V_{tra} : Voltage of Transformer Primary Side

V_{trp} : Voltage Between Middle Points of Leg3 and Leg4 at Stage B

V_{trs} : Voltage Between Middle Points of Leg1 and Leg2 at Stage A

Z_{sh} : Voltage of Output Inductor

δ : Phase Angle

μ : Micro

LIST OF ABBREVATIONS

AC	: Alternative Current
BDC	: Bidirectional DC-DC Converter
DC	: Direct Current
DCSR	: Direct Current Slew Rate Control
DPS	: Dual Phase Shift
EPS	: Extended Phase Shift
EV	: Electric Vehicle
FB	: Full Bridge
FC	: Fuel Cell
HB	: Half Bridge
HEV	: Hybrid Electric Vehicle
HV	: High Voltage
HZ	: Hertz
IBDC	: Isolated Bidirectional DC-DC Converter
IEEE	: Institute of Electrical and Electronics Engineers
IGBT	: Insulated Gate Bipolar Transistor
LV	: Low Voltage
MOSFET	: Metal Oxide Semiconductor Field Effect Transistor
MV	: Medium Voltage
NBDC	: Non-isolated Bidirectional DC-DC Converter
PF	: Power Flow
PI	: Proportional Integral
PPS	: PWM Plus Phase Shift
PQ	: Power Quality
PS	: Phase Shift
PSBC	: Phase Shift Shoot Through Bivariate Coordinated
PSC	: Phase Shift Control
PSCAD/EMTDC	: Power System Computer Aided Design / Electromagnetic Transient DC Program

PU	:	Per Unit
PV	:	Photovoltaic
PWM	:	Pulse Width Modulation
RMS	:	Root Mean Square
SC	:	Snubber Capacitor
SE	:	Solar Energy
SMC	:	Sliding Mode Control
SPS	:	Single Phase Shift
SS	:	Soft Switching
ST	:	Settling Time
TPS	:	Triple Phase Shift
TS	:	Triggering Signals
UDC	:	Unidirectional DC-DC Converter
UPS	:	Uninterruptable Power Supplies
WE	:	Wind Energy
ZCS	:	Zero Current Switching
ZVRT	:	Zero Voltage Resonant Transition
ZVS	:	Zero Voltage Switching

1. INTRODUCTION

1.1.Overview

From the production of electrical energy to consumption of electrical energy in all stages (transmission and distribution are included), the existence of continuity, stable frequency and voltage values and voltage and current pure sine waveforms are not a problem of power quality of having a rough definition. Power quality components (Continuity of supply of electrical energy, frequency, the effective value of voltage, sags and swells are temporary formed at voltage, sudden voltage changes, phase-to-phase imbalance, harmonic components in voltage and current waveforms, flicker) are continuously rated values remain constant (frequency, voltage, etc…) or not (sag and swells, sudden voltage changing, imbalance, flicker) or 100% continuity of supply (never be power block out) is an ideal situation that does not applied to any existing electrical system in the world.

In recent years, different types of power hybrid electric vehicles, uninterruptable power supplies, fuel cells, solar panel cells as energy sources are searched in order to improve the quality of power at the transmission and distribution lines and other areas and those systems' devices have been developed day by day. In these systems, for maximum efficiency in cases of charge and discharge via bi-directional voltage system between storage elements and direct current way require independent power sources. That's why bidirectional dc-dc converters between different dc sources provide energy exchanging and control mechanisms. These restrictions on the systems reveal importance of energy efficiency (Lee et. al., 2006). Thus, researchers design a lot of different topologies and control methods for improving the converter system in literature.

Generally bi-directional dc-dc converters are isolated and non-isolated stand and they are divided into various topologies. (buck, boost, buck-boost, cuk are non-isolated; forward, push-pull and flyback are isolated.) These topologies are evaluated in order to use at maximum efficiency in systems which are improved to increase performance by changing some properties on it day by day and produced new topologies. Occurring power losses during energy transfer should be reduced for

working bidirectional dc-dc converter with maximum efficiency. For this, equipments of the system should be chosen by using the best way and it must be easy to operate and applicability. However, under these conditions, the resulted system is healthy and can work in an efficient manner.

1.2.Purpose of Thesis

Bidirectional dc-dc converter is proposed by Matsuo in 1984. In this study, two bidirectional dc-dc converters are connected to battery and it is used for increasing dc voltage between solar system and load (Matsuo et. al., 1984).

In this thesis work, bidirectional dc-dc converter simulation studies are performed. A lot of topologies are worked with various control methods in literature. Therefore, these topologies and control methods are introduced firstly in order to emphasize place of this work in the literature.

In recent years, working principles of bidirectional dc-dc converters are improved for increasing system efficiency. At this point, calculation of system components, mitigation of power losses and improvements on control methods play an important roles for developing bidirectional dc-dc converters. According to these studies, isolated full bridge dc-dc converter topology that is the most common used topology in literature is investigated in this thesis work. Moreover, new type of Proportional-Integral (PI) based control methods are researched and phase shift control methods are applied to the full bridge topology. These control methods are performed by using PSCAD/EMTDC simulation program and compared each other by measuring voltages and currents waveforms, triggering signals, power losses, efficiencies at different frequencies. Design of the system components are also calculated and modes of operation are defined for the main buck-boost structure by using these three different phase shift control methods that are Single Phase Shift (SPS), Extended Phase Shift (EPS) and Dual Phase Shift (DPS).

1.3.Outline of the Thesis

After the introduction section, the outline of the thesis is organized as follows;

In second chapter, BDC working principles and using areas of BDCs are introduced for defining importance of BDCs at power quality issue. Then, literature survey on BDC topologies and their control methods are presented. There are a lot of different BDC topologies in literature and common used topology is studied in this thesis in order to provide more contribution to literature.

In the third chapter, firstly the circuit topology of the proposed BDC is investigated. Secondly, the design of circuit elements are presented. Thirdly, conduction and switching loss calculations are presented and finally, analysis of simulation parameters are defined in detail.

The fourth chapter presents phase shift control methods and their simulation results with single phase full bridge BDC topology. In this chapter, input – output voltages, IGBTs, inductors and capacitors current waveforms are demonstrated by PSCAD/EMTDC simulation graphics. Moreover, system efficiencies are calculated for different frequency levels with power loss calculations in order to compare these control methods each other.

In the fifth chapter, comparison of the phase shift control methods is presented with tables by giving system parameters, settling times of dc link voltages, switching and conduction losses and efficiencies at different frequency values.

In the sixth chapter, conclusions of the thesis are given and the future work studies are discussed.

Finally all references used in this thesis study are presented.

2. LITERATURE SURVEY

2.1. Bidirectional DC-DC Converter

Most of the existing bidirectional DC-DC converters classified as the generic circuit structure illustrated at Figure 2.1 that is characterized by current fed or voltage fed on one side. Bidirectional DC-DC converters work buck or boost type. Buck type converters decrease voltage from high voltage side to low voltage side and boost type converters increase voltage from low voltage side to high voltage side.

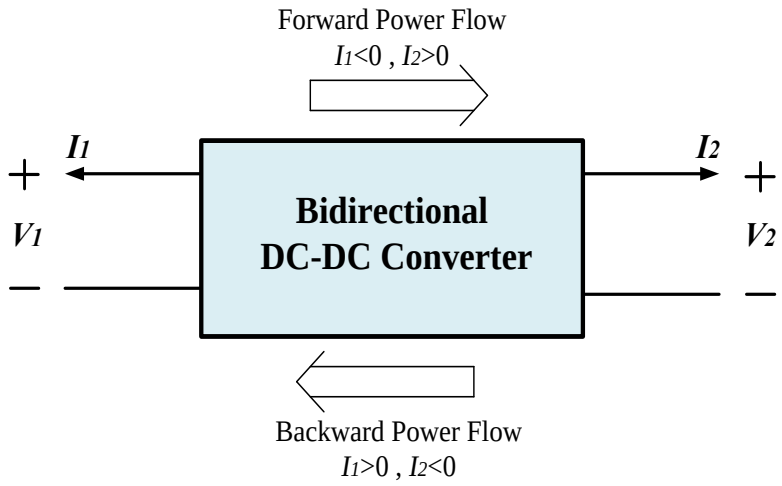

Figure 2.1. Illustration of Bidirectional Power Flow

Switches that is located in the above box, provide bidirectional power flow in converter model. They carry current on both directions. It is usually used unidirectional semiconductor power switch MOSFET (Metal-Oxide-Semiconductor-Field-Effect-Transistor) or IGBT (Insulated-Gate-Bipolar-Transistor) in parallel with a diode for double sided current flow. Because the double sided current flow power switch is not available.

In the literature, these converters usually used with fully controlled elements and generally used DC PWM control method. It produces stable or adjustable and isolated or non-isolated dc voltage. According to control method, it can be seen

fluctuations at output voltage. Also current waveform of input side shows fluctuations too. So, it can be summarized as follows.

DC-DC Converters are classified as single domain, double domain and triple domain chopper circuits and these classification is shown in Figure 2.2.

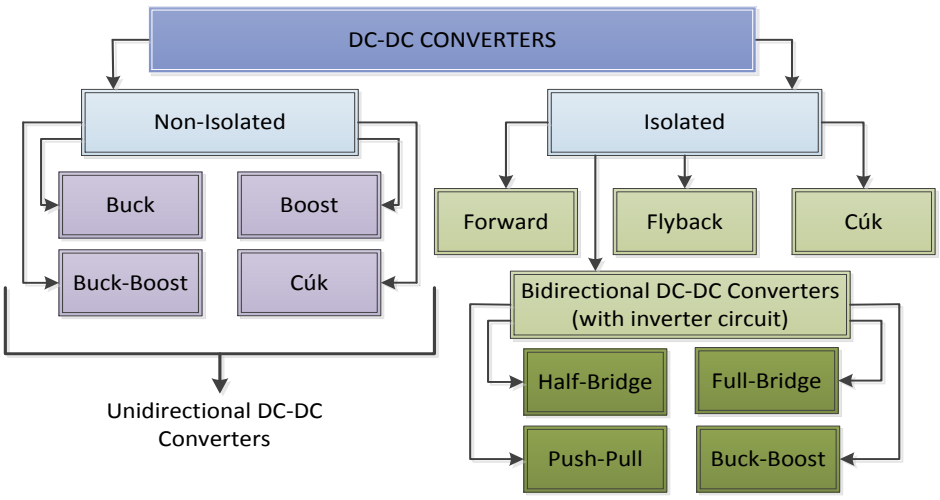

Figure 2.2. Classification of DC-DC Converters with Block Diagrams

Generally DC-DC converters are isolated and non-isolated stand and they are divided into various topologies. (usually buck, boost, buck-boost, cuk are nonisolated; forward, push-pull and flyback are isolated.) These topologies are evaluated in order to reach maximum efficiency in systems. Thus, changing materials of circuit elements and production of new topologies help to improve efficiency. Occurring power losses during energy transfer should be reduced for working bidirectional DC-DC converter with maximum efficiency. For this, equipments of the system should be chosen by using the best way and it must be easy to operate and applicability. Under these conditions, the resulting system is healthy and can work in an efficient manner.

Bidirectional DC-DC converters are used in a lot of parts in industrial applications such as hybrid or electrical vehicles, renewable energy sources (solar and wind energy), power electronic equipments with battery systems, etc…

Figure 2.3 shows using areas of dc-dc converters at industrial applications. According to necessity of the system using of DC-DC converters are changeable. So,

they can be used as unidirectional, bidirectional, isolated, non-isolated, half bridge, full bridge, three phase or cascade by creating different or new topologies with control methods.

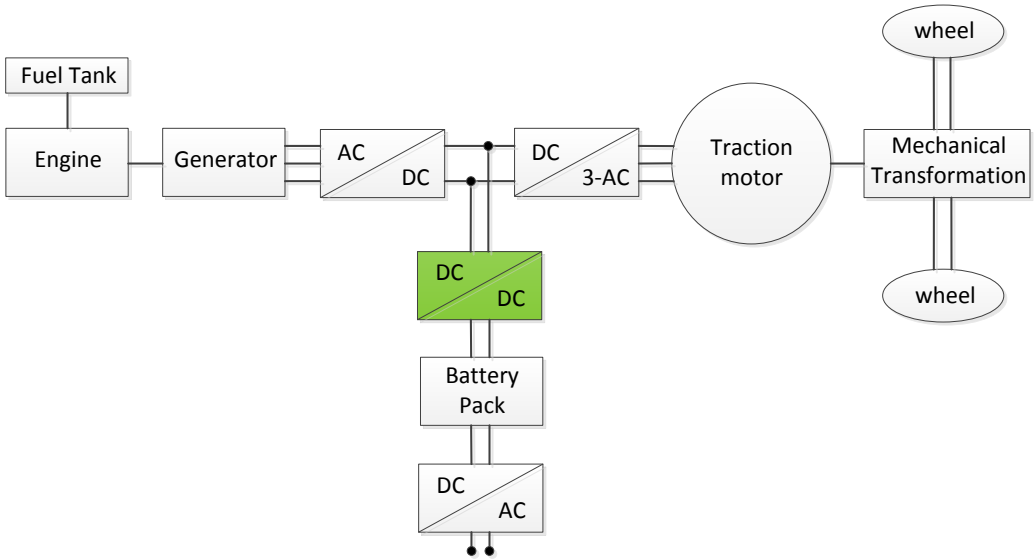

(a)

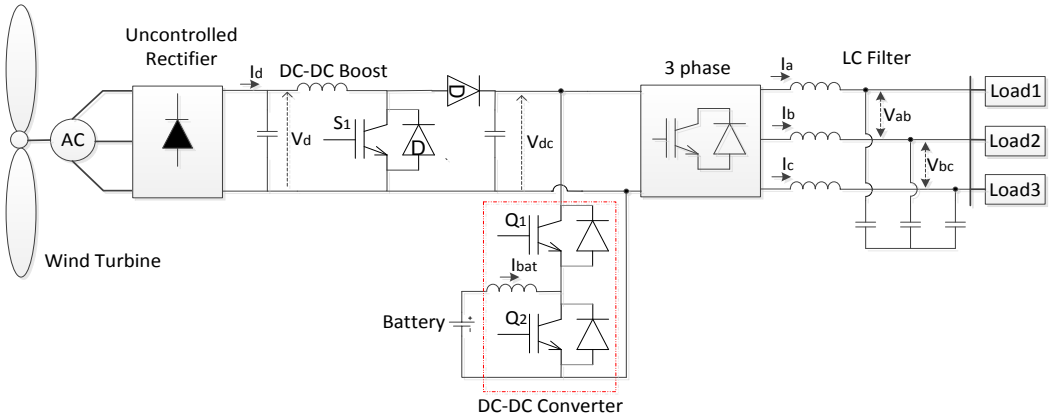

(b)

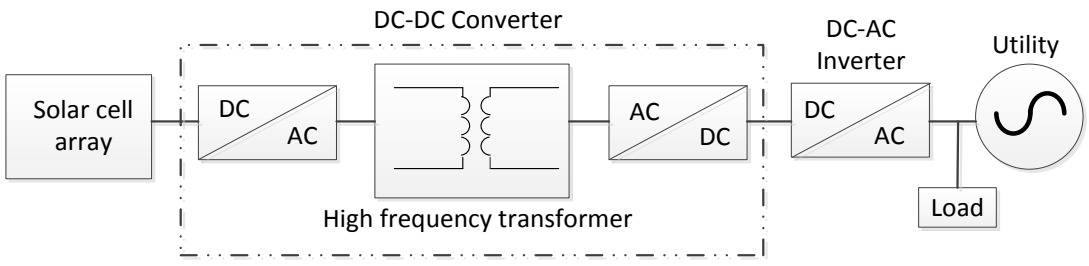

(c)

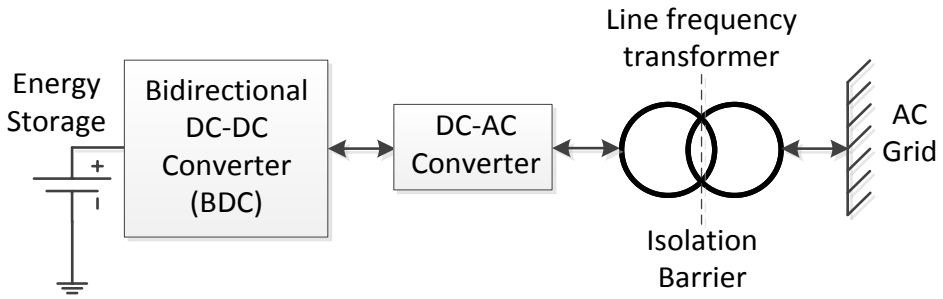

(d)

Figure 2.3. Using DC-DC converters of various industrial applications
(a) General Configuration of an Electric Vehicle (NPTEL, Module 4, Lecture 9)
(b) Power circuit topology of a variable speed stand-alone wind energy supply system (Hussein et. al., 2013)
(c) Using of DC-DC converter with high frequency transformer at photovoltaic system (Shen et. al., 2011)
(d) Basic structure of an energy storage device connected to an ac grid through a line frequency transformer (Karshenas et. al., 2011)

Moreover, Figure 2.4 shows general usage of DC-DC, DC-AC and AC-DC converters with operational components such as mobile phone, laptops, desktops and television. Some electronic components include multiple DC-DC converters since they have different operating voltages. Therefore, the input and output voltages can be used by increasing or decreasing. Also different types of AC-DC and DC-AC converters are used for necessities of electronic devices.

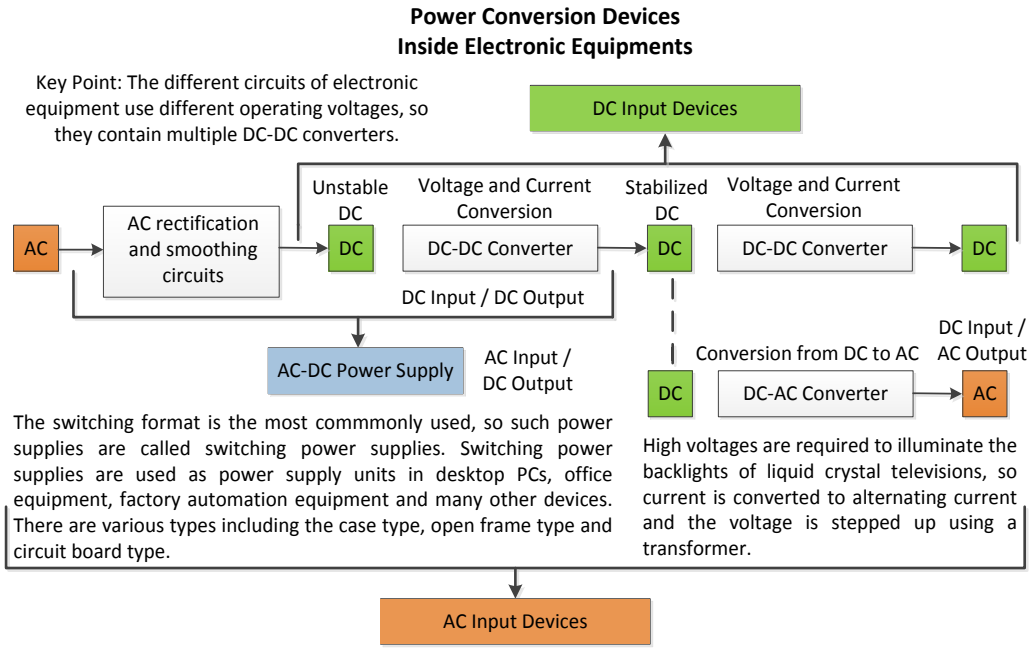

Figure 2.4. General Usage of DC-DC, DC-AC and AC-DC Converters (TDK Power Electronics World)

2.2. BDC Topologies

Different types of bidirectional isolated DC-DC converter topologies are studied by researchers. These studies provide to obtain maximum efficiency for fulfilling different application needs. But some topologies are common used because their analysis and practicability are simple. Therefore, these different bidirectional dc-dc converter topologies are introduced briefly at this chapter.

In the literature, the mostly used topologies are summarized at Tan et. al., 2011. According to this study, energy storage system topology, full bridges and half bridges topologies are given with their working principles. Moreover, its experimental setup consists of three-phase PWM converter with Li-ion battery bank at the low voltage side and single phase shift control method is used.

First of all, common used topology is full bridge, voltage source BDC. Figure 2.5 shows the converter model and this topology is studied in this thesis work without snubber capacitors.

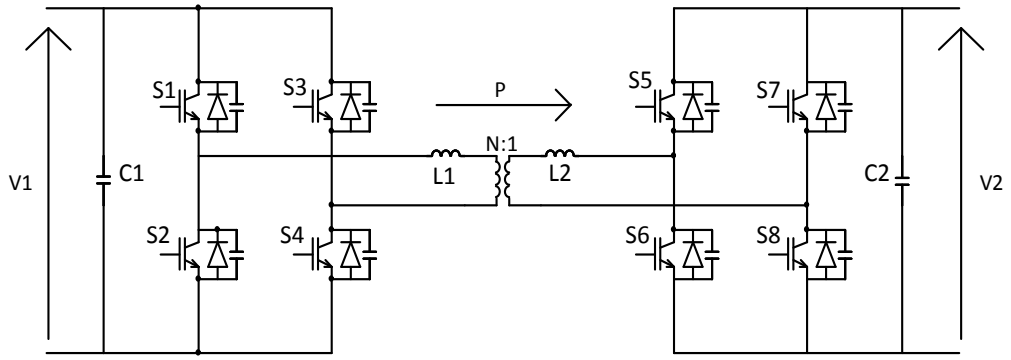

Figure 2.5. Full Bridge, Voltage Source BDC Topology

Figure 2.5 demonstrates full bridge topology with high frequency isolation transformer that is proposed in (De Doncker et. al., 1991) and (Kheraluwala et. al., 1992). The DC-DC converter provides zero voltage switching (ZVS) by using parasitic or external snubber capacitors to minimize losses. It can be used electric double layer capacitors and batteries. Thus, this topology usually preferred for various applications. The bidirectional isolated DC-DC converter has an optimal operating point when the voltage ratio of input and output voltages is equal to transformer turn ratio. It is also capable of high power transfer when using simple phase shift method. This method is useful, even for the half-bridge bidirectional isolated DC-DC converters. This converter is not suitable for low power applications. Because it gives poor efficiency. Therefore, for example, EV and HEV use this topology in order to obtain better efficiency.

Figure 2.6 presents bidirectional isolated DC-DC converter based on a series resonant converter that has been considered as an interface between a low voltage bus (11-16 V) and a high voltage bus (220-447 V) in HEVs and EVs (Krismer et. al., 2005). The drawback of the converter is that the series capacitor has to handle the full-load current, leading to increasing volume and cost.

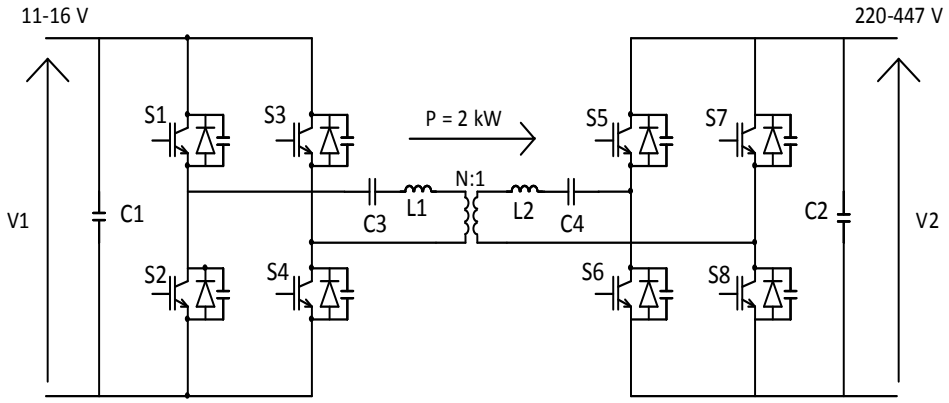

Figure 2.6. Bidirectional isolated DC-DC converter based on a series resonant converter

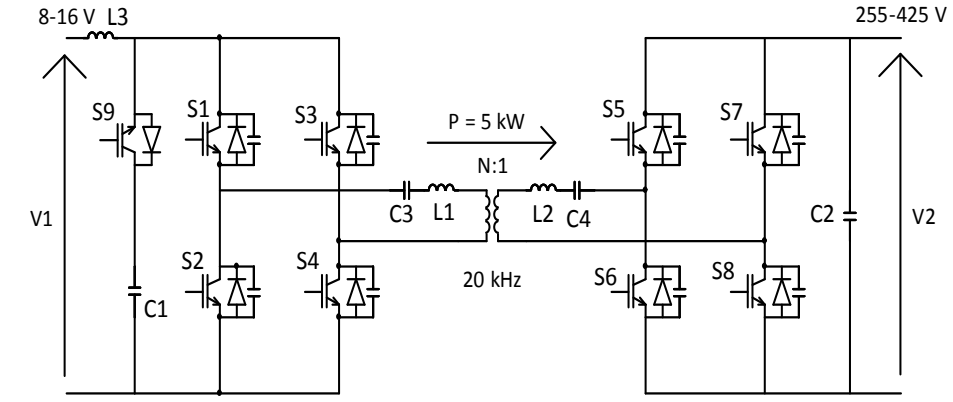

(a)

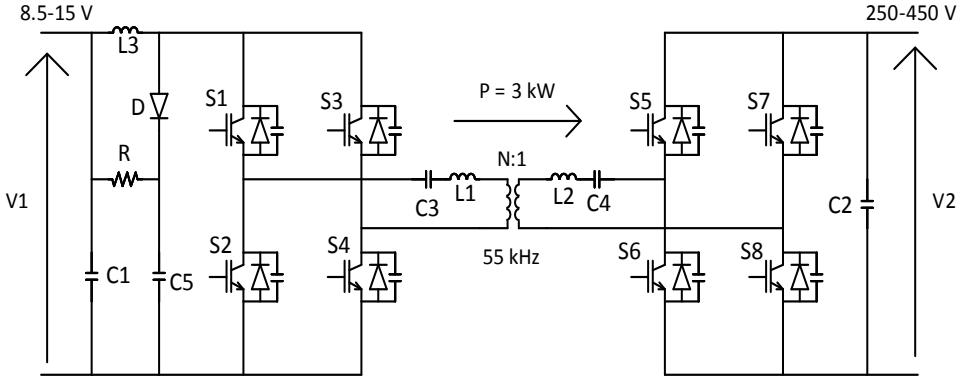

(b)

Figure 2.7. Full bridge bidirectional isolated DC-DC converter with a current source converter at low voltage side and a voltage source converter at high voltage side.
(a) Employing an active-clamp snubber
(b) Employing a passive-clamp snubber

Figure 2.7 shows the current source (boost) full-bridge converter with an active-clamp snubber (Wang et. al., 1998) and a passive clamp snubber (Zhu et. al.,

2006) to fulfill high power, high current and a high voltage conversion ratio of a fuel-cell vehicle system. Moreover, the authors of (Wang et. al., 1998) proposed the dc-link inductor should be placed at the low voltage battery side to improve the battery charging efficiency and minimize the ripple current. But, the low voltage side of the converter suffer from high transient voltage that necessitates the active or passive clamping snubbers.

Figure 2.8 explains the bidirectional isolated dc-dc converter employed for an EDLC energy storage system (Rufer et. al., 2002). The voltage source converter is connected to the high voltage side, while the current source converter is connected to the EDLC bank with a decoupling inductor. Although ZVS is achieved at the high voltage side, the conduction loss in the current source converter is non-negligible due to the series connection of a diode with each IGBT.

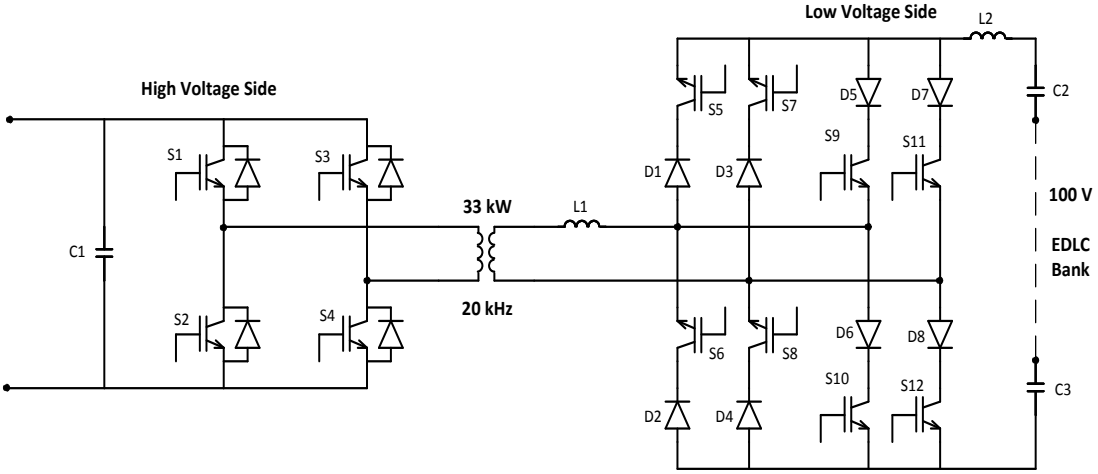

Figure 2.8. An EDLC energy storage system for elevators, employing a combined voltage and current source bidirectional isolated DC-DC converter

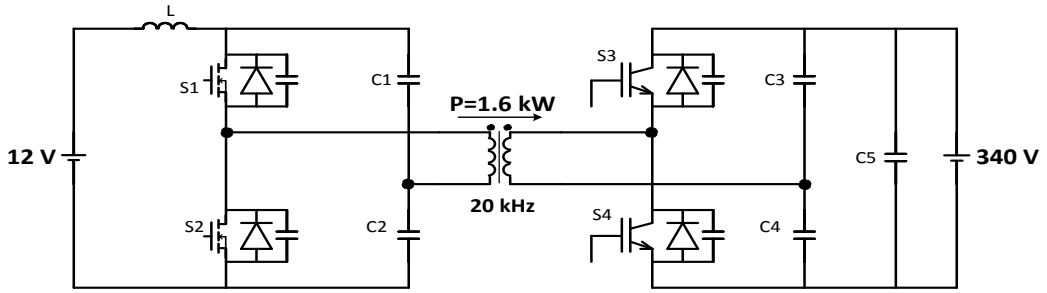

Figure 2.9. Half-bridge bidirectional isolated DC-DC converter for battery and fuel cell applications

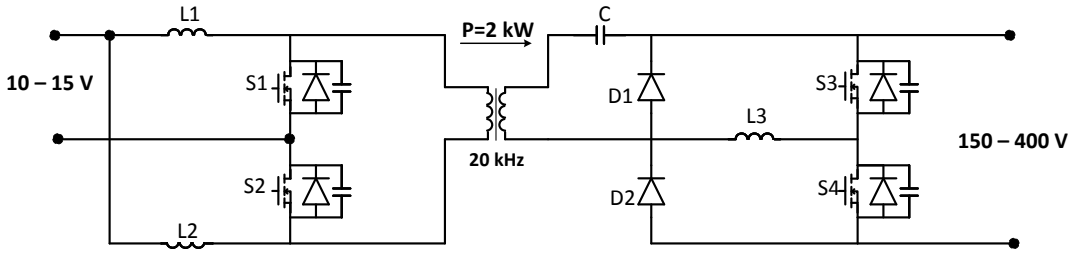

Figure 2.10. Asymmetrical bidirectional isolated dc-dc converter with a low component count for fuel cell electric vehicles

Figure 2.9 indicates half bridge bidirectional isolated DC-DC converter for battery and fuel cell applications (Li et. al., 2003), (Peng et. al., 2004). The low voltage side is a current source half bridge converter that functions as a boost converter and an inverter. The high voltage side is a voltage source half bridge converter. Lossless snubber capacitors are used to achieve ZVS in the converter. A 20 kHz high frequency transformer isolates the low voltage side and the high voltage side. Power is transferred by the simple phase shift method, in a similar way with the full bridge DC-DC converter. The half bridge topology has a minimum count of active devices and ZVS is achieved without additional active devices. It has the same total device rating as the full bridge topology and a reasonable ripple DC current at the low voltage side.

If the battery voltage is lower than 12 V, it may be reasonable to employ this topology. But, the half bridge topology may not be suitable for connection with higher battery voltages because MOSFETs with a higher blocking voltage will be required, thus increasing device loss. Also the split DC capacitors in the half bridge topology have to withstand the rated current value. This would be a burden for the capacitors at the low voltage low voltage, high current side. Additionally, voltage balancing circuits may be required for the split capacitors on low-voltage and high-voltage sides. The buck and boost operations of the converter in (Figure 2.9) have been verified at the rated power of 1.6 kW. Also an efficiency of more than 94% was achieved at the rated power.

Figure 2.10 shows a 2 kW asymmetrical half bridge bidirectional isolated DC-DC converter (Chiu et. al., 2006). The efficiency of the converter varies between 88% and 96% for power transfer between 200 W (10%) and 2 kW (100%). This

converter topology is asymmetrical, and the low voltage side switches are subjected to a higher voltage stress which would make the topology inappropriate for applications to batteries with higher voltage rating. In addition, two inductors are required at the low voltage side and a series blocking capacitor is required to prevent transformer saturation. A significant increase at the capacitor size may not be acceptable for high power applications.

2.3. BDC Control Methods

In bidirectional DC-DC converter literature, a lot of various control methods are tried for improving system efficiency. Generally they use pulse width modulation (PWM) method and using control methods are single (traditional) phase shift (SPS) (Zhao et. al., 2010), extended phase shift (EPS) (Reddy et. al., 2013), dual phase shift (DPS) (Bai et. al., 2008), triple phase shift (TPS) (Wu et. al., 2012), PWM plus phase shift (PPS) (Dehong et. al., 2004), direct current slew rate control (DCSR) (Lingyu et. al., 2014), sliding mode control (SMC) (Wang et. al., 2015), phase-shifting shoot-through bivariate coordinated control (PSBCC) (Zhao et. al., 2012), etc…

In addition to these control methods, it can be created various control methods or novel switching signals generation methods (Meral et. al., 2009). But above control methods are commonly used.

General expressional, how can be done transistor triggering is demonstrated at Figure 2.11 for introducing aim.

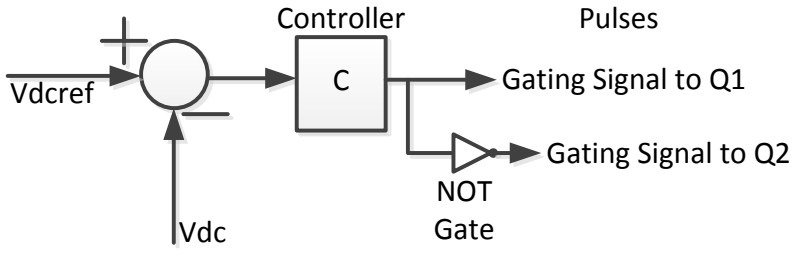

Figure 2.11. General Control Method for triggering transistors in Bidirectional DC-DC Converters

Figure 2.11 presents block diagram of triggering signals for IGBTs. Firstly, measured value is extracted from reference value and then it can be evaluated by control method. Then, switching pulses are produced. If the two IGBTs are named with Q_1 and Q_2, Q_2 should be taken opposite signal. So, the not gate is needed for the opposite signal.

Phase-Shift control methods (SPS, EPS and DPS) will be studied detailed at 4^{th} Chapter and other control methods can be introduced below.

Triple phase shift (TPS) control is used for improving system efficiency to be better than SPS, EPS and DPS. (Wu et. al., 2012) defined three phase shift angles in the paper. The first phase shift angle between the primary control signal and the corresponding secondary control signal. For example, if all switches are named like Figure 3.1 between Q_1 and S_1 in dual active bridge topology, the second is the phase shift between the diagonal control signals in the primary power circuit. Moreover, Q_1 and Q_4 produce the third phase shift angle between the diagonal control signals in the secondary power circuit, also between S_1 and S_4 too. Additionally, one period of the converter is separated into eight stages and these stages are described in this paper.

Briefly, phase shift angles are produced for defining TPS by using different methods and its mathematical complexity is harder than DPS. But it is useful for possible arbitrary parameters change in nonlinear systems.

PWM plus phase shift control (PPS) is used in the reference (Dehong et. al., 2004). In this control method, PWM control and phase-shift control are combined to reduce current stress, conduction losses and expand ZVS range. Compared with SPS control, PPS control can reduce RMS currents of the converter. The losses of the converter can also decrease. Moreover, converter can achieve ZVS in larger load variation. In PPS control, all switch devices are assumed as ideal switches with paralleled diodes and capacitors. The inductance is composed of the leakage inductance of the transformer and additional series inductance. Also the values of DC link capacitors must be chosen large in order to obtain small voltage ripples.

This paper used variation of half bridge topology and its control block diagram is shown at Figure 2.12. In this figure, UC3875 generates signal g1 and g2. Signal g1 has leading phase according to the error signal of command power (P_o*)

and actual power (P_o) to signal g2. Signal g1 and g2 connect to UC3525 respectively. Signal g1 has the same phase vgs1 and signal g2 has the same phase as vgs3. The signal NV_2/V_1 modulates the duty cycles of vgs1 and vgs3. By inverting vgs1 and vgs3, it can be get other two gate signals.

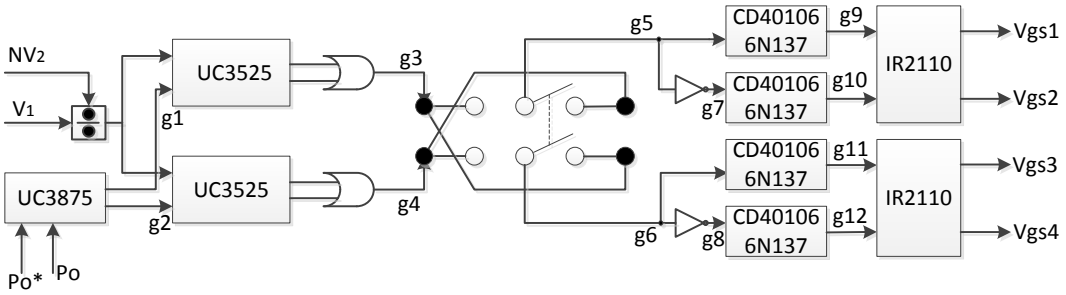

Figure 2.12. PPS control block diagram (Dehong et. al., 2004)

Direct current slew rate control (DCSR) is given in reference (Lingyu et. al., 2014). This control method provides lower conduction loss, lower peak current. The proposed topology consist of current-fed half bridge with active clamping circuits and a three-level half bridge topology. 1kW prototype is built and DCSR control method is employed. Working principle of DCSR is similar with DPS but (Lingyu et. al., 2014) explained implementation is easy with using the proposed topology. Therefore, control strategy based on the proposed topology, the voltages of HVS power devices are balanced perfectly.

S_1, S_2, S_3 and S_4 are defined as high voltage side switches, Q_1, Q_{1a}, Q_2, Q_{2a} are defined as low voltage side switches according to proposed topology in Figure 2.13.

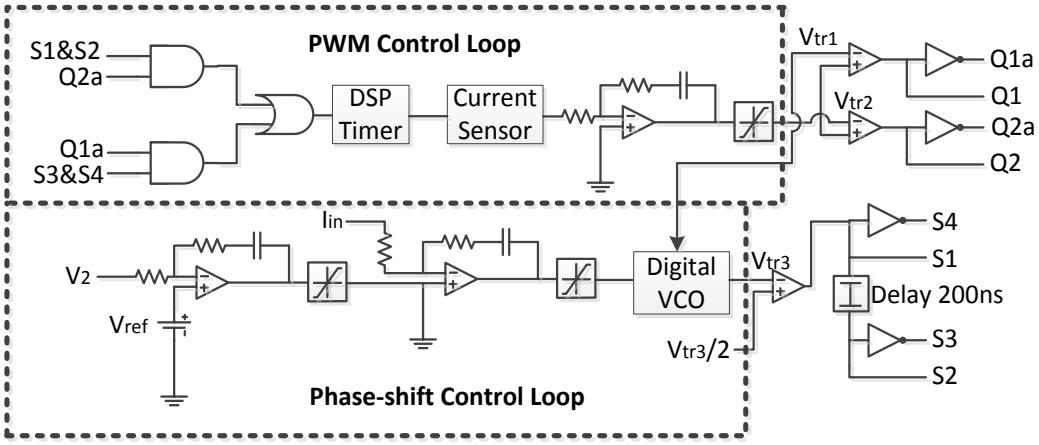

Figure 2.13. DCSR control block diagram (Lingyu et. al., 2014)

Sliding mode control (SMC) is used in reference (Wang et. al., 2015). This control method is based on extended state observer (ESO). In this paper, it is studied mismatch disturbance rejection problem of the DC-DC buck converter. A novel sliding control composed of following two steps. First, ESO is employed to estimate the mismatched and matched disturbances, respectively. SMC is then designed for DC-DC buck converter system based on the disturbance observation. This control structure is shown in Figure 2.14, where the voltage and current information can be obtained from sensors, and the control output will generate PWM signal.

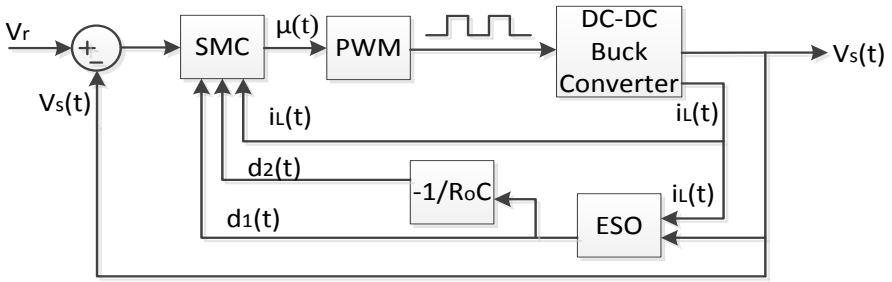

Figure 2.14. SMC control block diagram (Wang et. al., 2015)

Phase-shifting shoot-through bivariate coordinated control (PSBCC) is used in reference (Zhao et. al., 2012). This control method is used full bridge bidirectional DC-DC converter passive clamp circuit with two unique switched impedance networks on both sides and it is named by Z-source isolated bidirectional DC-DC converter (SZIBDC). This topology is useful for preventing current backflow and

extra two switches (G_{11}-G_{12}), (G_{21}-G_{22}) are used at both directions. Moreover, boost factors α and β are used for defining control modes of PSBCC. Figure 2.15 shows the PSBCC block diagram and effect of control strategy is given.

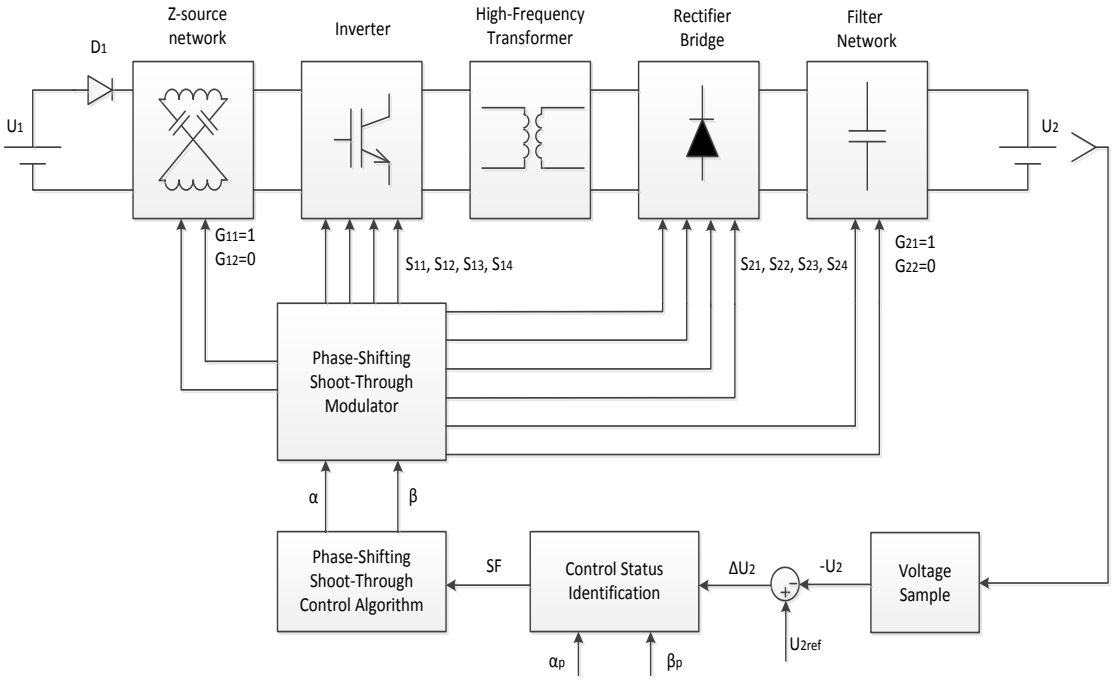

Figure 2.15. PSBC control block diagram (Zhao et. al., 2012)

3. MODELLING OF BIDIRECTIONAL DC-DC CONVERTER

In this chapter, single-phase full-bridge bidirectional isolated buck-boost dc-dc converter topology is given and its designing parameters are calculated. Mathematical analysis of power losses are also included.

3.1 Circuit Topology

Single-phase full-bridge bidirectional isolated buck-boost DC-DC converter topology (Figure 3.1) contains high frequency isolated transformer in order to provide smooth current flowing and the transformer is generally used 1:1. Therefore, 1:1 isolated transformer is used at this study. Authors sometimes use transformers with different winding ranges. For example, 6:1 transformer studied at three-phase system (Tan et. al., 2010). Moreover, one of the two full-bridge construction includes 4 IGBTs and the other H-bridge has 4 IGBTs too. Totally 8 IGBTs are triggered by cosine signals. These signals can be different (1 or 0) according to control method algorithm that is created to fulfill the working necessities. Moreover, conditions of switches are represented by power flow ways. For PF1: A_1 and B_2 are ON, A_2 and B_1 are OFF. For PF2: A_1 and B_2 are OFF, A_2 and B_1 are ON. R_1=R_2=20ohm. In this thesis, snubber capacitors did not use for triggering. The effect of the snubber capacitors decrease switching losses. Thus, the aim of the study is comparing efficiencies of phase shift control methods and snubber capacitors can be great affected to efficiency study on phase shift control methods. Namely, the effect of snubber capacitors will be explained for the efficiency at this chapter. Also, two inductors and two dc link capacitors are used at this circuit topology. Describing of inductors and capacitors will be calculated at Section 3.2.

The aim of the converter is converting DC voltage to another DC voltage by increasing (boost mode) or decreasing (buck mode). These operation modes are important for working of the converter because characteristics of current and voltage waveforms change their shapes according to these modes.

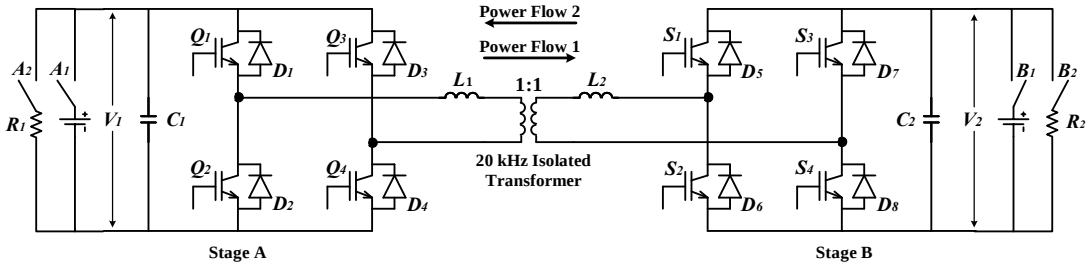

Figure 3.1. Circuit Topology of Single-Phase Full-Bridge Bidirectional Isolated Buck-Boost DC-DC Converter

If the system works at low to middle power rating applications, MOSFETs can be used instead of IGBTs. When only MOSFETs are used in the circuit, both stage A and stage B of the converter can be snubberless. Hence, it provides minimizing switching losses. Like high voltage side of the Fig 2.8, from Table 3.1, it can be clearly seen that if symmetrical (zero voltage switching + zero current switching) ZVS+ZCS soft-switching techniques could be achieved in a BDC, regardless of the direction of power flow (Chen et. al., 2010).

- Power Flow 1: ZVS for Inverting Stage A, ZCS for Rectifier Stage B.
- Power Flow 2: ZVS for Inverting Stage B, ZCS for Rectifier Stage A.

Table 3.1. Soft Switching Technique Combination According to the Applied Power Devices (Chen et. al., 2010)

BDC Type	**As Input Inverting Choppers**	**As Output Rectifier Switches**	**Preferred soft-switching techniques (For inverting choppers + For rectifier switches)**
MOSFET+MOSFET	MOSFET	MOSFET (SR)	ZVS+ZCS
MOSFET+IGBT (with anti-paralleled diode)	MOSFET	Anti-paralleled Diode (IGBT disabled)	ZVS+ZCS
	IGBT	MOSFET (SR)	ZCS+ZCS
IGBT(with antiparalleled diode)+ IGBT(with antiparalleled diode)	IGBT	Anti-paralleled Diode (IGBT disabled)	ZCS+ZCS

3.2. Defining of Circuit Elements

3.2.1. Inductance Calculation

The inductor design has a significant impact on a system performances, such as realization of complementary control ZVRT (Zero Voltage Resonant Transition) soft switching, device switching loss, system volume, inductor power loss, etc… It is necessary to optimize the inductance with all the design considerations.

The relationship between inductor peak current I_{peak}, minimum current I_{min}, and inductor RMS current I_{RMS} can be expressed in 3.1-3.5, where T_s is the switching period, I_{Load} is load current, P is the load power and ΔI is the inductor current ripple.

$$\Delta I = \frac{1}{2} \cdot \frac{V_{in} - V_o}{L} \cdot \frac{V_o}{V_{in}} \cdot T_{sw} \tag{3.1.}$$

$$I_{Load} = \frac{P}{V_o} \tag{3.2.}$$

$$I_{peak} = I_{Load} + \Delta I \tag{3.3.}$$

$$I_{\min} = I_{Load} - \Delta I \tag{3.4.}$$

$$I_{RMS} = \sqrt{I_{Load}^{\,2} + \frac{\Delta I^{\,2}}{3}} \tag{3.5.}$$

Where (Zhang, 2008):

ΔI : Inductor current ripple

V_{in} : Input voltage

V_{out} : Output voltage

T_{sw} : Switching period

I_{RMS} : Inductor root mean square current

I_{peak} : Inductor peak current

I_{min} : Inductor minimum current

I_{Load} : Load current

The optimization of the inductor design should satisfy the following conditions: zero voltage switching condition under all operating conditions and lowest volume.

Data sheets often give a range of recommended inductor values. If this is the case, choose an inductor from this range. The higher the inductor value, the higher is the possible maximum output current because of the reduced ripple current.

Normally, the low inductor values cause to the small size. Note that if the inductor value decrease, the peak current increases.

For device data sheets, where no inductor range is given, an inductor that satisfies both buck and boost mode conditions must be chosen. Select the largest value of inductance calculated from either equations (3.6) and (3.7).

Buck Mode:

For buck mode, the following equation is a good estimate for the right inductance value.

$$L > \frac{V_{out} \times (V_{in\max} - V_{out})}{K_{ind} \times F_{sw} \times V_{in\max} \times I_{out}} \tag{3.6.}$$

Where:

V_{inmax} : Maximum input voltage

V_{out} : Desired output voltage

I_{out} : Desired maximum output current

F_{sw} : Switching frequency of the converter

K_{ind} : Estimated coefficient that represents the amount of inductor ripple current relative to the maximum output current.

A good estimation for the inductor ripple current is 20% to 40% of the output current, or $0.2<K_{ind}<0.4$. (Green M., 2012)

Boost Mode:

For boost mode following equation is a good estimate for the right inductance.

$$L > \frac{V_{in\min}{}^{2} \times (V_{out} - V_{in\min})}{K_{ind} \times F_{sw} \times V_{out}{}^{2} \times I_{out}} \tag{3.7.}$$

Where:

V_{inmin} : minimum input voltage

V_{out} : desired output voltage

I_{out} : desired maximum output current

F_{sw} : switching frequency of the converter

K_{ind} : estimated coefficient that represents the amount of inductor ripple current relative to the maximum output current.

A good estimation for the inductor ripple current is 20% to 40% of the output current, or $0.2<K_{ind}<0.4$. (Green M., 2012)

There is a formula that is used in (Inoue et. al., 2007) for calculating input and output inductors with phase-shift angle.

$$P = \frac{V_1 V_2 N}{wL} \times \left(\frac{\delta(\pi - \delta)}{\pi} \right) \tag{3.8.}$$

Where; V_1 and V_2 are input and output voltages while considering buck and boost modes, N is high frequency transformer turn ratio, L is sum of the transformer leakage inductance and auxiliary inductor, δ is a phase shift angle and finally w is equal to $2\pi f$. δ is presented to 5.78μs (charging mode) and 7.35μs (discharging mode) at (Tan et. al., 2012). Thus, δ can be chosen between 4μs and 8μs for buck and boost modes of the converter.

Using the below equation for calculating inductors at buck and boost modes;

$$L = L_{Trans} + 2L_{Auxiliary} = \frac{V_1 V_2 N \times (\delta(\pi - \delta))}{2 \cdot P \cdot f \cdot \pi^2} \quad (3.9.)$$

For Buck Mode:

P=15kW, V_1=200V, V_2=160V, N=1, δ=4.6, f=20kHz, L_{Trans}=1.6µH → L_1=18µH

For Boost Mode:

P=15kW, V_1=100V, V_2=160V, N=1, δ=5.1, f=20kHz, L_{Trans}=1.6µH → L_2=12µH

L_1 and L_2 are equal to $L_{Auxiliary}$ at equation (3.9.).

3.2.2. DC Link Capacitors Calculation

Firstly, the basic capacitor equation which is known. Capacitor current, i_c can be expressed as capacitor value, C times derivative of the voltage across this capacitor, V_{cap}.

$$i_{cap} = C \frac{dV_{cap}}{dt} \quad (3.10.)$$

Extracting the capacitance C can be calculated as;

$$C = \frac{i_{cap} dt}{dV_{cap}} \quad (3.11.)$$

At equation (3.11.) dV_{cap} is voltage ripple across the capacitor and it is known for a design. Generally, small capacitor values give rise to bigger voltage ripple and this bigger voltage ripples cause to transfer more harmonics at the ac side load. Therefore, both small capacitor and low harmonics to the load are necessary. Obviously, a contradiction occurs and designers should consider this condition.

However, the ripple voltage of the converter is generally determined and the equation (3.12.), (3.13,) can be used for buck and boost modes in order to calculate input and output capacitors. In this way, creating of two capacitor values is possible if it is used $C_1=C_{input}$, $C_2=C_{output}$ for buck mode and $C_1=C_{output}$, $C_2=C_{input}$ for boost mode.

Input capacitor (C_{input}) and output capacitors (C_{output}) are calculated as (Rafiq M. and Ul Hasan M. F., MSc Thesis);

$$C_{input} = \frac{\Delta I_L T_{sw}}{8\Delta V_o} \tag{3.12.}$$

$$C_{output} = \frac{I_0 D T_{sw}}{\Delta V_o} \tag{3.13.}$$

For Buck and Boost Modes:

ΔI_L should be calculated for finding C_{input}. Thus, equation (3.1.) should be used firstly.

$$\Delta I_L = \frac{1}{2} \cdot \frac{200-160}{18\times10^{-6}} \cdot \frac{160}{200} \cdot \frac{1}{20000} \tag{3.14.}$$

ΔI_L = 44.4A

And by using equation (3.12.);

$$C_{input} = \frac{44.4}{8\times3.96\times10^{-3}\times20000} = 70mF \tag{3.15.}$$

Equation (3.18.) should be used for calculating C_{output}. But, duty cycle D should be calculated firstly and equation (3.16.) presents duty cycle formula.

$$D = 1 - \frac{\Delta V_{in}}{V_o} \tag{3.16.}$$

$$D = 1 - \frac{0.02 \times 200}{160} = 0.975 \tag{3.17.}$$

And substituting this value into equation (3.13.);

$$C_{output} = \frac{14.62 \times 0.975}{3.96 \times 10^{-3} \times 20000} = 180mF \tag{3.18.}$$

Consequently, C_1=70mF , C_2=180mF for buck and boost modes of SPS control.

3.2.3. Effect of Snubber Capacitors

Generally, larger capacitances cause to reduce turn-off losses, but it should reduce turn-on losses too. The present aim is reducing the total of turn-off and turn-on losses. The snubber design can be simply done with energy equation that is charge balance of Cv^2 and 1/2Li^2 shown at (3.19.) (Zhang, 2008).

$$C \cdot v^2 = \frac{1}{2} \cdot L \cdot i^2 \tag{3.19.}$$

Here v is capacitor voltage and i is inductor current.

This calculation can be done for small capacitance values or total elimination of snubber capacitors, which is good for power MOSFETs. But this charge balance is insufficient to minimize the switching loss for significant IGBT tail current. For this case, an experimental research was made to determine better snubber capacitors at turn-on and turn-off losses under hard and soft switching conditions (Zhang, 2008).

In this study, five cases were tested experimentally for snubber capacitor optimization. 0.14μF, 0.1μF, 0.068μF, 0.033μF and 0F capacitors were tried. The prototype with 0.068μF gave the best efficiency result. Figure 3.2 shows turn-on and turn-off energy vs. current with various capacitance values (Zhang, 2008).

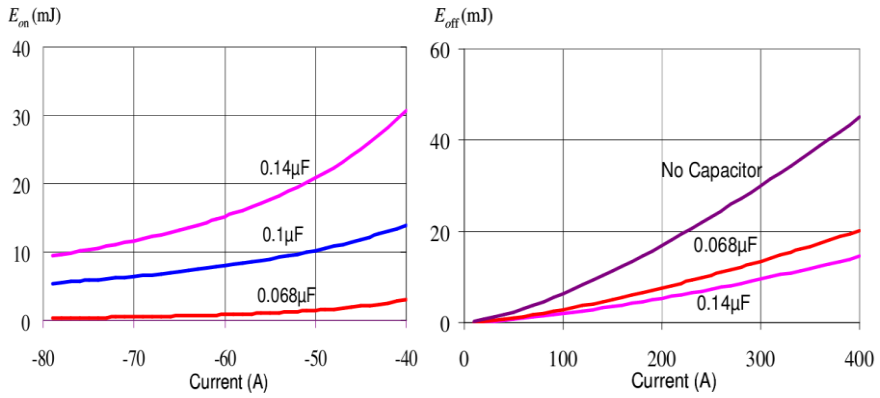

(a) (b)

Figure 3.2. Turn-on and turn-off energy vs. current with various capacitance values
(a) Turn-on energy vs. current
(b) Turn-off energy vs. current

According to the above graphics, using the most efficient snubber capacitor ($0.068\mu F$) affects 50% of the system performance. Therefore, if it is wanted to compare different phase shift control methods on efficiency, nonuse of snubber capacitors will be given better results at turn-off condition. In this way, this study measures efficiencies with or without using snubber capacitors.

3.2.4. Power Loss Calculations

3.2.4.1. IGBT and Diode Losses

The IGBT and diode losses as well as the power losses in any semiconductor component can be divided in three groups:

(a) Conduction Losses ($P_{conduction}$)

(b) Switching Losses (P_{sw})

(c) Blocking leakage losses usually neglected

Therefore;

$$P_{Semiconductor} = P_{Conduction} + P_{SW} \tag{3.20.}$$

3.2.4.1.1. Conduction Losses

Important parameters can be read from the datasheet of IGBT, for calculating conduction losses of IGBT and anti-parallel diode. The instantaneous value of the IGBT conduction losses are;

$$P_{CT}(t) = u_{CE}(t) i_C(t) = u_{CE0} i_C(t) + r_C {i_C}^2(t) \tag{3.21.}$$

The average IGBT current value is I_{cav} and value of IGBT current is I_{crms} . Then the average power losses can be expressed as;

$$P_{CT}(t) = \frac{1}{T_{SW}} \int_0^{T_{SW}} p(t)dt = \frac{1}{T_{SW}} \int_0^{T_{SW}} (u_{CE0} i_C(t) + r_C {i_C}^2(t))dt = u_{CE0} I_{cav} + r_C {I_{crms}}^2 \tag{3.22.}$$

Same approximation, the instantaneous value of the diode conduction losses is

$$P_{CD}(t) = u_D(t) i_D(t) = u_{D0} i_F(t) + r_D {i_D}^2(t) \tag{3.23.}$$

If the average diode current is I_{Dav} and the rms diode current is I_{Drms}, the average diode conduction losses across the switching period ($T_{SW}=1/f_{SW}$) are

$$P_{CD}(t) = \frac{1}{T_{SW}} \int_0^{T_{SW}} p(t)dt = \frac{1}{T_{SW}} \int_0^{T_{SW}} (u_{D0} i_D(t) + r_D {i_D}^2(t))dt = u_{D0} I_{Dav} + r_D {I_{Drms}}^2 \tag{3.24.}$$

3.2.4.1.2. Switching Losses

The switching losses are obtained from production of switching energies and the switching frequency f_{sw}.

$$P_{swT}(t) = (E_{onT} + E_{offT})\, f_{sw} \tag{3.25.}$$

$$P_{swD}(t) = (E_{onD} + E_{offD})\, f_{sw} \tag{3.26.}$$

Where the energy during on and off period can be written as,

$$E_{onM} = E_{refon} \frac{\Delta V_{in} I_{in}}{V_{ref} I_{ref}} \tag{3.27.}$$

$$E_{offM} = E_{refoff} \frac{\Delta V_{in} I_{in}}{V_{ref} I_{ref}} \tag{3.28.}$$

E_{refon} and E_{refoff} can be taken from datasheet of IGBT in order to calculate switching losses of both IGBT and diode.

Total losses;

$$P_T = P_{CT} + P_{swT} = u_{CE0} I_{cav} + r_C I_{crms}^{\ 2} + (E_{onT} + E_{offT})\, f_{sw} \tag{3.29.}$$

$$P_D = P_{CD} + P_{swD} = u_{D0} I_{Dav} + r_C I_{Drms}^{\ 2} + (E_{onD} + E_{offD})\, f_{sw} \tag{3.30.}$$

4. CONTROL METHODS AND SIMULATIONS

In this thesis, the simulation model of the system is studied by using EMTDC/PSCAD 4.2.0 Professional software. In order to investigate the performance of Bidirectional Isolated DC-DC Converter, Single Phase Shift (SPS), Extended Phase Shift (EPS) and Dual Phase Shift (DPS) control methods are modeled, simulated and analyzed in PSCAD 4.2.0 program. All control methods are developed in FORTRAN language.

4.1. Simulation Model

The simulation results are obtained from the system given in Figure 4.1 by using PSCAD software in a way to compare the phase shift control methods effect on performance of the bidirectional isolated dual active bridge DC-DC converter.

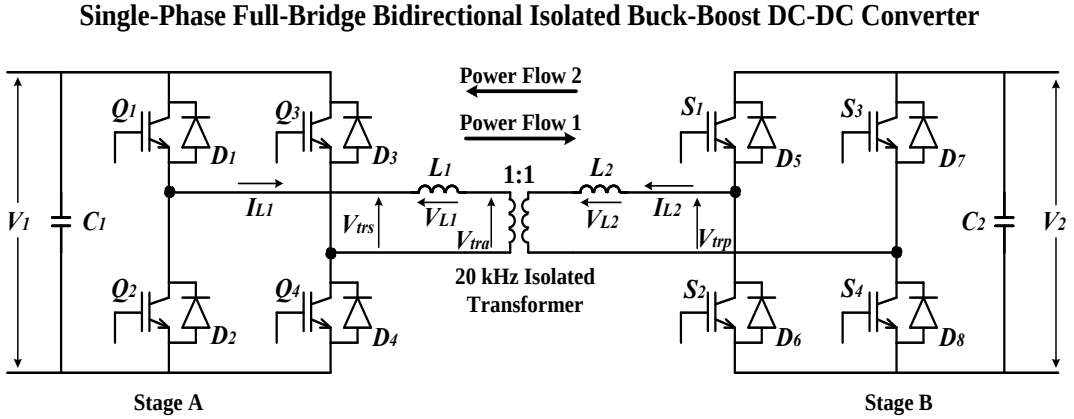

Figure 4.1. Simulation Model of Isolated Bidirectional DC-DC Converter

In this part of the thesis, modeling and analysis of different phase shift control methods are studied and simulated. Effects of phase shift control methods are compared on the performance of bidirectional DC-DC converter. Therefore, a lot of different cases should be examined in order to understand which phase shift control method is better than the others. Initially, each of the control methods will be introduced with the circuit parameters, triggering signals, switching states, buck-

boost modes and calculation of phase shift angle codes. Moreover, all cases are given after the simulation results. Then, comparison results are given with tables in fifth chapter before conclusion.

4.2. Single Phase Shift (SPS) Control

SPS is common used control method for bidirectional dc-dc converters in literature. These researchers (Xie et. al., 2010), (Chan et. al., 2003), (Mi et. al., 2008), (Zhao et. al., 2010), (Qin et. al., 2012), (Zhao et. al., 2014), (Wen et. al., 2014), (Kheraluwala et. al., 1992), (Inoue et. al., 2007), (Tan et. al., 2012), (Bai et. al., 2008) used SPS control method.

SPS control is operated by creating phase shift angle between Stage A IGBTs triggering signals and Stage B IGBTs triggering signals in Figure 4.1. In other words, when Q_1 and Q_3 are 1, Q_2 and Q_4 are 0. The same condition is valid for Stage B (when S_1 and S_3 are 1, S_2 and S_4 are 0.) But it contains addition of phase angle at the current or voltage waveform.

These triggering signals are produced with reference signal that is created by addition of P and I parameters. These parameters are PI (Proportional-Integral) control parameters and P value is obtained from multiplication of Error and K_p constant value. But I is produced by addition of previous I value and multiplication of K_i, T_s and Error. Then, cos(*wt*) signal defines IGBT triggering signals according to conditions which are changeable. It can be bigger or smaller than 0 and IGBTs take 1 and 0 values according to these conditions.

In SPS control, reference signal is extracted from cosine function. In this way, phase shift angle is created between Stage A and Stage B of the bidirectional dc-dc converter. Fortran codes are demonstrated at 4.2.4. part.

Moreover, SPS simulation and its control block diagram are shown at Figure 4.2 and Figure 4.3 respectively.

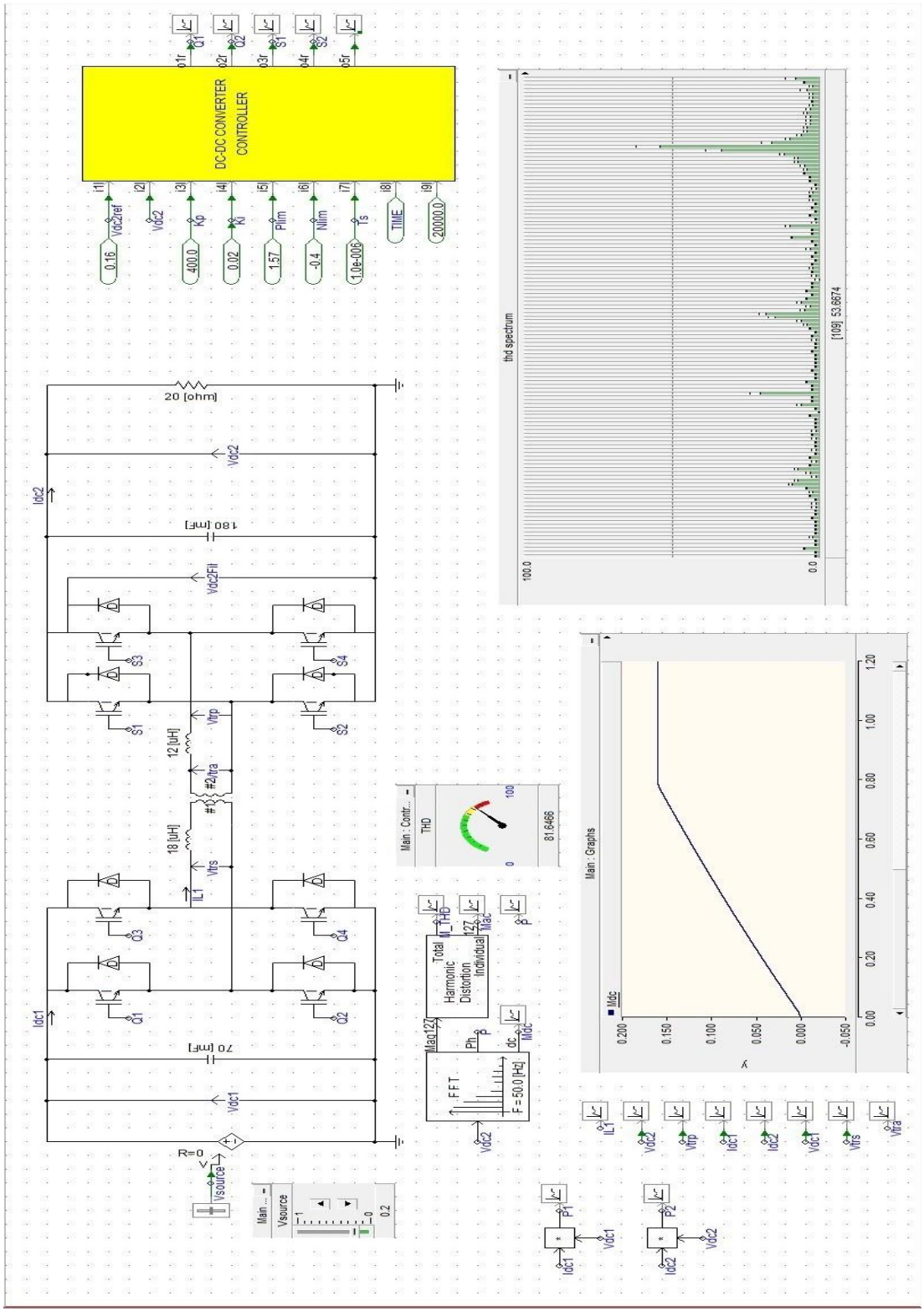

Figure 4.2. PSCAD Simulation of SPS Control

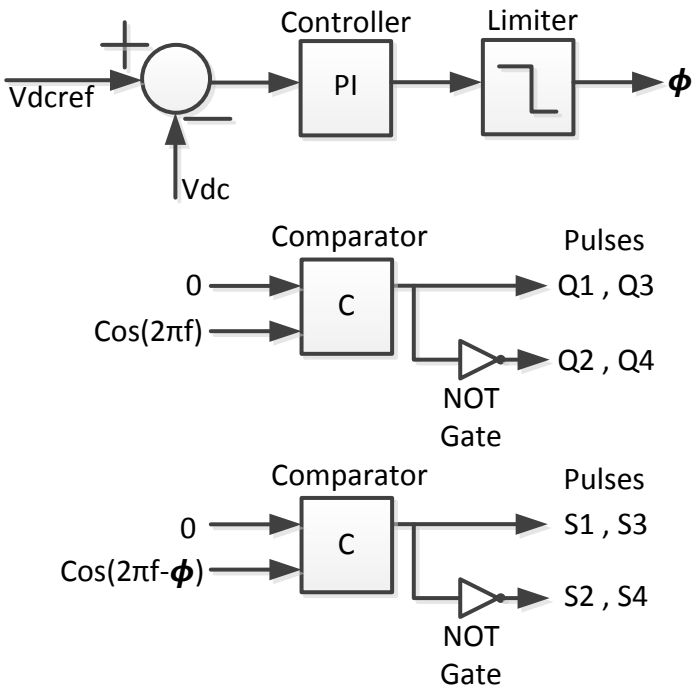

Figure 4.3. SPS Control Block Diagram

4.2.1. Triggering Signals

In SPS control method, IGBTs triggering signals can be showed at Table 4.1 and Figure 4.4.

Table 4.1. Triggering Signals of IGBTs at SPS Control

Stage A				**Stage B**			
Q_1	Q_2	Q_3	Q_4	S_1	S_2	S_3	S_4
1	0	1	0	1	0	1	0

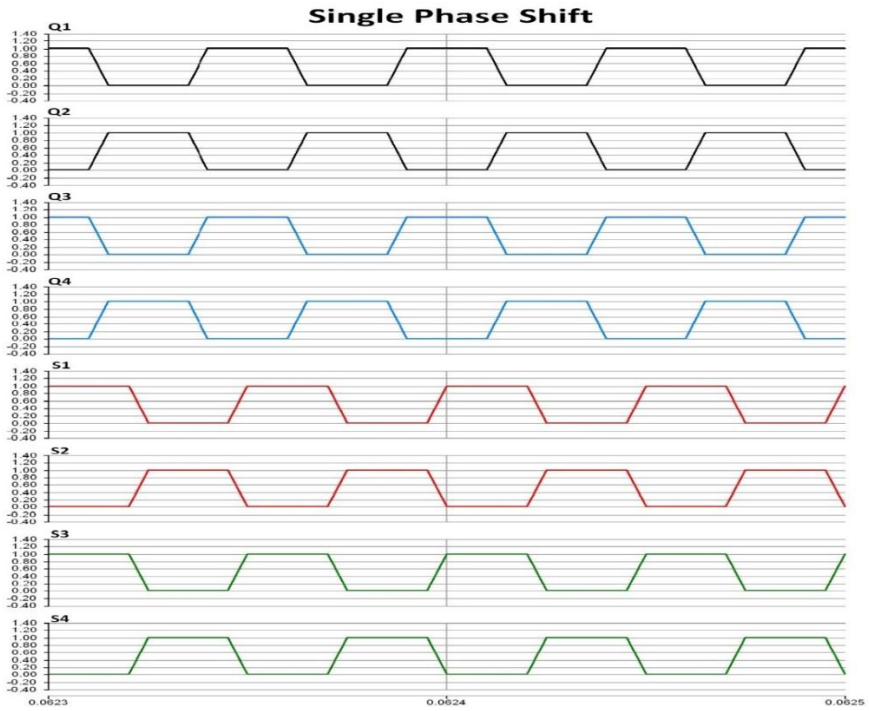

Figure 4.4. Triggering Signals of IGBTs at SPS Control Method

4.2.2. Switching States for Buck-Boost Modes

The switching cycle can be broken into 4 main intervals. During each of these 4 intervals, two IGBTs on each of the bridges conduct. During the transitions between intervals, certain capacitors and diodes also conduct. In order to illustrate the logic behind this, the following diagrams and tables are given. The circuit diagrams are incomplete and intervals continue. Thus, the circuits which have same current ways, are omitted and these diagrams given at Figure 4.5 and Figure 4.6.

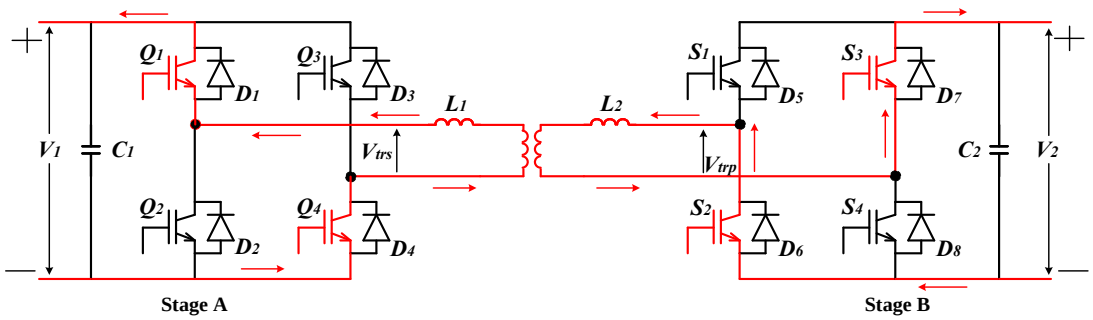

(a) Interval 1 (Inductor Current Negative, $V_{trs}=V_1$, $V_{trp}=-V_2$)

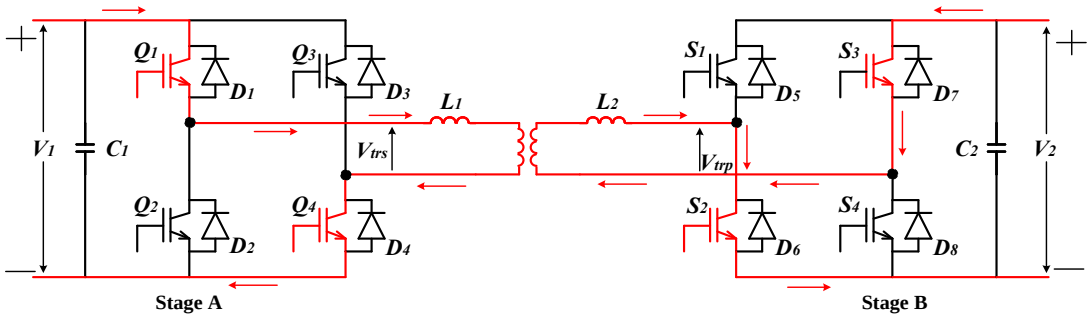

(b) Interval 1 (Inductor Current Positive, $V_{trs}=V_1$, $V_{trp}=-V_2$)

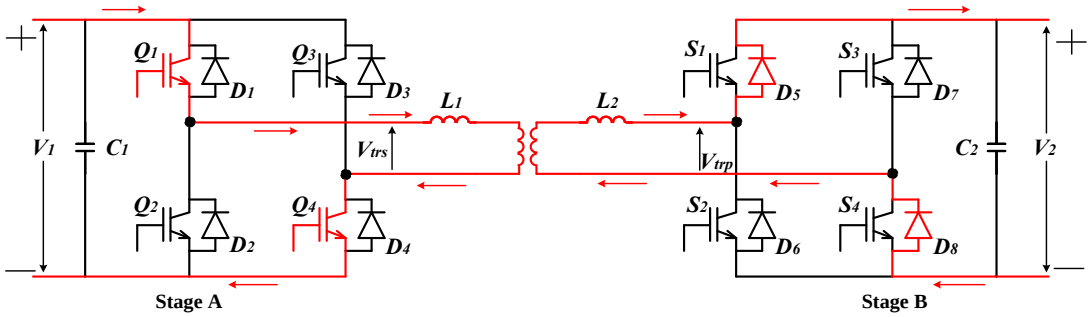

(c) Transition from interval 1 to Interval 2 (Ind. Current Negative, $V_{trs}=V_1$, $V_{trp}=V_2$)

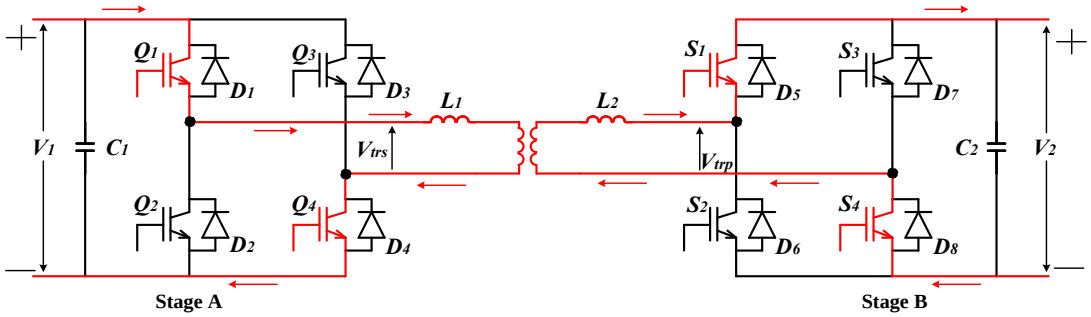

(d) Interval 2 (Inductor Current Positive, $V_{trs}=V_1$, $V_{trp}=V_2$)

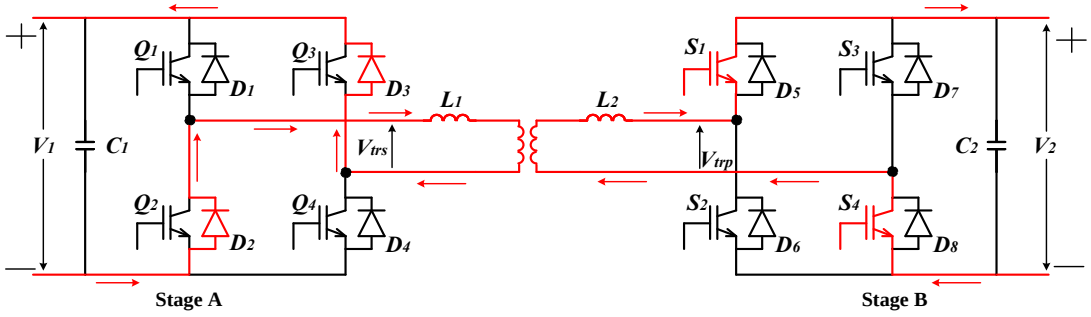

(e) Transition from Interval 2 to Interval 1' (Ind. Current Negative, $V_{trs}=-V_1$, $V_{trp}=V_2$)

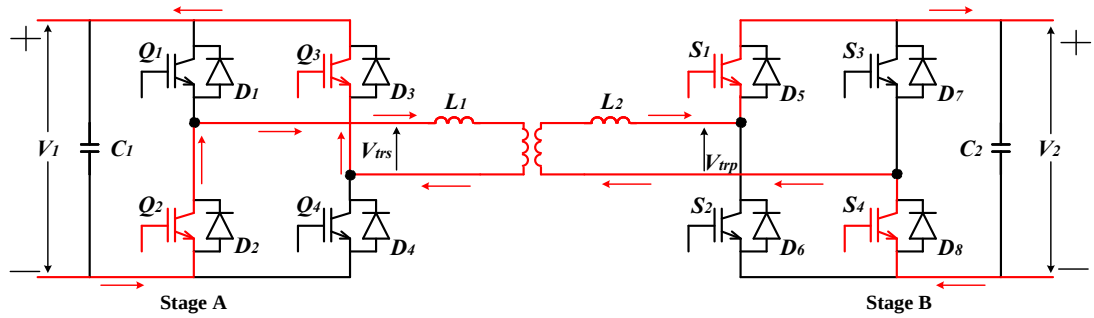

(f) Interval 1' (Inductor Current Positive, V_{trs}=-V_1 , V_{trp}=V_2)

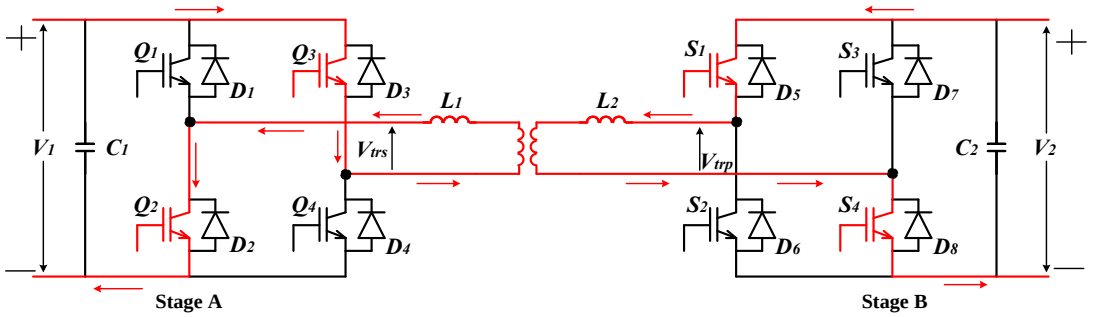

(g) Interval 1' (Inductor Current Negative, V_{trs}=-V_1 , V_{trp}=V_2)

Figure 4.5. SPS Switching States Current Diagrams for Buck-Boost Modes

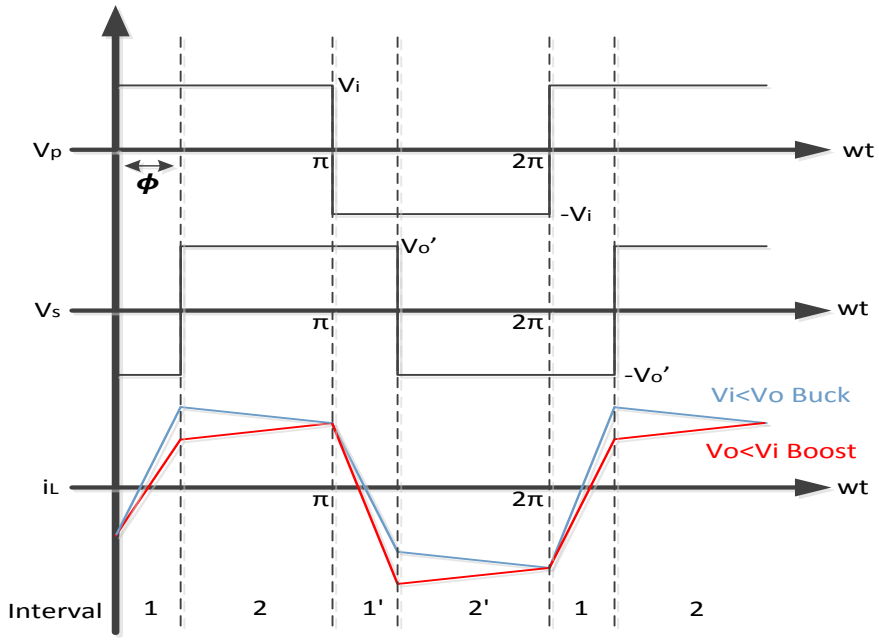

Figure 4.6. Current and Voltage Waveforms During Intervals (Electronics Stackexchange Web Page)

Figure 4.6 parameters can be defined according to below equations for theoretical analysis. ($V_p=V_{trs}$, $V_s=V_{trp}$, $i_L=I_{L1}$, $V_i=V_1$, $V_0=V_2$)

4.2.3. Simulation Cases and Results

Simulations are performed for the Table 4.2. Cases are changeable according to power flow way, buck-boost modes and parameters of circuit components.

Table 4.2. Cases of SPS Control Simulation; PF1: Power Flow 1, PF2: Power Flow 2

Converter Parameters			V_1	V_2	C_1	C_2	L_1	L_2	n	f
PF1	**Buck**	**Case1**	200V	160V	70mF	180mF	18µH	12µH	1:1	20kHz
		Case2	300V	100V	70mF	180mF	18µH	12µH	1:1	10kHz
	Boost	**Case3**	100V	160V	70mF	180mF	18µH	12µH	1:1	20kHz
PF2	**Buck**	**Case4**	160V	200V	70mF	180mF	18µH	12µH	1:1	20kHz
	Boost	**Case5**	160V	100V	70mF	180mF	18µH	12µH	1:1	20kHz
		Case6	300V	100V	70mF	180mF	18µH	12µH	1:1	10kHz

Simulation Results of Case 1:

V_1=200V, V_2=160V, C_1=70mF, C_2=180mF, L_1=18µH, L_2=12µH, n=1:1, f=20kHz

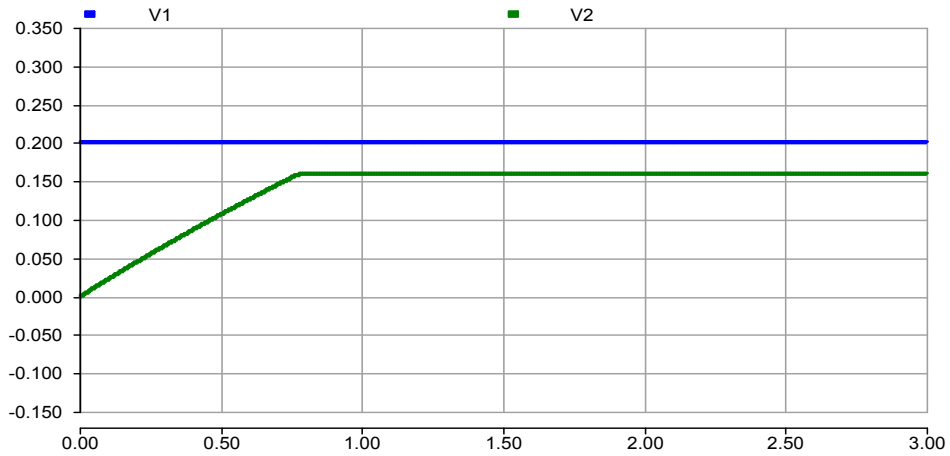

Figure 4.7. DC Link Voltages

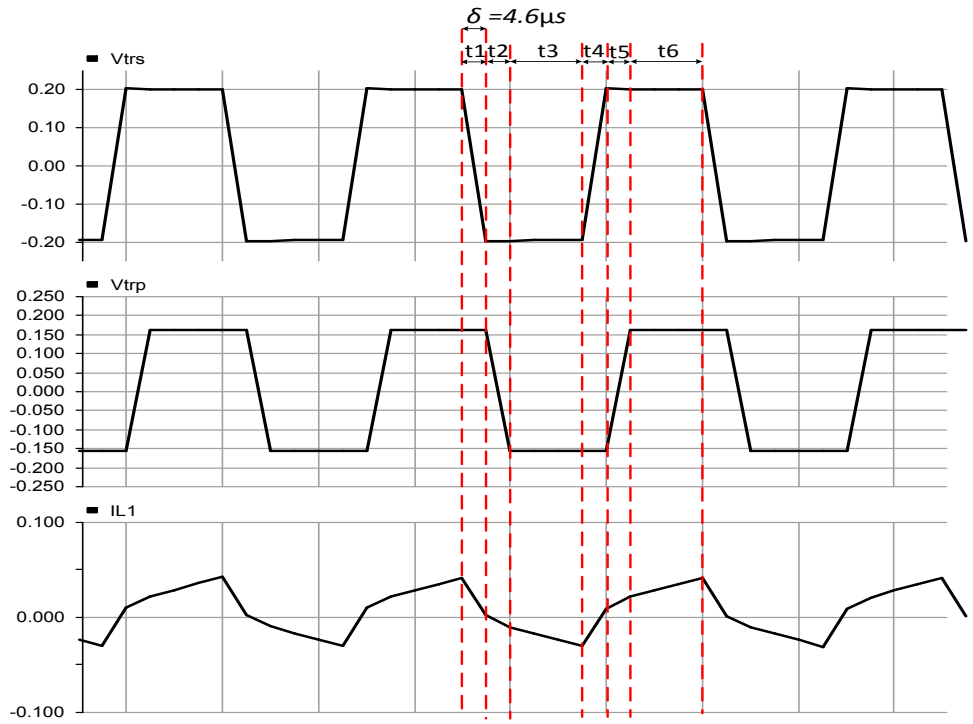

Figure 4.8. Transformer Voltages and Primer Inductor Current with phase-shift angle (Period is $T=t_1+t_2+t_3+t_4+t_5+t_6$)

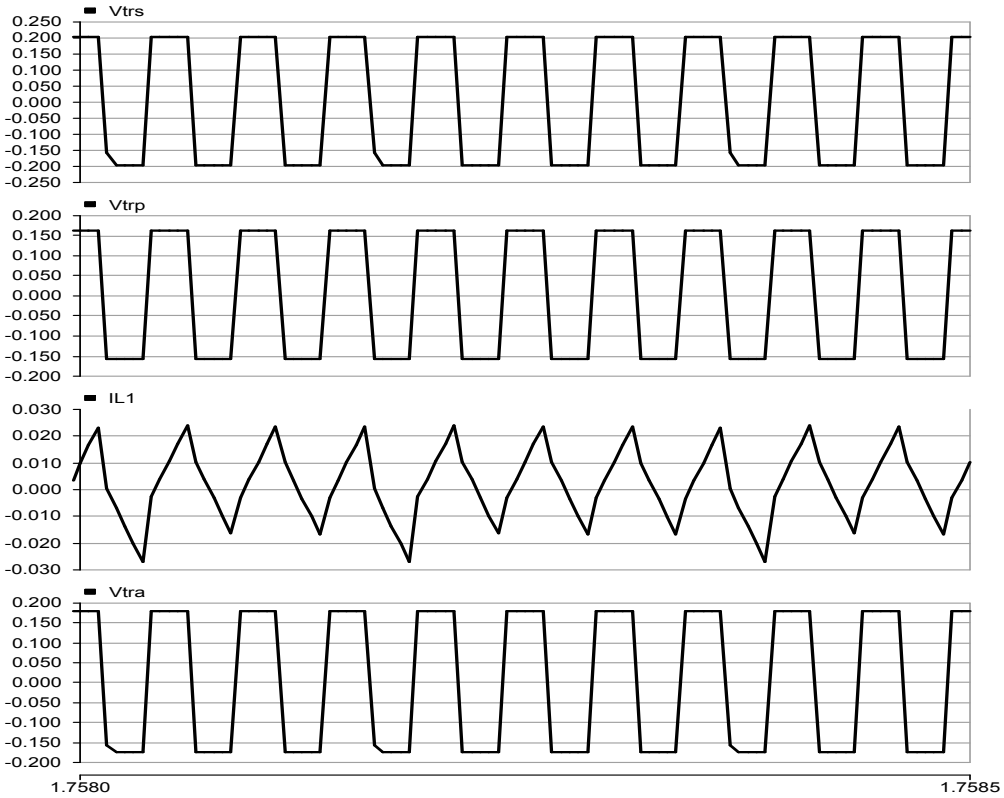

Figure 4.9. Transformer Voltages and Primer Inductor Current when the dc-link settling

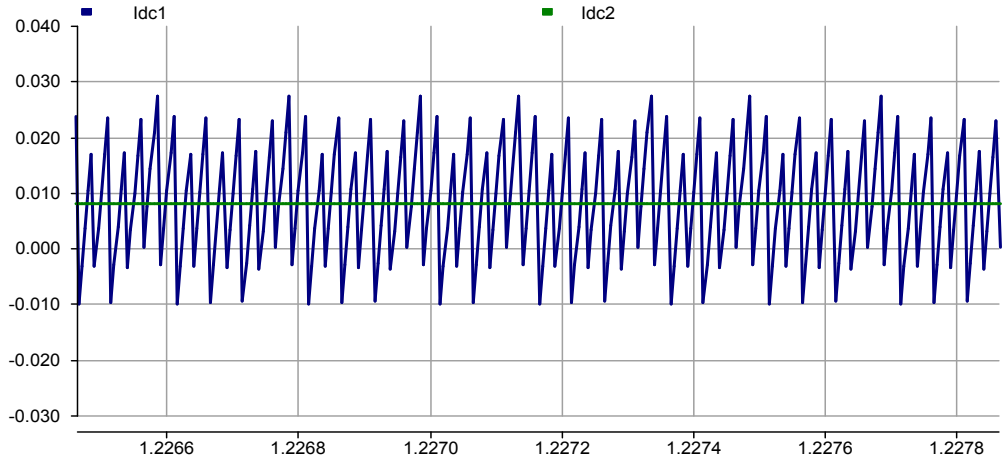

Figure 4.10. DC-Link Input and Output Currents

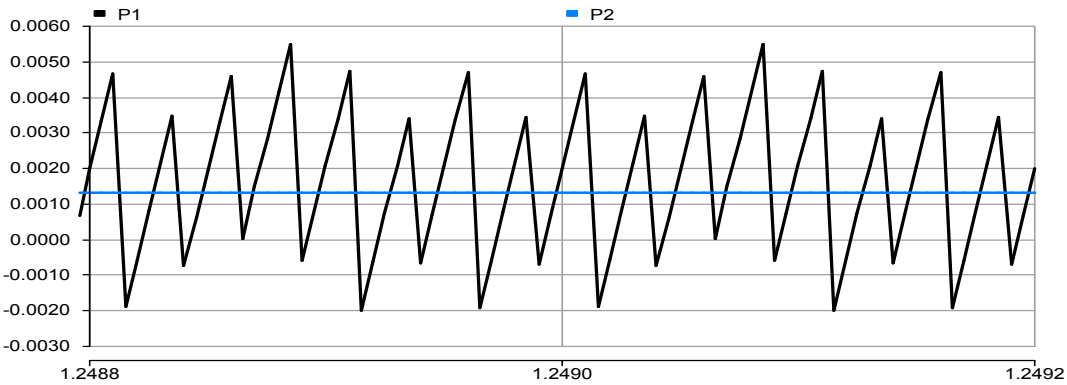

Figure 4.11. Input and Output Power Waveforms

Also, it is examined harmonics at primary side of the transformer and load side of the converter for this case.

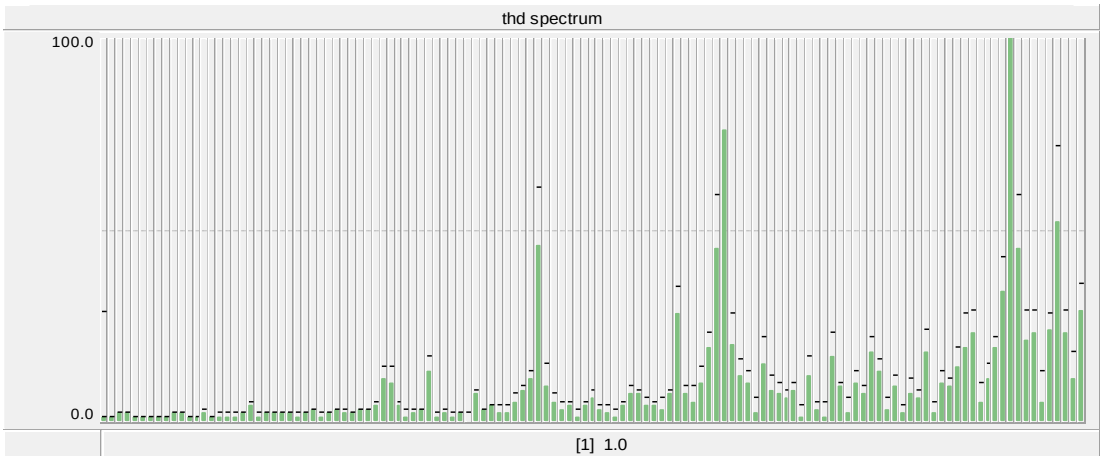

Figure 4.12. Harmonics Spectrum at Primary Side of Transformer

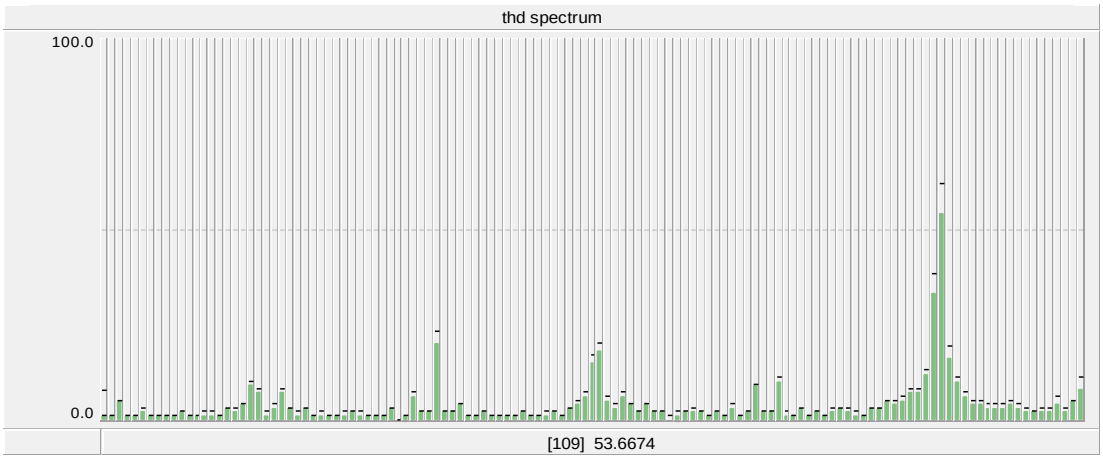

Figure 4.13. Harmonics Spectrum at Load Side

Simulation Results of Case 2:

V_1=300V, V_2=100V, C_1=70mF, C_2=180mF, L_1=18µH, L_2=12µH, n=1:1, f=10kHz

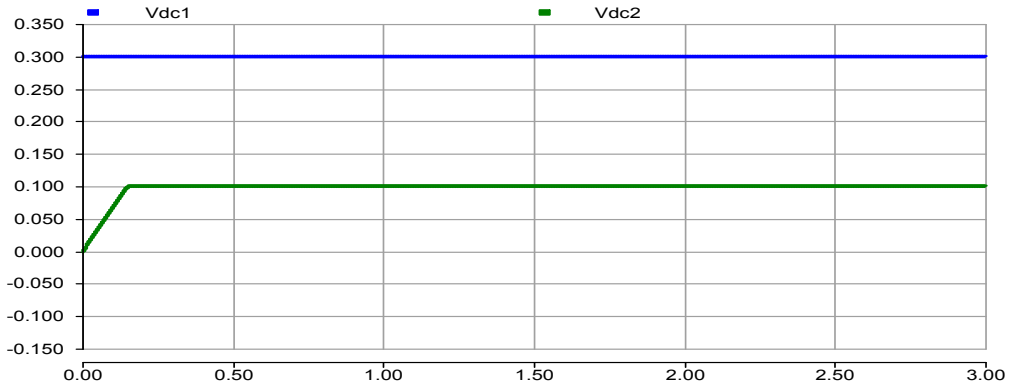

Figure 4.14. DC Link Voltages

Figure 4.15. Transformer Voltages and Primer Inductor Current before the dc-link settling

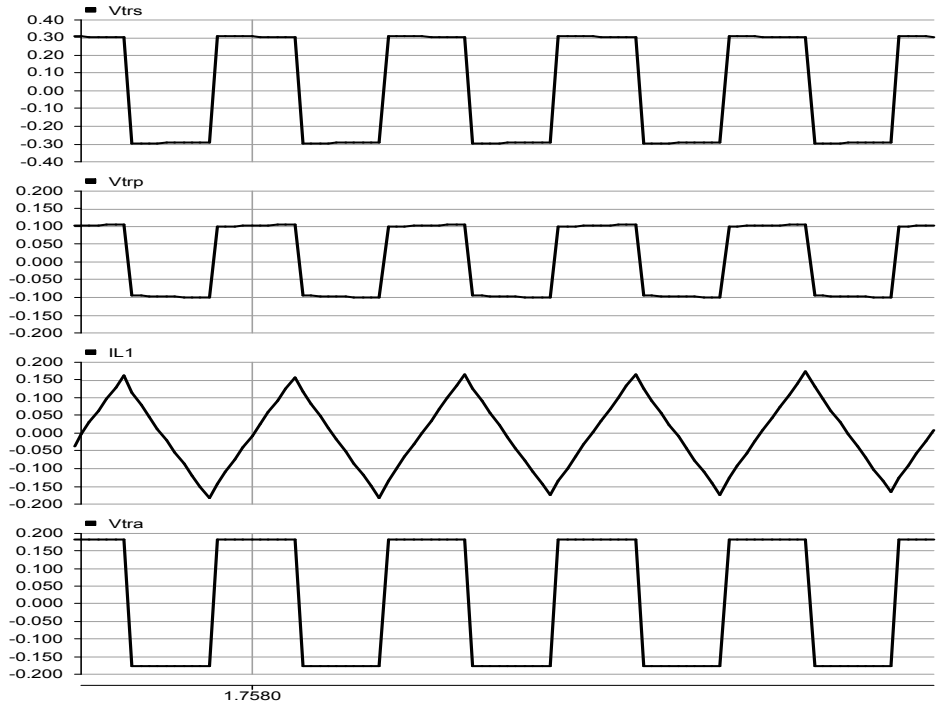

Figure 4.16. Transformer Voltages and Primer Inductor Current when the dc-link settling

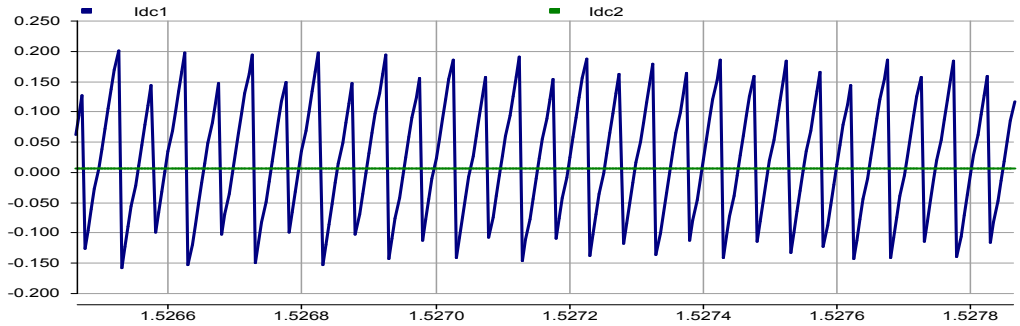

Figure 4.17. DC-Link Input and Output Currents

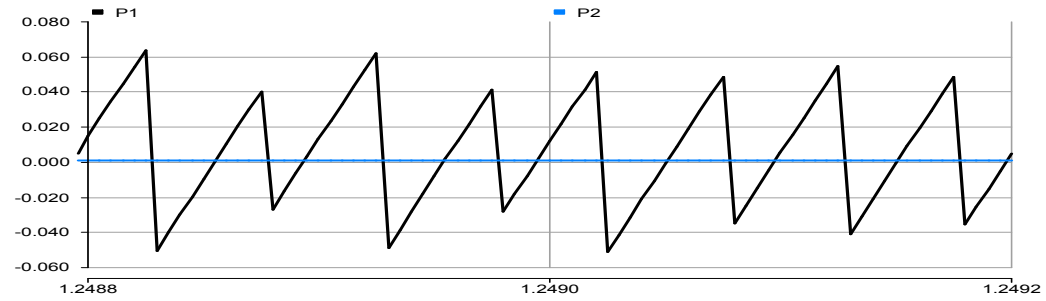

Figure 4.18. Input and Output Power Waveforms

Simulation Results of Case 3:

V_1=100V, V_2=160V, C_1=70mF, C_2=180mF, L_1=18µH, L_2=12µH, n=1:1, f=20kHz

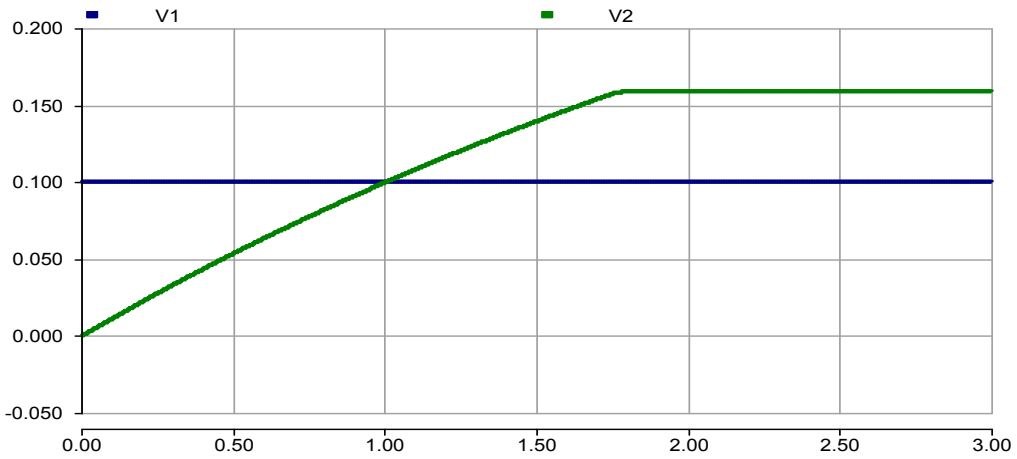

Figure 4.19. DC Link Voltages

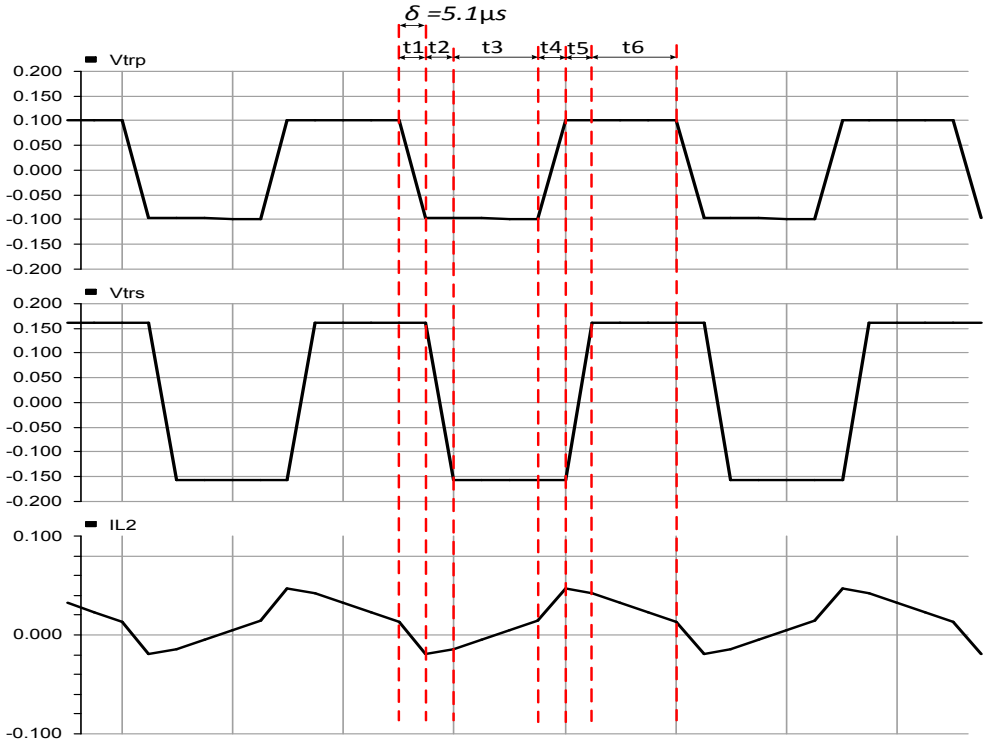

Figure 4.20. Transformer Voltages and Primer Inductor Current with phase-shift angle (Period is $T=t_1+t_2+t_3+t_4+t_5+t_6$)

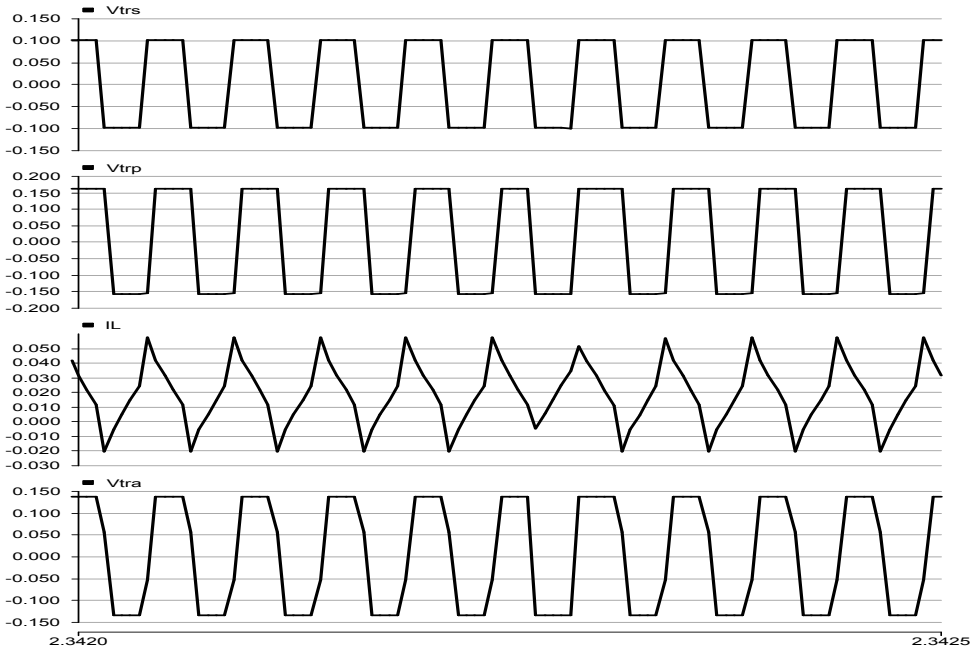

Figure 4.21. Transformer Voltages and Primer Inductor Current when the dc-link settling

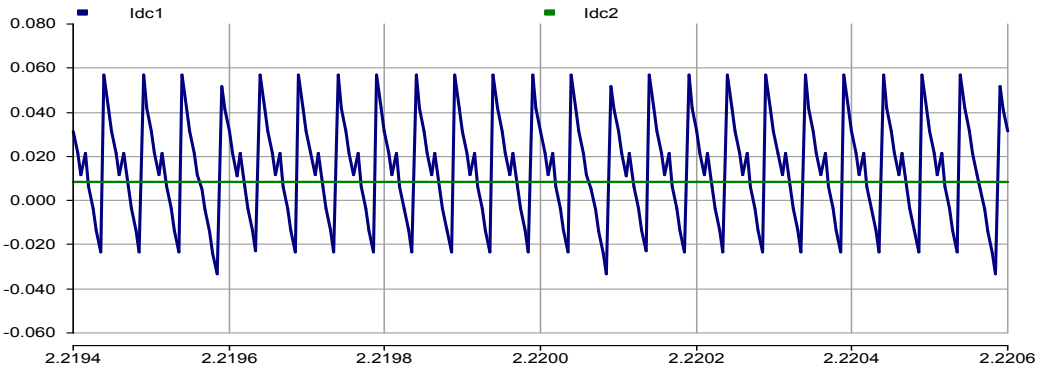

Figure 4.22. DC-Link Input and Output Currents

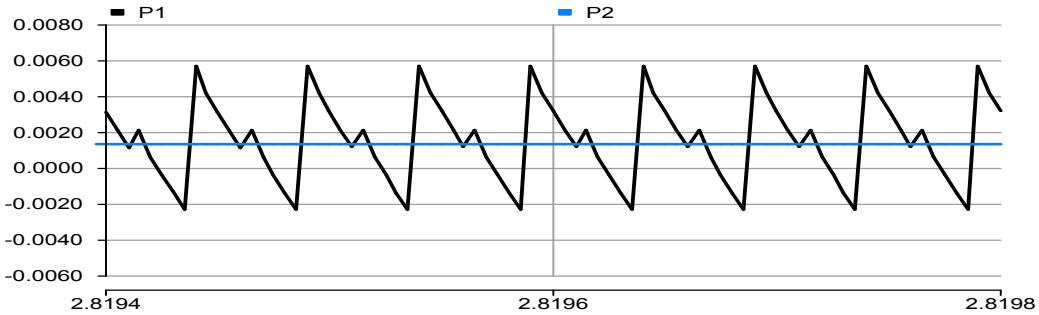

Figure 4.23. Input and Output Power Waveforms

Simulation Results of Case 4:

V_1=160V, V_2=200V, C_1=70mF, C_2=180mF, L_1=18µH, L_2=12µH, n=1:1, f=20kHz

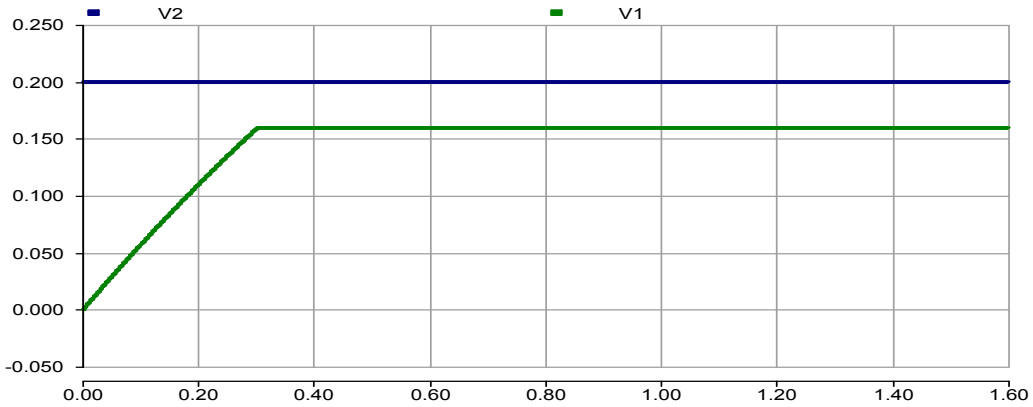

Figure 4.24. DC Link Voltages

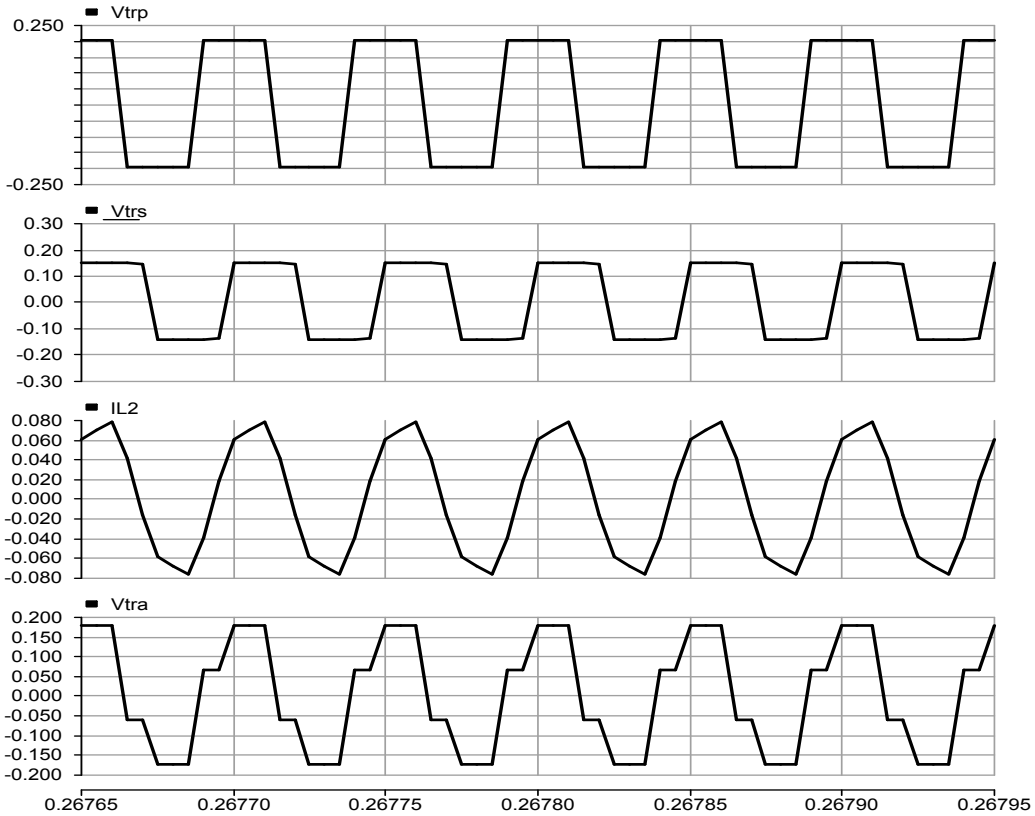

Figure 4.25. Transformer Voltages and Primer Inductor Current before the dc-link settling

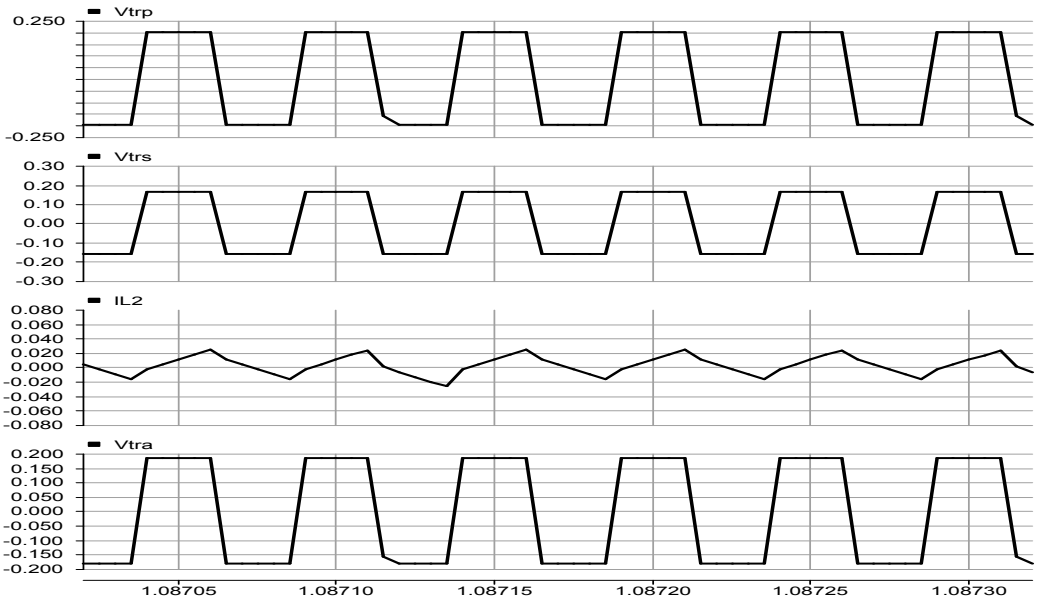

Figure 4.26. Transformer Voltages and Primer Inductor Current when the dc-link settling

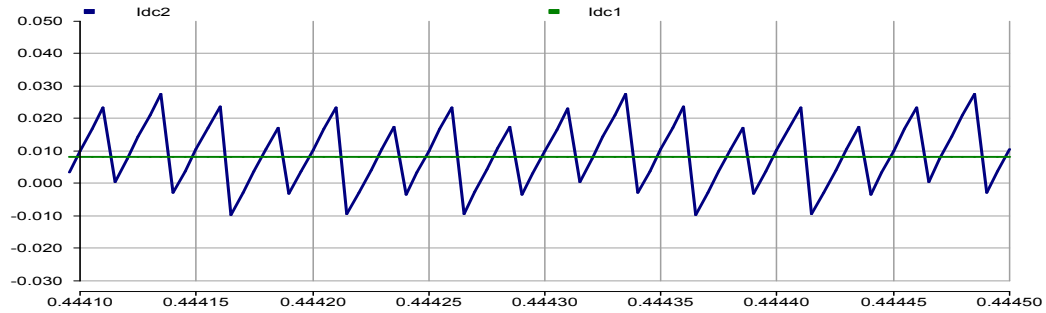

Figure 4.27. DC-Link Input and Output Currents

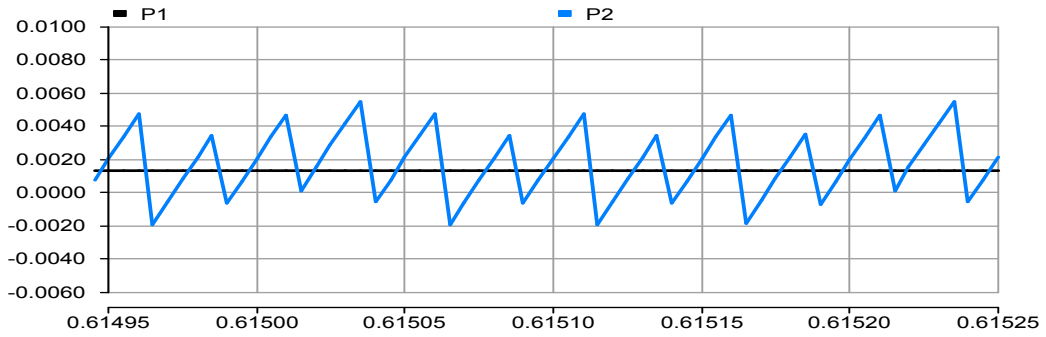

Figure 4.28. Input and Output Power Waveforms

Simulation Results of Case 5:

V_1=160V, V_2=100V, C_1=70mF, C_2=180mF, L_1=18µH, L_2=12µH, n=1:1, f=20kHz

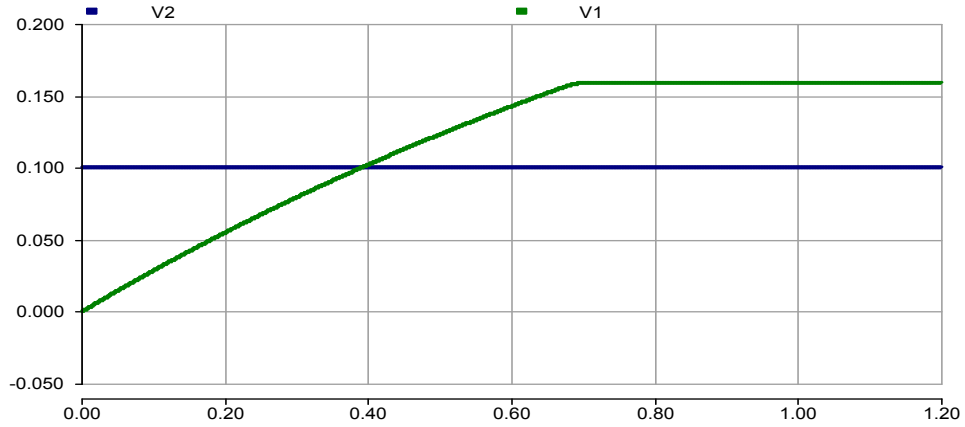

Figure 4.29. DC Link Voltages

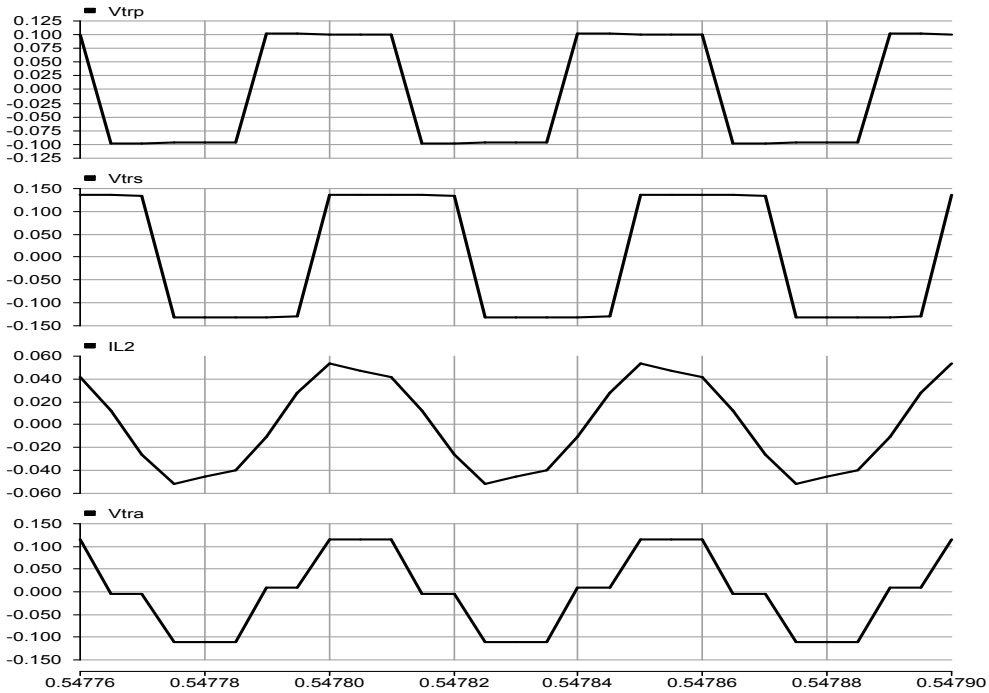

Figure 4.30. Transformer Voltages and Primer Inductor Current before the dc-link settling

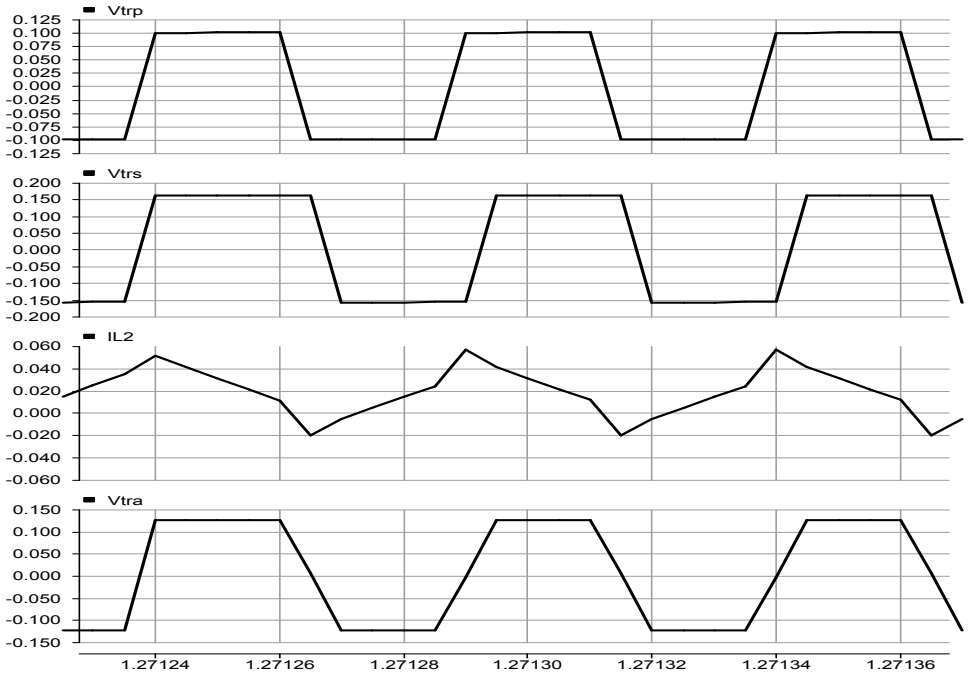

Figure 4.31. Transformer Voltages and Primer Inductor Current after the dc-link settling

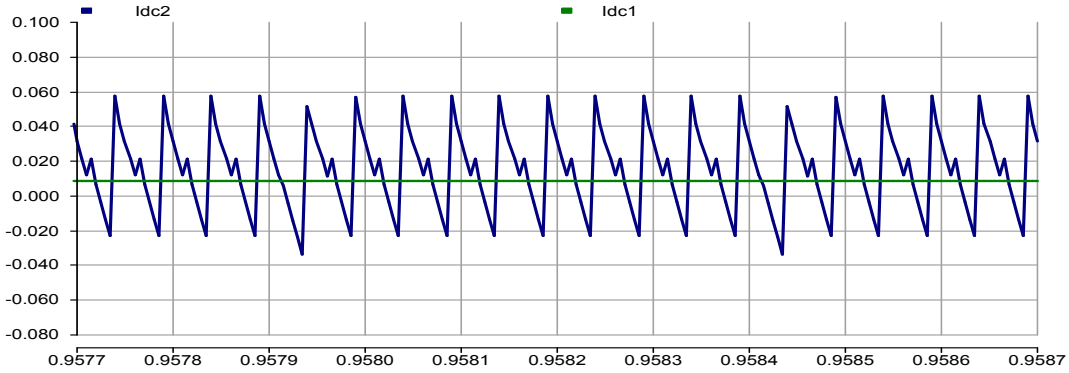

Figure 4.32. DC-Link Input and Output Currents

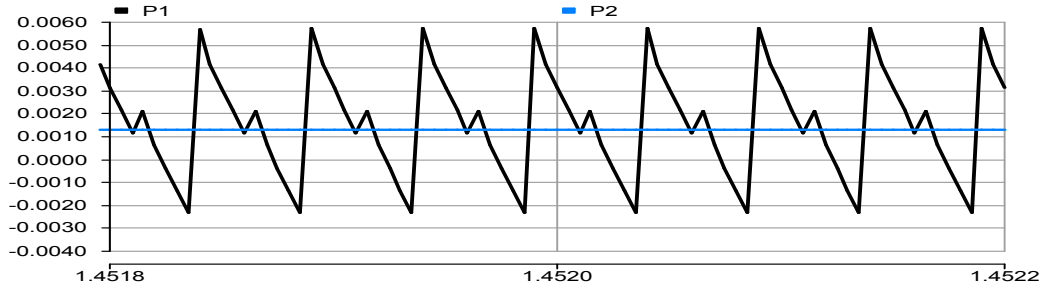

Figure 4.33. Input and Output Power Waveforms

Also, it is examined harmonics at primary side of the transformer and load side of the converter for this case.

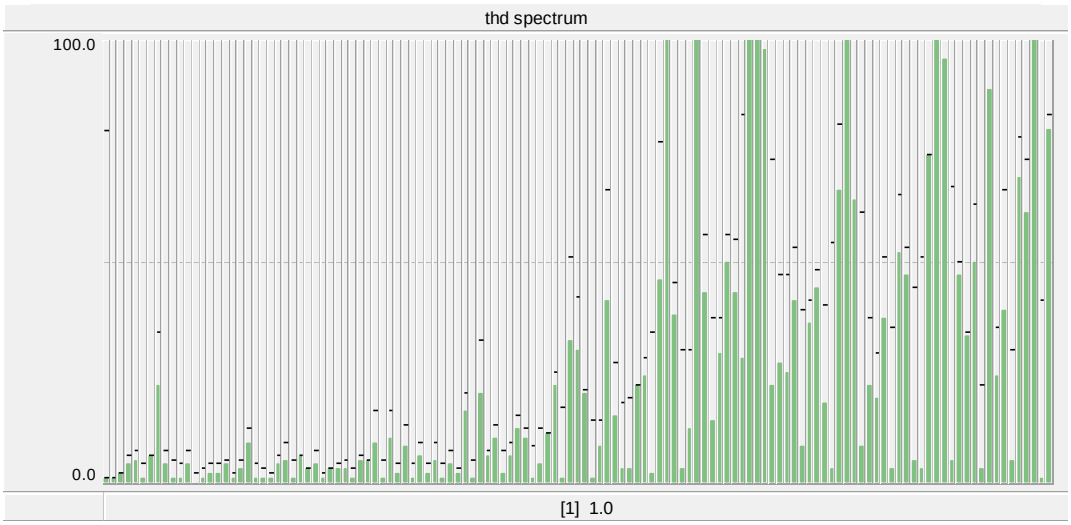

Figure 4.34. Harmonics Spectrum at Primary Side of Transformer

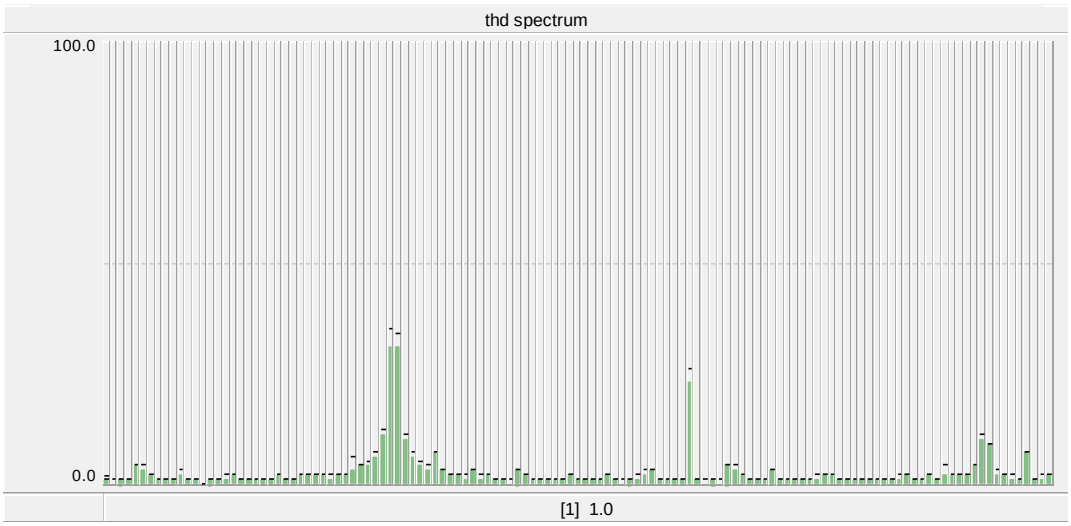

Figure 4.35. Harmonics Spectrum at Load Side

Simulation Results of Case 6:

V_1=300V, V_2=160V, C_1=70mF, C_2=180mF, L_1=18µH, L_2=12µH, n=1:1, f=10kHz

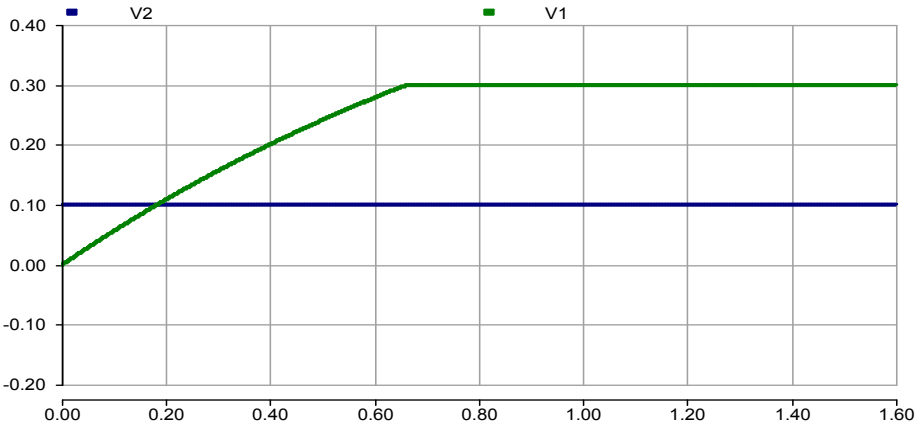

Figure 4.36. DC Link Voltages

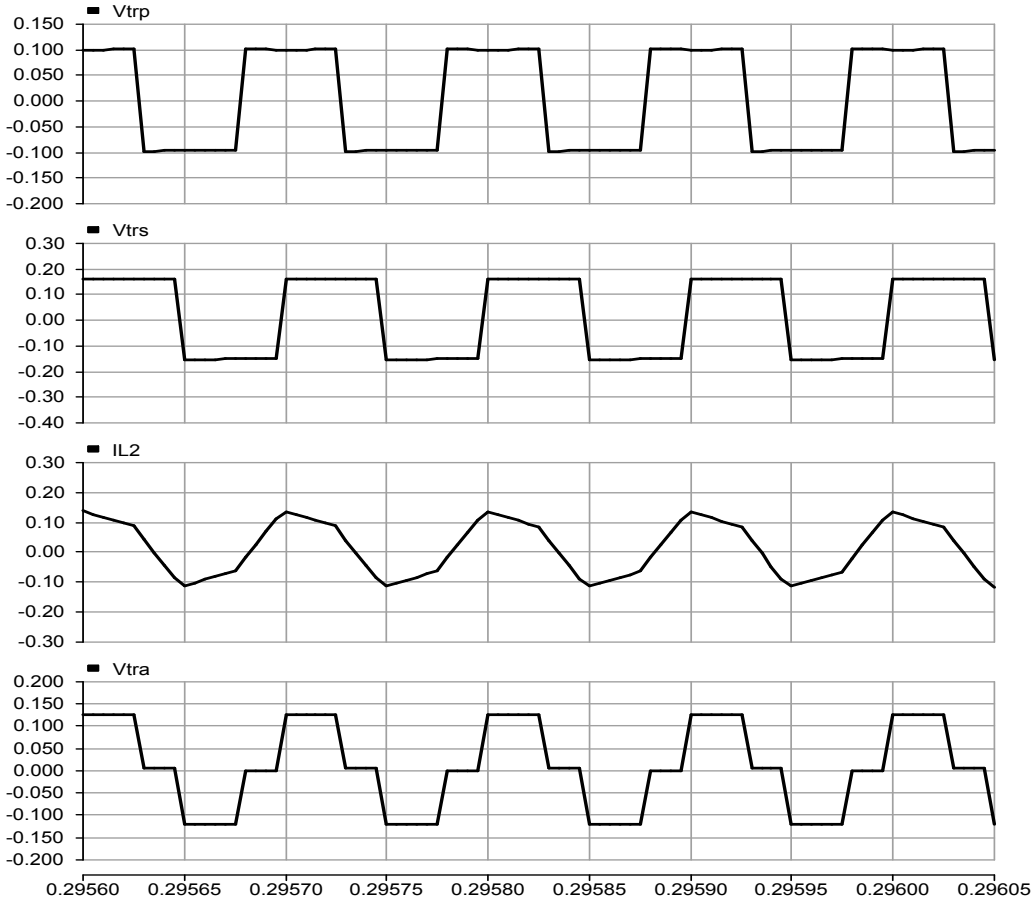

Figure 4.37. Transformer Voltages and Primer Inductor Current before the dc-link settling

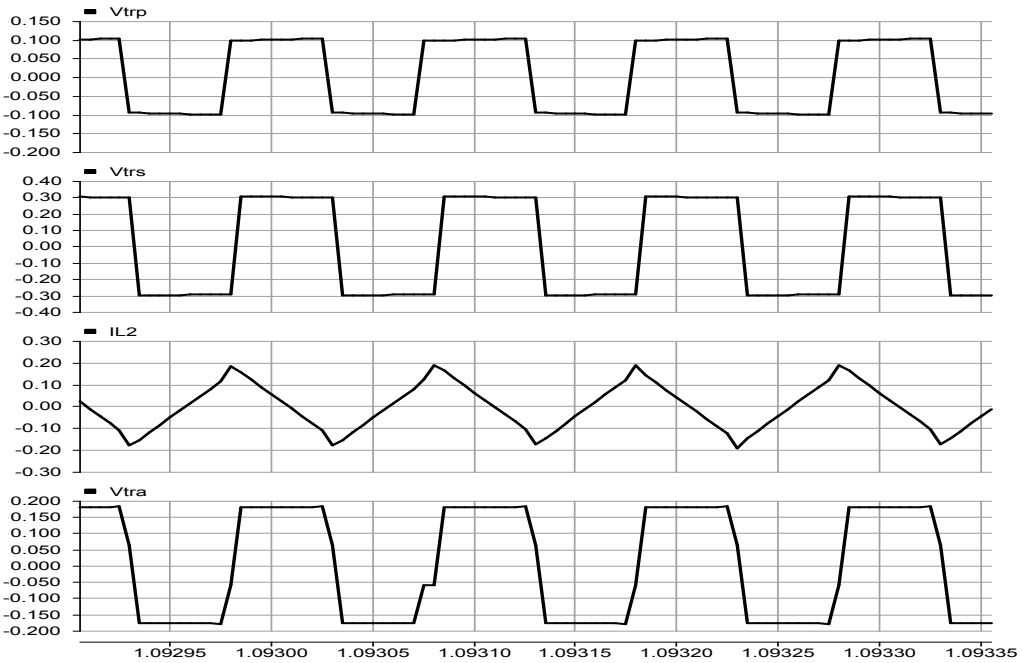

Figure 4.38. Transformer Voltages and Primer Inductor Current after the dc-link settling

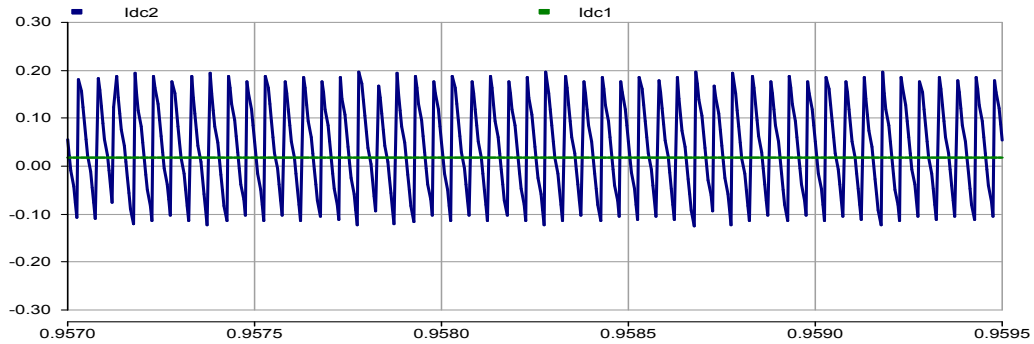

Figure 4.39. DC-Link Input and Output Currents

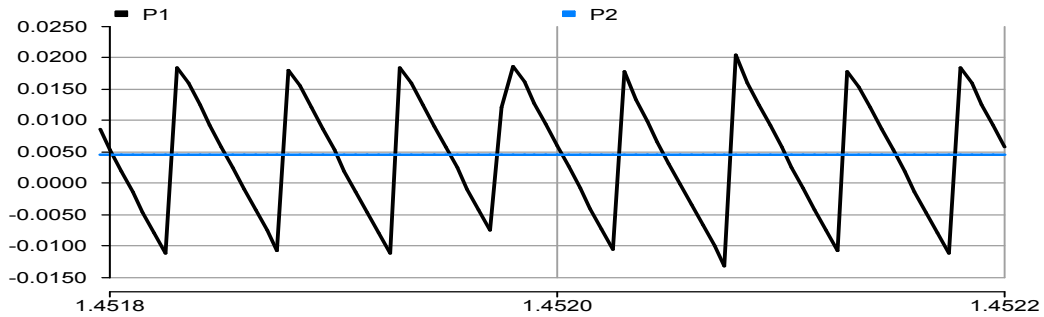

Figure 4.40. Input and Output Power Waveforms

4.2.4. Fortran Codes of SPS

```
#LOCAL REAL xVdc1_Err
#LOCAL REAL xP_dcdc
#LOCAL REAL xI_dcdc
#LOCAL REAL xRefdcdc

#LOCAL INTEGER xS1
#LOCAL INTEGER xS2
#LOCAL INTEGER xQ1
#LOCAL INTEGER xQ2

#LOCAL REAL xyA
#LOCAL REAL xyB
#LOCAL REAL xyphaseshift
#LOCAL REAL xfreq

#LOCAL INTEGER DCCounter

! !!!!!!!!!!!!!!!! INPUTS !!!!!!!!!!!!!!!!
xVdc1ref=$i1l
xVdc1=$i2l
xKp_dcdc=$i3l
xKi_dcdc=$i4l
xLimP_dcdc=$i5l
xLimN_dcdc=$i6l
xTs=$i7l
xTime=$i8l
xfreq=$i9l

! !!! Taking Datas from Memory !!!!!!!
xI_dcdc = STORF(NSTORF)
DCCounter = STORI(NSTORI)

DCCounter=DCCounter + 1
IF (DCCounter == 50) THEN
      DCCounter = 0

xVdc2_Err = xVdc2ref - xVdc2Fil
xP_dcdc = xKp_dcdc * xVdc2_Err
xI_dcdc = xI_dcdc + xKi_dcdc * xTs * xVdc2_Err
xRefdcdc = xP_dcdc + xI_dcdc

IF (xRefdcdc > xLimP_dcdc) THEN
      xRefdcdc = xLimP_dcdc
ENDIF

IF (xRefdcdc < xLimN_dcdc) THEN
      xRefdcdc = xLimN_dcdc
ENDIF
ENDIF

xyA=COS(6.28318530717958647692528676655 9*xTime*xfreq)
IF (xyA>=0) THEN
xS1=1
xS2=0
ELSE
xS1=0
xS2=1
ENDIF

xyB=COS(6.28318530717958647692528676655 9*xTime*xfreq-xRefdcdc)
IF (xyB>=0) THEN
xQ1=1
xQ2=0
ELSE
xQ1=0
xQ2=1
```

```
ENDIF

! !!!!!!!! Saving Datas !!!!!!!!!!!!!!!!!!
STORF(NSTORF) = xI_dcdc
STORI(NSTORI) = DCCounter

! !!!!!!!! OUTPUT !!!!!!!!!!!!!!!!!!!!!!!!!!!!!!!!!
$o1r= xS1
$o2r= xS2
$o3r= xQ1
$o4r= xQ2
$o5r= xRefdcdc

NSTORF = NSTORF+1
NSTORI = NSTORI+1
```

4.3. Extended Phase Shift (EPS) Control

EPS control method is harder than SPS control and it is not common in literature. These researchers (Zhao et. al., 2012), (Reddy et. al., 2013), (Shi et. al., 2013) used EPS control method in their studies.

(Zhao et. al., 2012) studied comparison of SPS and EPS by investigating current stress and backflow power experimentally with mathematical models. It emphasized EPS that gives better efficiency results than SPS. Additionally, (Reddy et. al., 2013) specified EPS reduces current stress, expands regulating range and enhances regulating flexibility. Lastly, (Shi et. al., 2013) indicates EPS improve the efficiency 30% more than the SPS experimentally at 10kW IBDC prototype for energy storage systems.

EPS control method is operated by creating phase shift angles between Stage A and Stage B of the dc-dc converter in Figure 4.1. Moreover, one more phase shift angle should be defined between the one of the full bridges. It can be changeable to rectifier or inverter side. In short, there are two phase shift angles and first angle represents between of the S type IGBTs and Q type IGBTs. The other one can be represented between of the S_1-S_2 leg and S_3-S_4 leg or Q_1-Q_2 leg and Q_3-Q_4 leg. In this way, IGBTs are triggered with 1 or 0. Triggering signals are shown at part 4.3.1. and switching states (direction of current against minor time intervals) are demonstrated at part 4.3.2. Moreover, EPS simulation and its control block diagram are shown at Figure 4.41. and Figure 4.42 respectively.

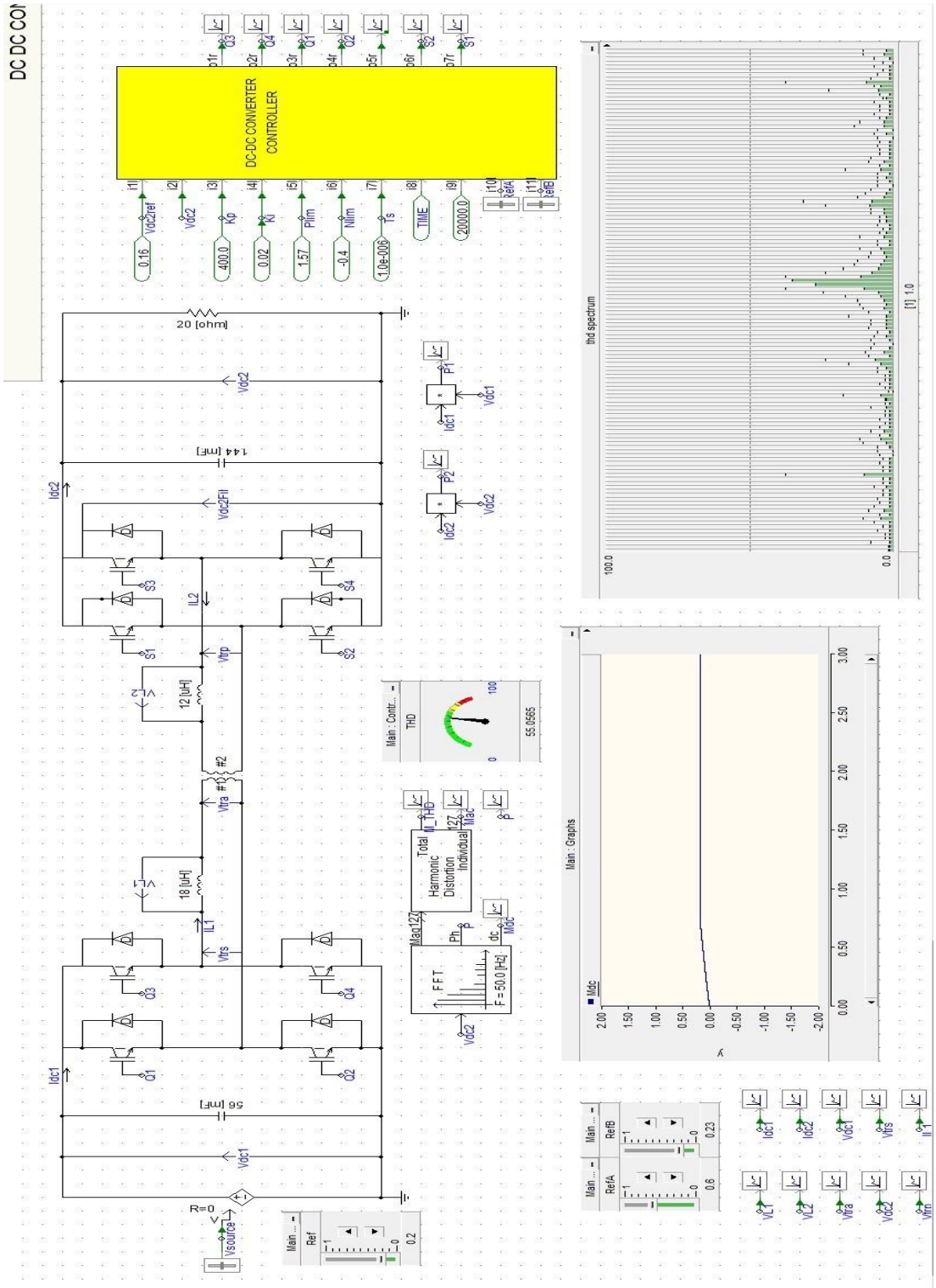

Figure 4.41. PSCAD Simulation of EPS Control

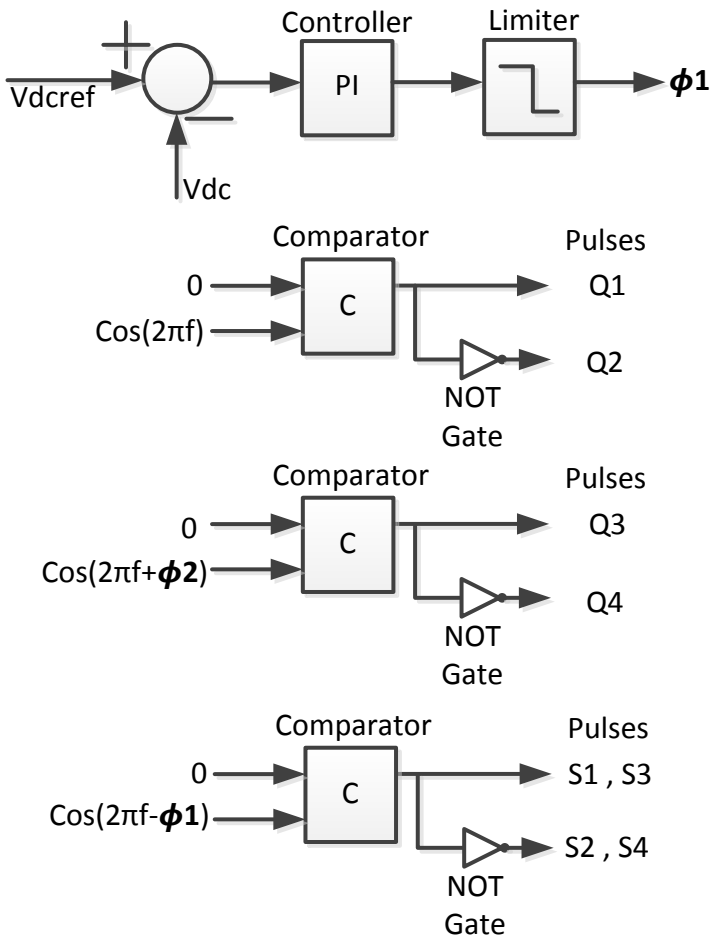

Figure 4.42. EPS Control Block Diagram

4.3.1. Triggering Signals

In EPS control method, IGBTs triggering signals can be showed at Table 4.3 and Figure 4.43.

Table 4.3. Triggering Signals of IGBTs at EPS Control

Stage A				**Stage B**			
Q_1	Q_2	Q_3	Q_4	S_1	S_2	S_3	S_4
1	0	1	0	1	0	1	0

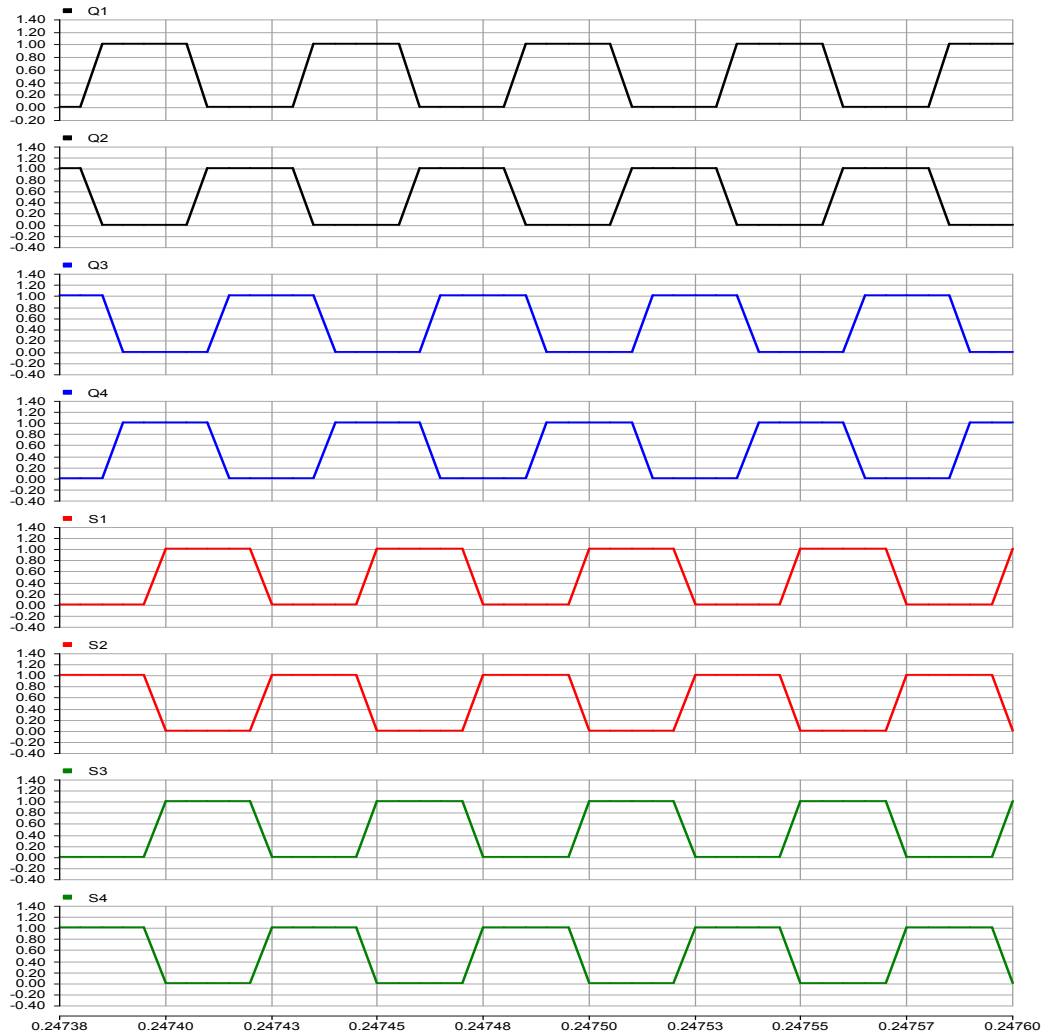

Figure 4.43. Triggering gate signals of EPS control method

When one period is divided into 6 parts and comparing with square pulses and triangular pulses, it can be obtained the below switching states (Xiaolong S. et. al., 2013) that is shown at Table 4.4.

Table 4.4. Switching States of EPS Control with 6 parts. (Xiaolong et. al., 2013)

t_1	t_2	t_3	t_4	t_5	t_6
D_2,Q_4 D_5,D_8	Q_2,D_4 S_1,S_4	Q_2,Q_3 D_6,D_7	D_1,Q_3 D_6,D_7	Q_1,D_3 S_2,S_3	Q_1,Q_4 D_5,D_8

4.3.2. Switching States for Buck-Boost Modes

The switching cycle can be broken into 8 main intervals and operation modes are explained below the Figure 4.44 that shows switching states of EPS control.

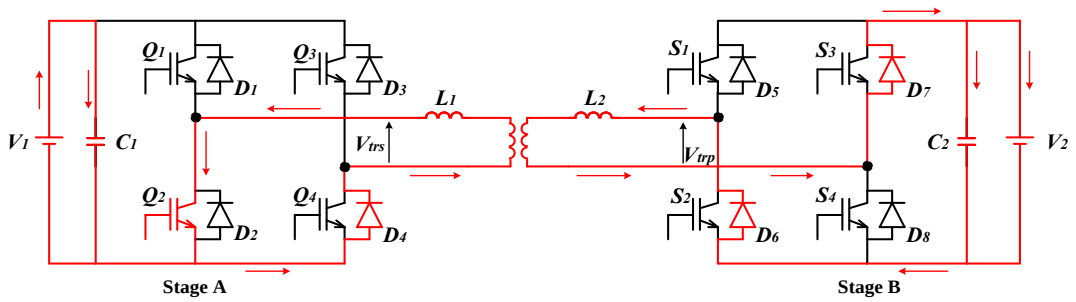

(a) Mode 1

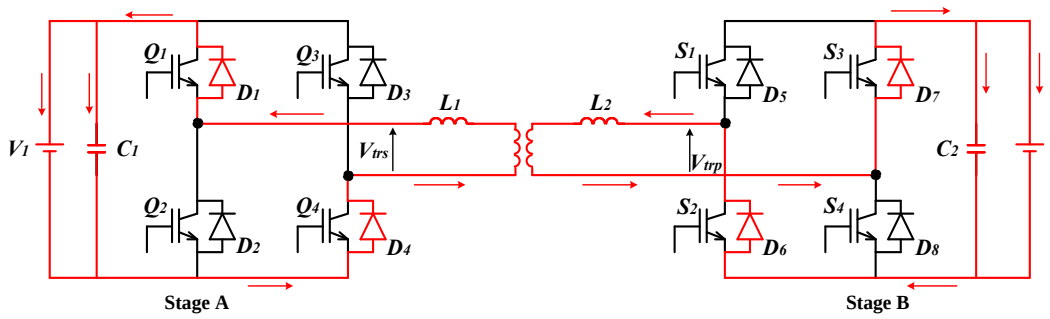

(b) Mode 2

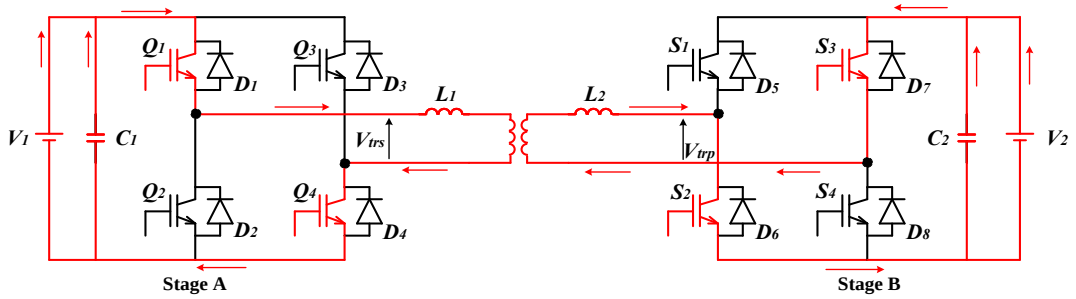

(c) Mode 3

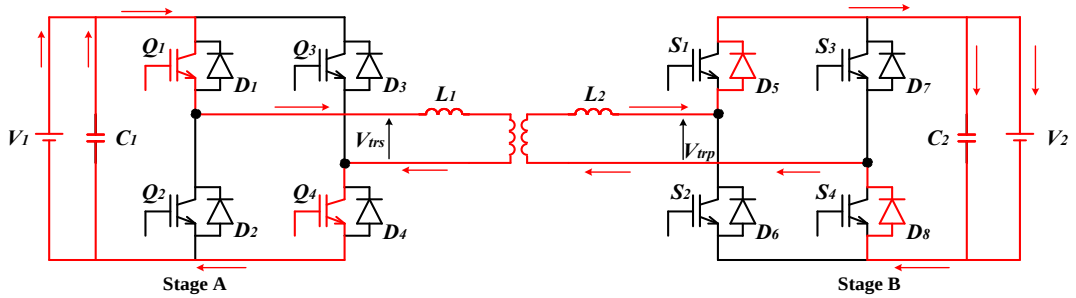

(d) Mode 4

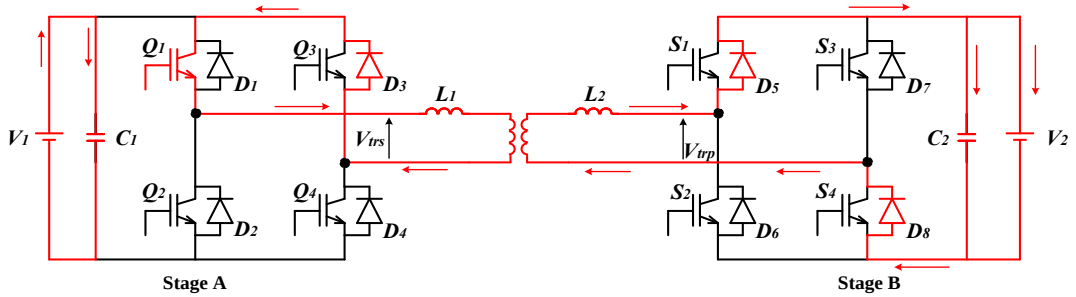

(e) Mode 5

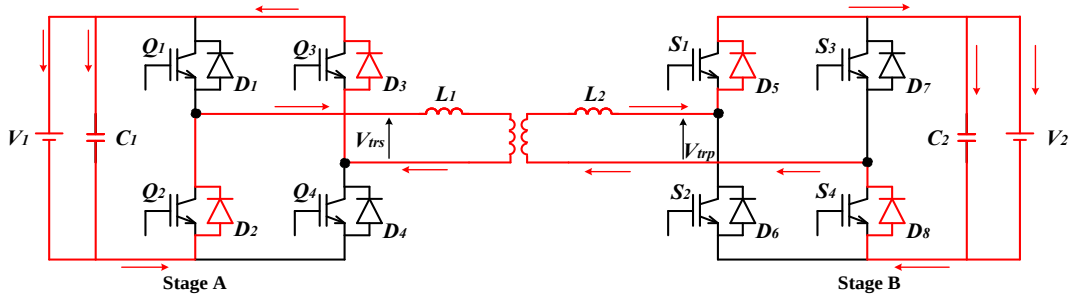

(f) Mode 6

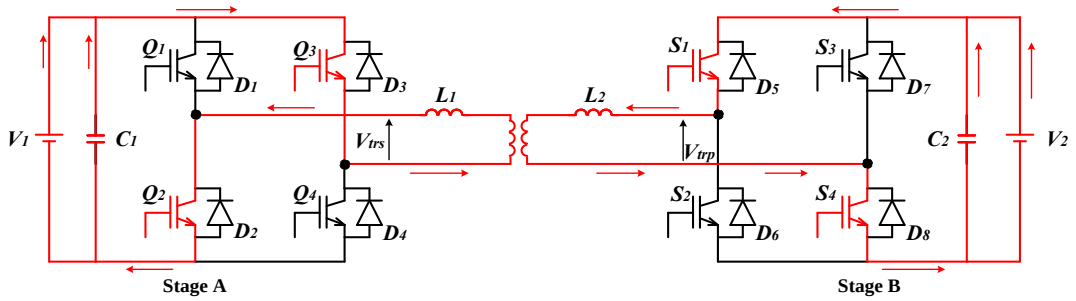

(g) Mode 7

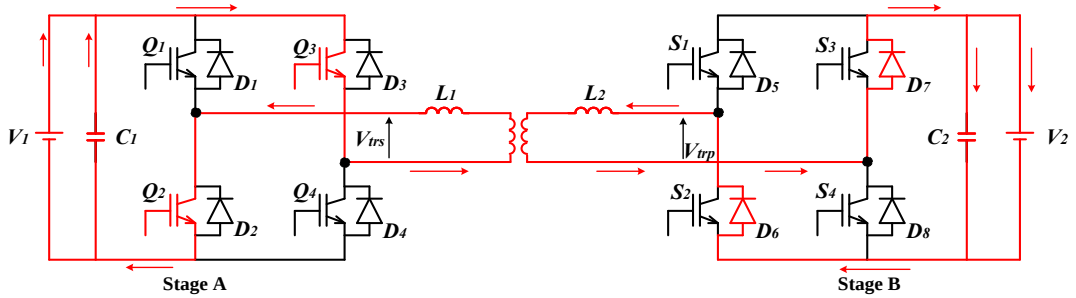

(h) Mode 8

Figure 4.44. EPS Switching States Current Diagrams for Buck-Boost Modes (Biao Z. et. al., 2012)

These operation modes are explained by benefiting from (Biao Z. et. al., 2012) and switching cycle can be divided into eight operation modes which are explained as follows based on power flow 1 (from Stage A to Stage B).

1) *Mode 1 (t_0 - t_1):* Figure 4.44(a) shows the equivalent circuit of mode 1. Just before t_0, Q_2 and Q_3 are conducting. The current i_L is in negative direction. At t_0, Q_3 is turned OFF and Q_4 is turned ON at zero current, and D_4 starts to conduct. On the secondary side (Stage B), the current is carried from L_1 to V_2 by D_6 and D_7. The voltage across L_1 is clamped at nV_2, and the current i_{L1} decreases linearly. This mode ends up when Q_2 is turned OFF. During this mode, the current of L_1 is

$$i_{L1}(t) = i_{L1}(t_0) + \frac{nV_2}{L_1}(t - t_0) \tag{4.1}$$

2) *Mode 2 (t_1 – t_1):* Figure 4.44(b) shows the equivalent circuit of mode 2. If current i_{L1} is still in negative direction at t_1 then at t_1, Q_2 is turned OFF and Q1 is turned ON

at zero current, i_{L1} is carried from L_1 to V_1 by D_6 and D_7. The voltage across L_1 is clamped at $V_1 + nV_2$ and i_{L1} decreases linearly. This mode ends up with i_{L1} decreasing to zero. During this mode i_{L1} is

$$i_{L1}(t) = i_{L1}(t_1) + \frac{V_1 + nV_2}{L_1}(t - t_1) \tag{4.2}$$

3) *Mode 3 ($t_1' - t_2$):* Figure 4.44(c) shows the equivalent circuit of mode 3. At t_1', the polarity of i_{L1} changes from negative to positive. And because the driving signals Q_1, Q_4, S_2 and S_3 are already on, so Q_1, Q_4, S_2 and S_3 start to conduct. The voltage across L_1 is clamped at $V_1 + nV_2$, and i_{L1} increases linearly. This mode ends up when S_2 and S_3 are turned OFF. During this mode, i_L is the same with (2).

4) *Mode 4 ($t_2 - t_3$):* Figure 4.44(d) shows the equivalent circuit of mode 4. At t_2, S_2 and S_3 are turned off and S_1 and S_4 are turned on at zero current. D_5 and D_8 start to conduct. The voltage across L_1 is clamped at $V_1 - nV_2$, and i_{L1} still increases linearly due to $V_1 \geq nV_2$. This mode ends up when Q_4 is turned OFF. During this mode i_{L1} is

$$i_{L1}(t) = i_{L1}(t_2) + \frac{V_1 - nV_2}{L_1}(t - t_2) \tag{4.3}$$

5) *Mode 5 ($t_3 - t_4$):* Figure 4.44(e) shows the equivalent circuit of mode 5. At t_3, Q_4 is turned OFF and Q_3 is turned ON at zero current, D_3 starts to conduct. On the secondary side, the current is carried from L_1 to V_2 by D_5 and D_8. The voltage across L_1 is clamped at $-nV_2$ and the current i_{L1} decreases linearly. This mode ends up when Q_1 is turned OFF. During this mode, the current of L_1 is

$$i_{L1}(t) = i_{L1}(t_3) + \frac{-nV_2}{L_1}(t - t_3) \tag{4.4}$$

6) ***Mode 6 ($t_4 - t_{4'}$):*** Figure 4.44(f) shows the equivalent circuit of mode 6. If current i_{L1} is still in positive direction at t_4, then at t_4, Q_2 is turned OFF and Q_1 is turned ON at zero current, i_{L1} is carried from L_1 to V_1 by D_2 and D_3. On the secondary side, the current is carried from L_1 to V_2 by D_5 and D_8. The voltage across L_1 is clamped at $-V_1 - nV_2$, and i_{L1} still decreases linearly. This mode ends up with i_{L1} decreasing to zero. During this mode i_{L1} is

$$i_{L1}(t) = i_{L1}(t_4) + \frac{-V_1 - nV_2}{L_1}(t - t_4) \tag{4.5}$$

7) ***Mode 7 ($t_{4'} - t_5$):*** Figure 4.44(g) shows the equivalent circuit of mode 7. At t_4', the polarity of i_{L1} changes from positive to negative. And, because the driving signals of Q_2, Q_3, S_1 and S_4 start to conduct. The voltage across L_1 is clamped at $-V_1 - nV_2$ and i_{L1} increases linearly. This mode ends up when S1 and S4 are turned OFF. During this mode, i_{L1} is the same with (5).

8) ***Mode 8 ($t_{4'} - t_5$):*** Figure 4.44(h) shows the equivalent circuit of mode 8. At t_5, S_1 and S_4, are turned OFF and S_2 and S_3 are turned ON at zero current. D_6 and D_7 start to conduct. The voltage across L_1 is clamped at $-V_1 + nV_2$ and i_{L1} still increases linearly due to $V_1 \geq nV_2$. This mode ends up when S_3 is turned OFF. During this mode, i_{L1} is

$$i_{L1}(t) = i_{L1}(t_5) + \frac{-V_1 + nV_2}{L_1}(t - t_5) \tag{4.6}$$

Above analysis are operated with sinusoidal square pulses. If analysis are operated with triangular signals, time intervals can be changed. But calculation of inductor current values do not change.

4.3.3. Simulation Cases and Results

Simulations are examined for the Table 4.5. Cases are changeable according to power flow way, buck-boost modes and parameters of circuit components.

Table 4.5. Cases of EPS Control Simulation; PF1: Power Flow 1, PF2: Power Flow 2

Converter / Parameters			V_1	V_2	C_1	C_2	L_1	L_2	n	f
PF1	**Buck**	**Case1**	200V	160V	56mF	144mF	18µH	12µH	1:1	20kHz
		Case2	300V	100V	56mF	144mF	18µH	12µH	1:1	10kHz
	Boost	**Case3**	100V	160V	56mF	144mF	18µH	12µH	1:1	20kHz
PF2	**Buck**	**Case4**	160V	200V	56mF	144mF	18µH	12µH	1:1	20kHz
	Boost	**Case5**	160V	100V	56mF	144mF	18µH	12µH	1:1	20kHz
		Case6	300V	100V	56mF	144mF	18µH	12µH	1:1	10kHz

Simulation Results of Case 1:

For this case study, the chosen parameters are;

V_1=200V, V_2=160V, C_1=56mF, C_2=144mF, L_1=18µH, L_2=12µH, n=1:1, f=20kHz

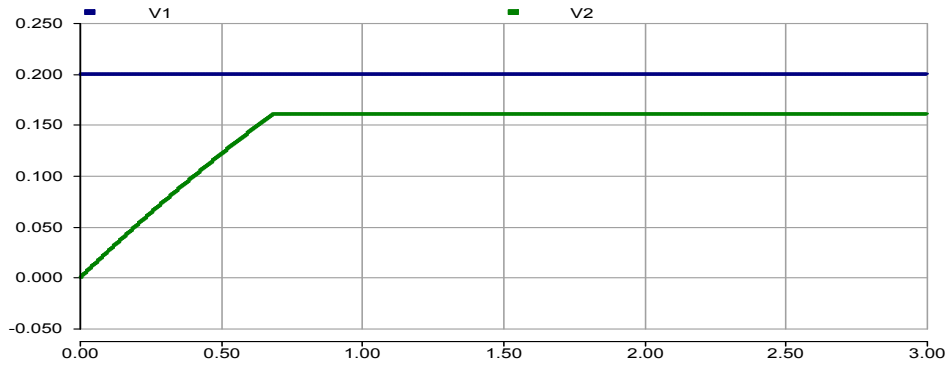

Figure 4.45. DC Link Voltages

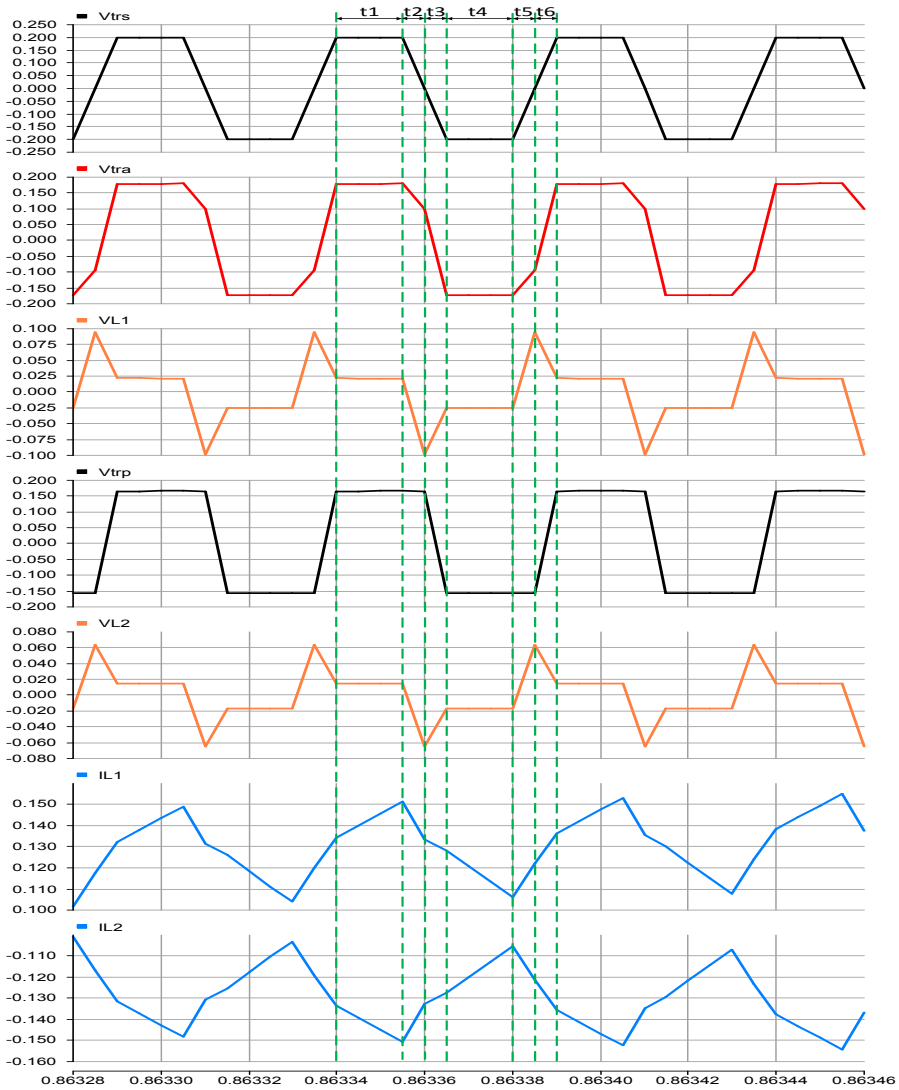

Figure 4.46. Voltage and Current Waveforms of Buck Mode at EPS Control

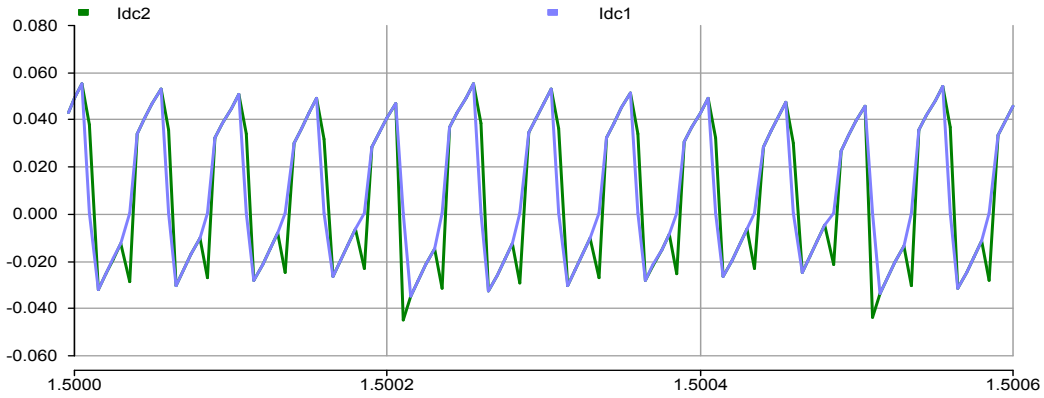

Figure 4.47. DC-Link Input and Output Currents

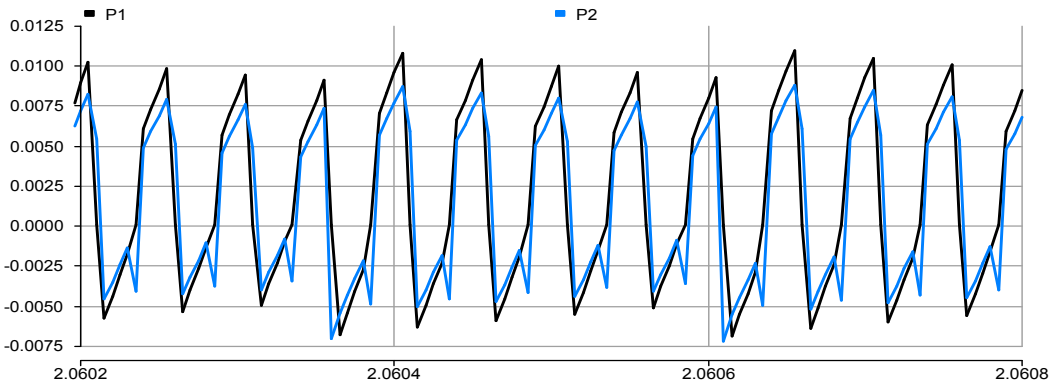

Figure 4.48. Input and Output Power Waveforms

Also, it is examined harmonics at primary side of the transformer and load side of the converter for this case.

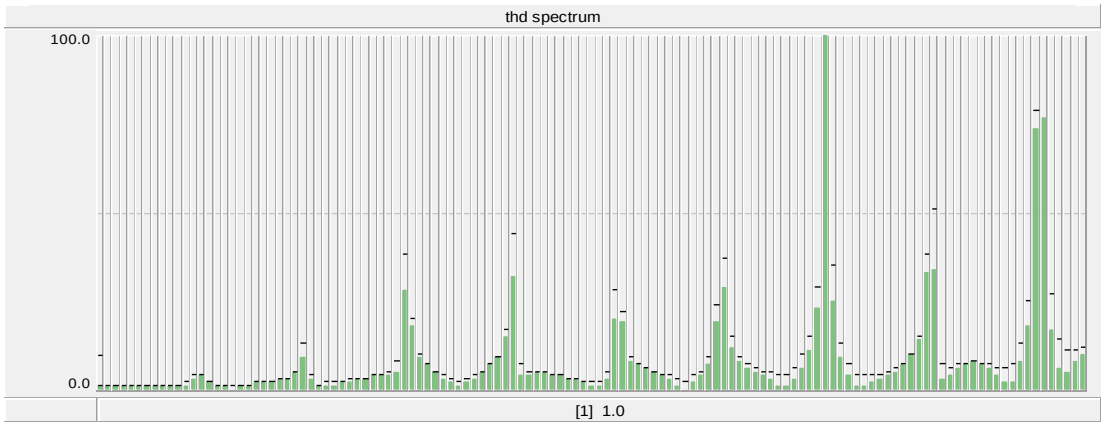

Figure 4.49. Harmonics Spectrum at Primary Side of Transformer

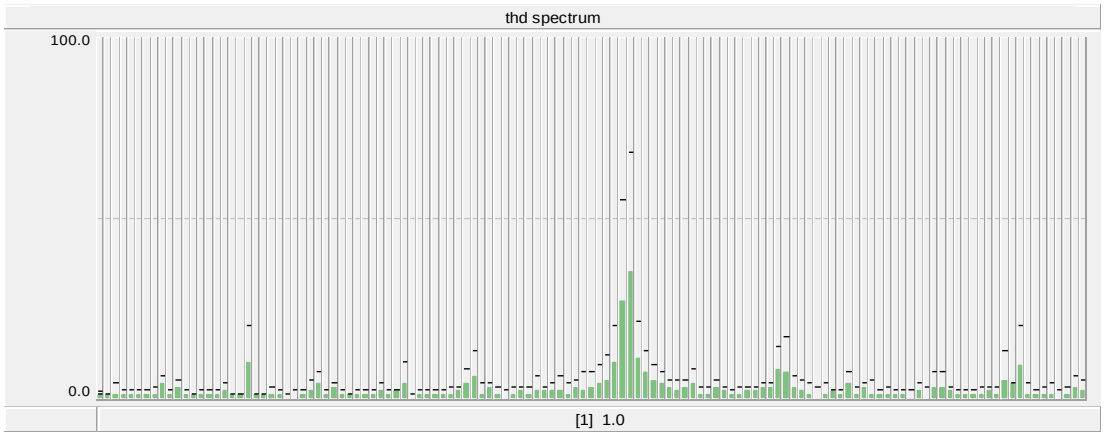

Figure 4.50. Harmonics Spectrum at Load Side

Simulation Results of Case 2:

V_1=300V, V_2=100V, C_1=56mF, C_2=144mF, L_1=18µH, L_2=12µH, n=1:1, f=10kHz

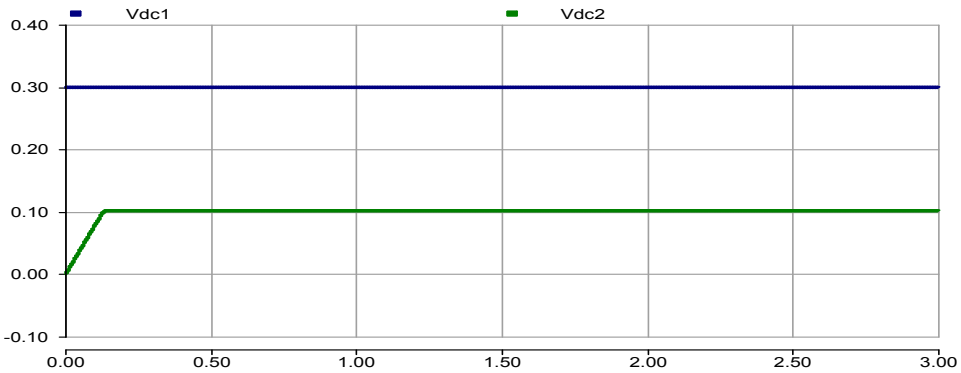

Figure 4.51. DC Link Voltages

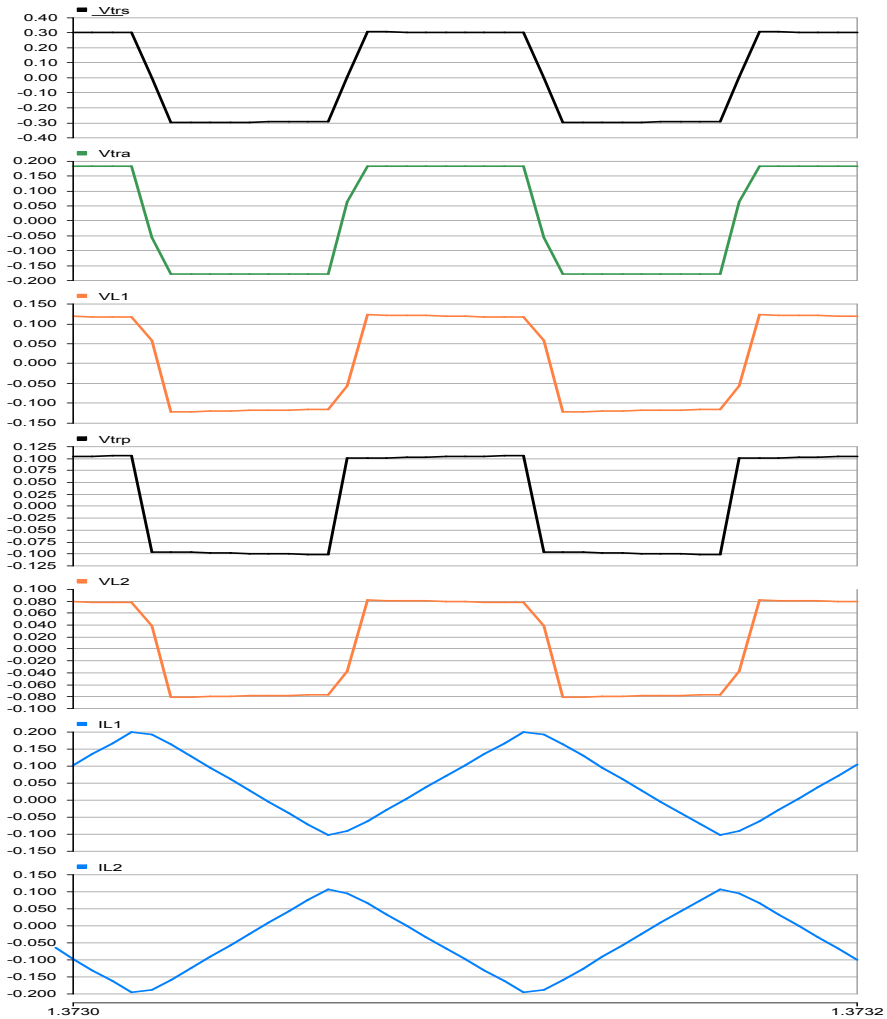

Figure 4.52. Voltage and Current Waveforms of Buck Mode at EPS Control

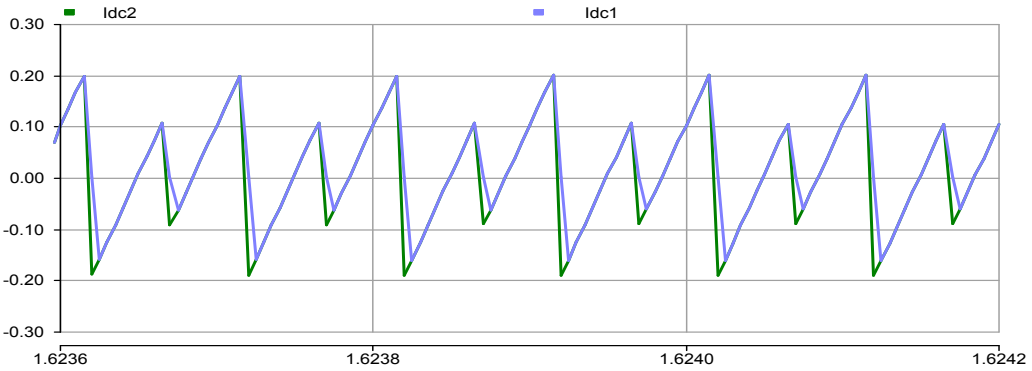

Figure 4.53. DC-Link Input and Output Currents

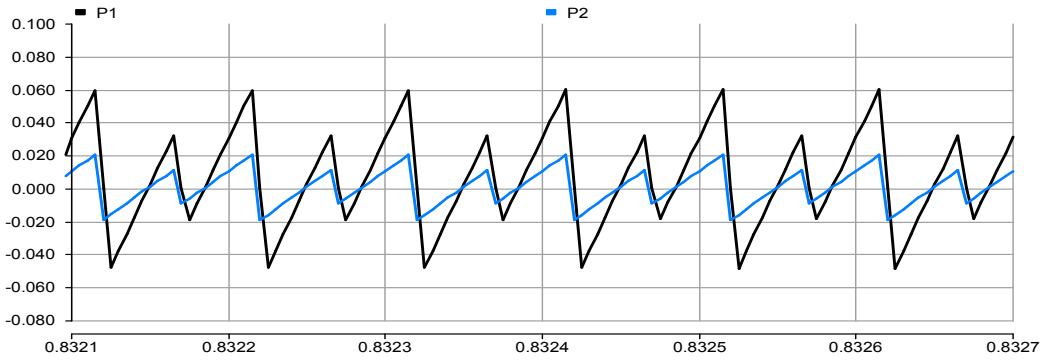

Figure 4.54. Input and Output Power Waveforms

Simulation Results of Case 3:

V_1=100V, V_2=160V, C_1=56mF, C_2=144mF, L_1=18µH, L_2=12µH, n=1:1, f=20kHz

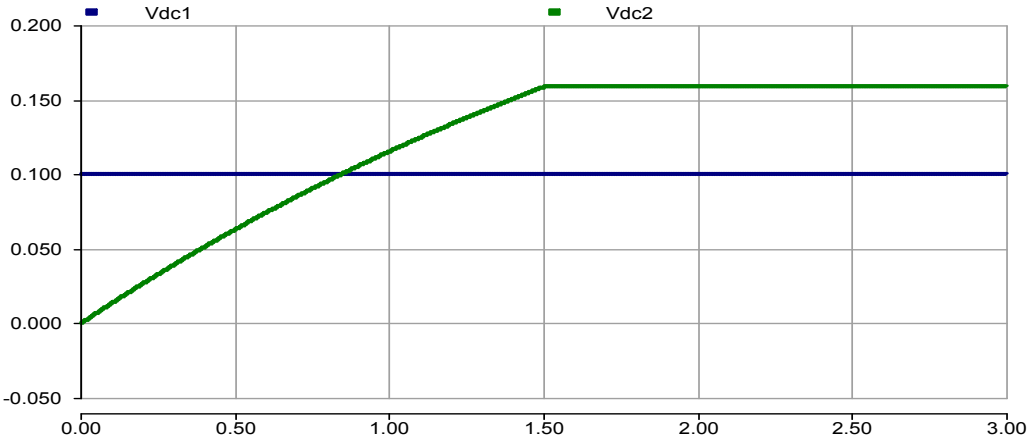

Figure 4.55. DC Link Voltages

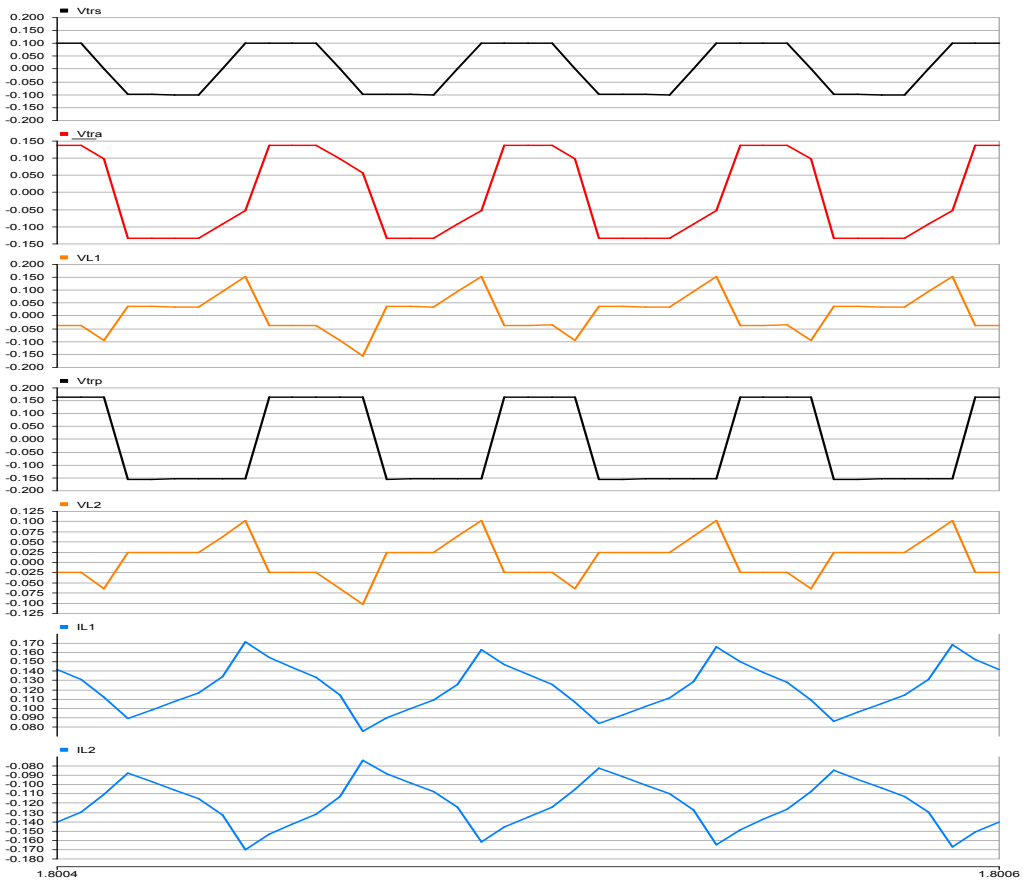

Figure 4.56. Voltage and Current Waveforms of Boost Mode at EPS Control

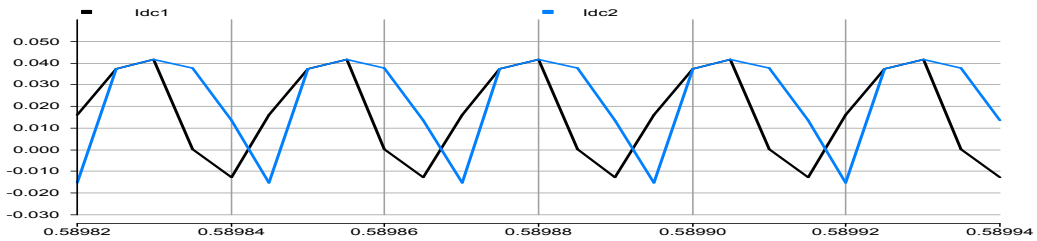

Figure 4.57. DC-Link Input and Output Currents

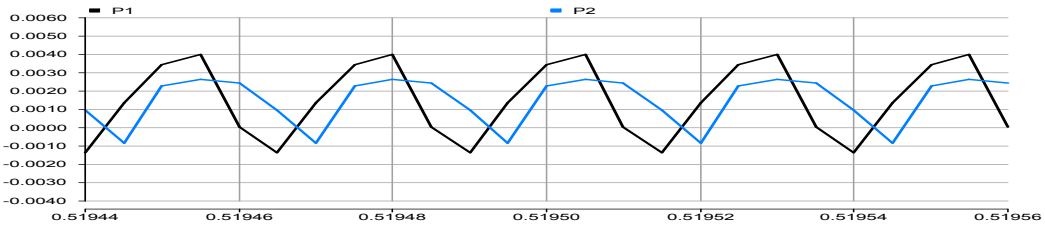

Figure 4.58. Input and Output Power Waveforms

Simulation Results of Case 4:

V_1=160V, V_2=200V, C_1=56mF, C_2=144mF, L_1=18µH, L_2=12µH, n=1:1, f=20kHz

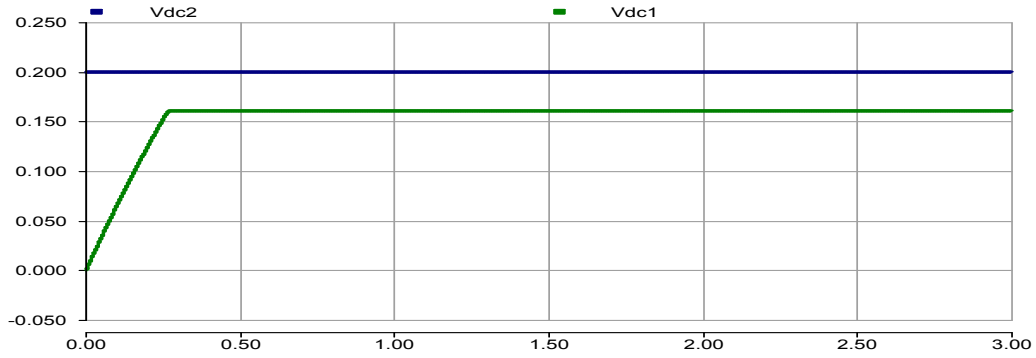

Figure 4.59. DC Link Voltages

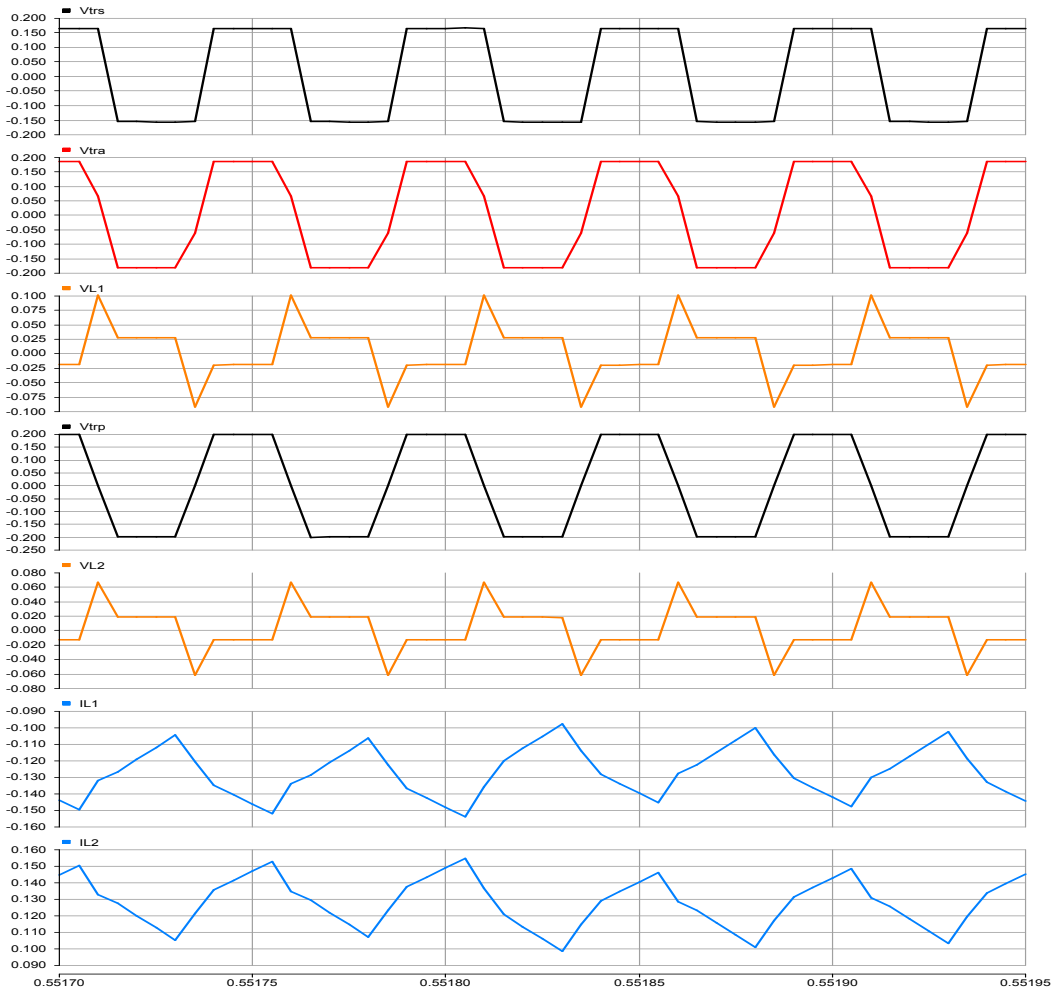

Figure 4.60. Voltage and Current Waveforms of Buck Mode at EPS Control

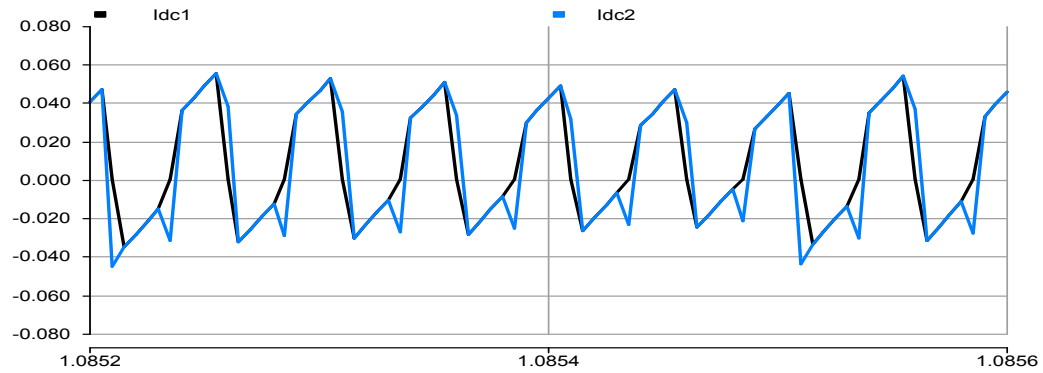

Figure 4.61. DC-Link Input and Output Currents

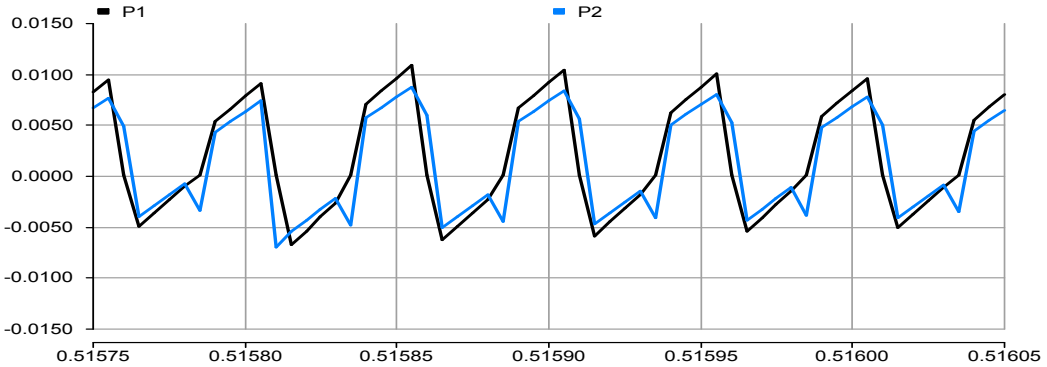

Figure 4.62. Input and Output Power Waveforms

Simulation Results of Case 5:

V_1=160V, V_2=100V, C_1=56mF, C_2=144mF, L_1=18µH, L_2=12µH, n=1:1, f=20kHz

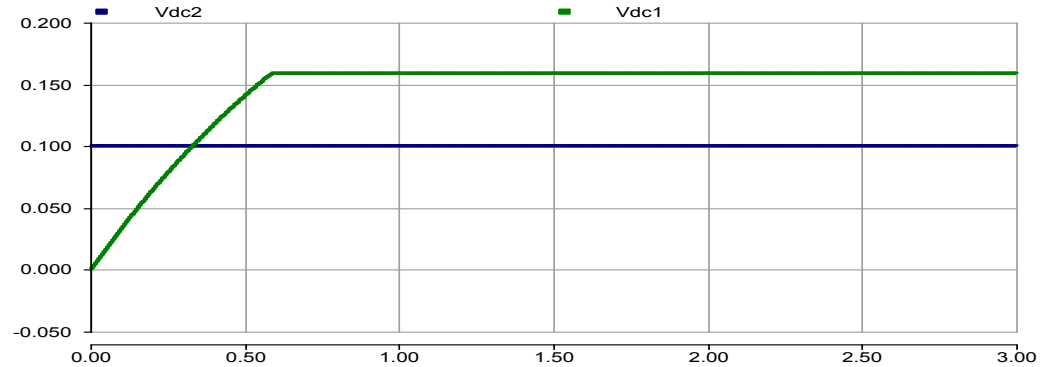

Figure 4.63. DC Link Voltages

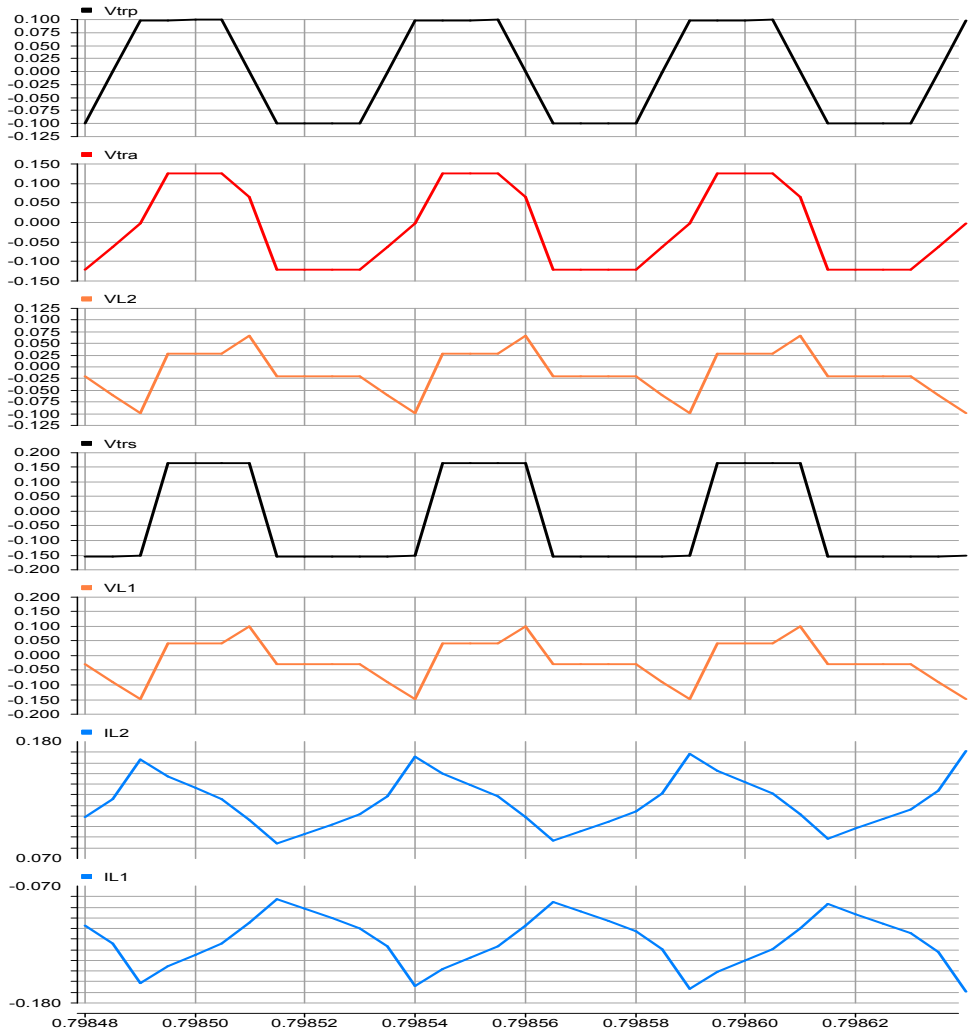

Figure 4.64. Voltage and Current Waveforms of Boost Mode at EPS Control

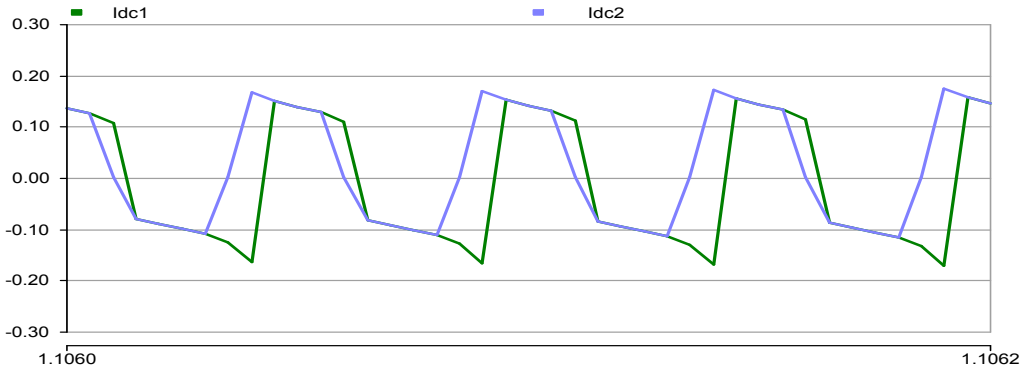

Figure 4.65. DC-Link Input and Output Currents

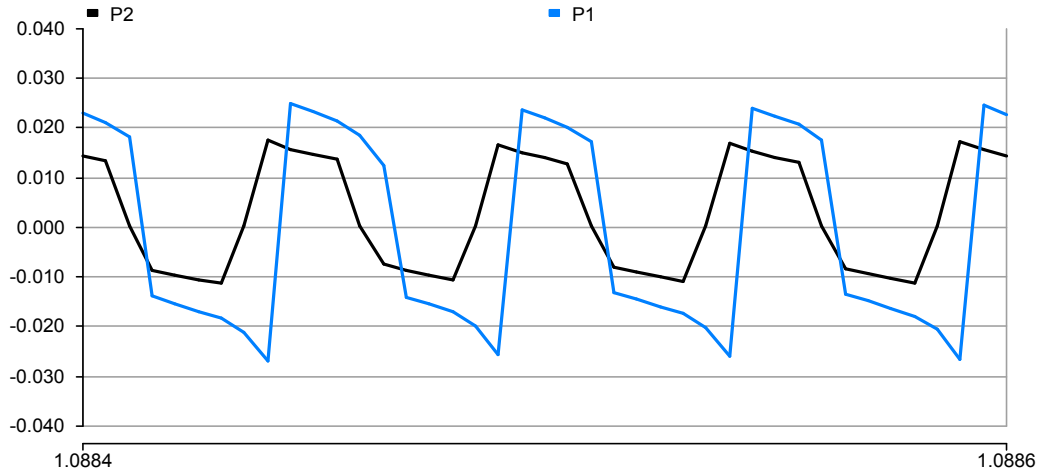

Figure 4.66. Input and Output Power Waveforms

Also, it is examined harmonics at primary side of the transformer and load side of the converter for this case.

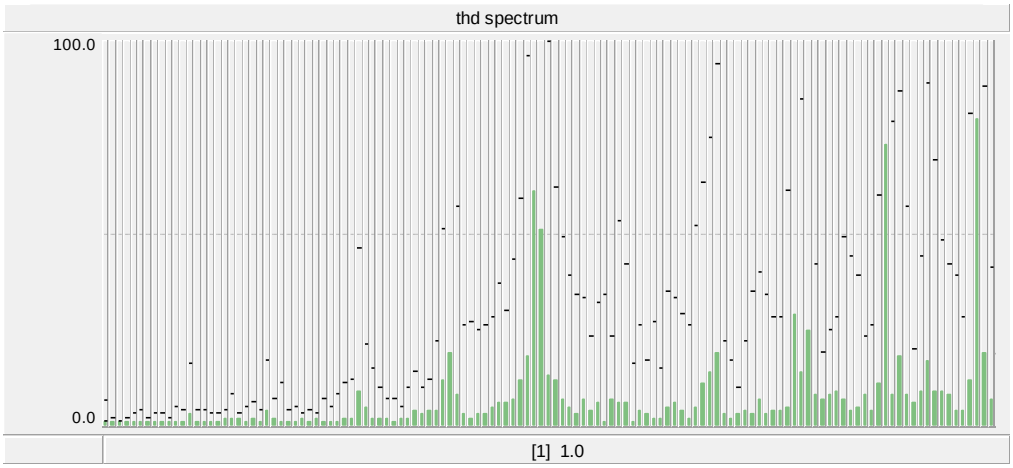

Figure 4.67. Harmonics Spectrum at Primary Side of Transformer

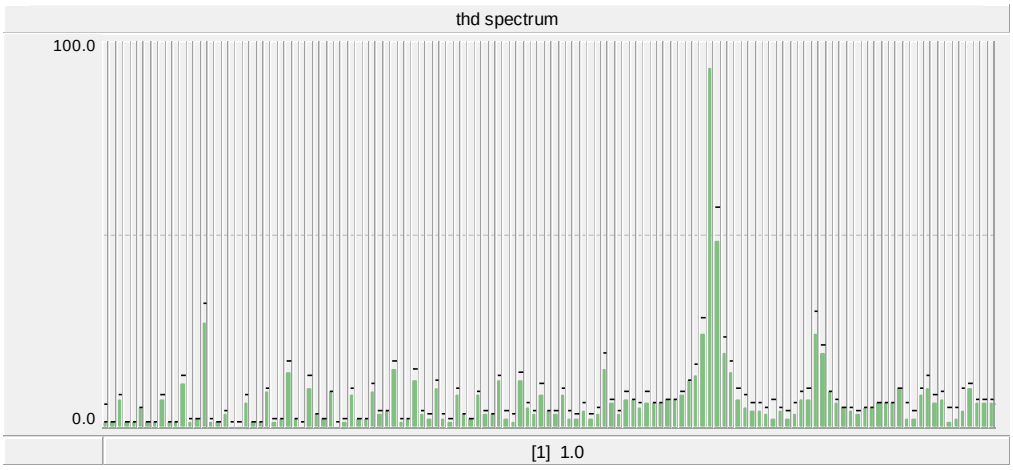

Figure 4.68. Harmonics Spectrum at Load Side

Simulation Results of Case 6:

V_1=300V, V_2=100V, C_1=56mF, C_2=144mF, L_1=18µH, L_2=12µH, n=1:1, f=10kHz

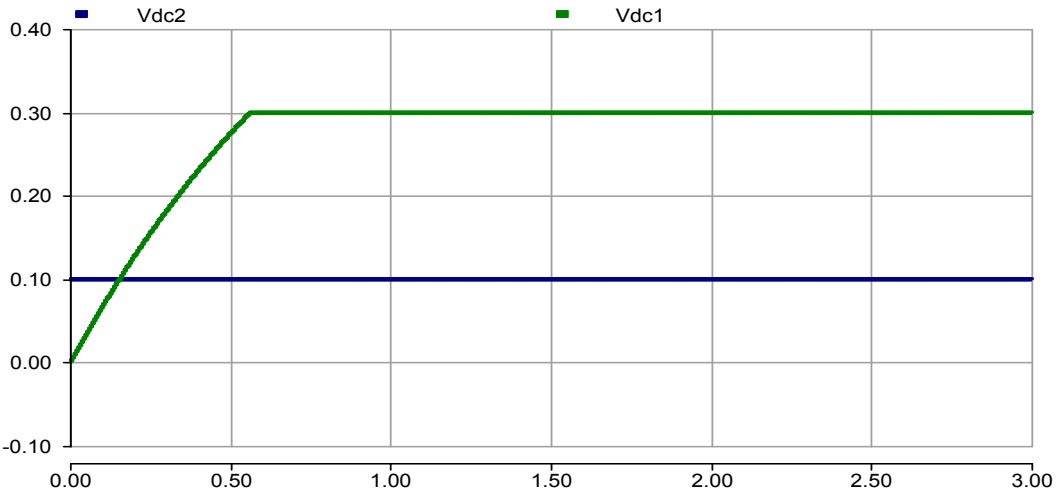

Figure 4.69. DC Link Voltages

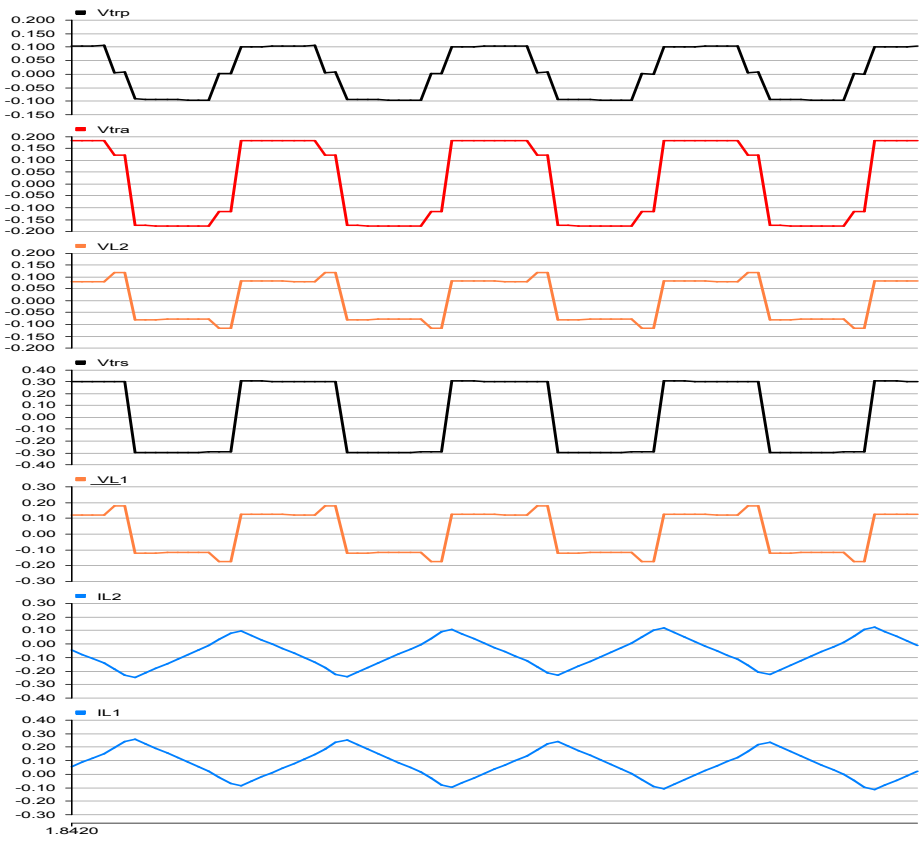

Figure 4.70. Voltage and Current Waveforms of Boost Mode at EPS Control

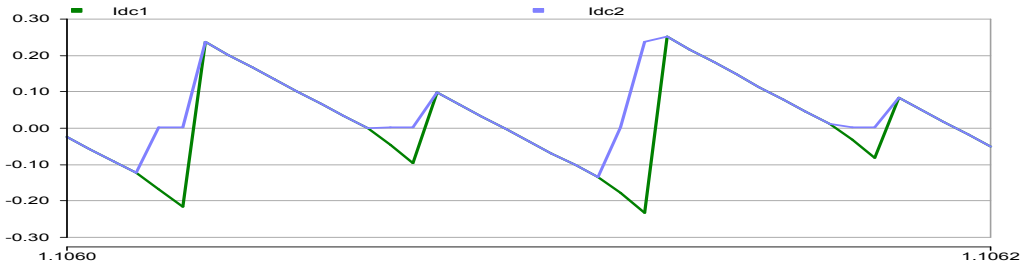

Figure 4.71. DC-Link Input and Output Currents

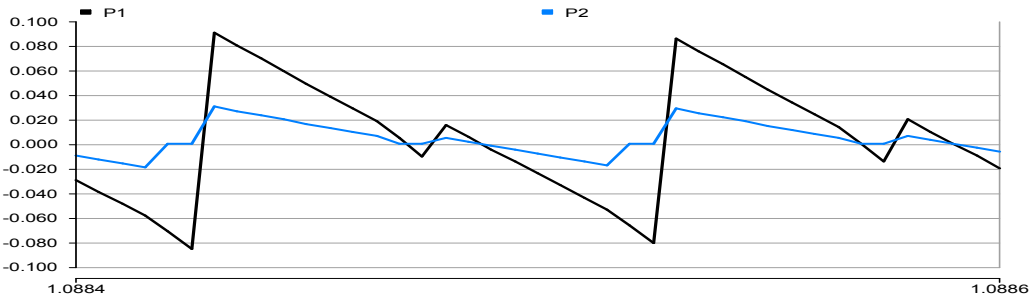

Figure 4.72. Input and Output Power Waveforms

4.3.4. Fortran Codes of EPS

```
#LOCAL REAL xVdc2_Err
#LOCAL REAL xP_dcdc
#LOCAL REAL xI_dcdc
#LOCAL REAL xRefdcdc

#LOCAL INTEGER xQ1
#LOCAL INTEGER xQ2
#LOCAL INTEGER xQ3
#LOCAL INTEGER xQ4
#LOCAL INTEGER xS1
#LOCAL INTEGER xS2

#LOCAL REAL xyA
#LOCAL REAL xyB
#LOCAL REAL xyC
#LOCAL REAL xyphaseshift
#LOCAL REAL xfreq

! !!!!!!!!!!!!!!! INPUTS !!!!!!!!!!!!!!!
xVdc2ref=$i1l
xVdc2=$i2l
xKp_dcdc=$i3l
xKi_dcdc=$i4l
xLimP_dcdc=$i5l
xLimN_dcdc=$i6l
xTs=$i7l
xTime=$i8l
xfreq=$i9l
xRefA=$i10l
xRefB=$i11l

! !!! Taking Datas from Memory !!!!!!!

xI_dcdc = STORF(NSTORF)

xVdc2_Err = xVdc2ref - xVdc2Fil
xP_dcdc = xKp_dcdc * xVdc2_Err
xI_dcdc = xI_dcdc + xKi_dcdc * xTs * xVdc2_Err
xRefdcdc = xP_dcdc + xI_dcdc


IF (xRefdcdc > xLimP_dcdc) THEN
      xRefdcdc = xLimP_dcdc
ENDIF

IF (xRefdcdc < xLimN_dcdc) THEN
      xRefdcdc = xLimN_dcdc
ENDIF

xyA=COS(6.28318530717958647692528676655 9*xTime*xfreq)
IF (xyA>=0) THEN
xQ1=1
xQ2=0
ELSE
xQ1=0
xQ2=1
ENDIF

xyC=COS(6.28318530717958647692528676655 9*xTime*xfreq + xRefA)
IF (xyC>=0) THEN
xQ3=0
xQ4=1
ELSE
xQ3=1
xQ4=0
ENDIF
```

```
xyB=COS(6.28318530717958647692528676655 9*xTime*xfreq - xRefdcdc )
IF (xyB>=0) THEN
xS1=1
xS2=0
ELSE
xS1=0
xS2=1
ENDIF

! !!!!!!!! Saving Datas !!!!!!!!!!!!!!!!!
STORF(NSTORF) = xI_dcdc

! !!!!!!!! OUTPUT !!!!!!!!!!!!!!!!!!!!!!!!!!!!!!!!!
$o1r= xQ1
$o2r= xQ2
$o3r= xQ3
$o4r= xQ4
$o5r= xRefdcdc
$o6r= xS1
$o7r= xS2

NSTORF = NSTORF+1
```

4.4. Dual Phase Shift (DPS) Control

DPS control method is rarely used at isolated bidirectional dc-dc converter applications. This method has different types and these types are presented as some novel controls in the literature. (Bai et. al., 2008), (Zhao et. al., 2012), (Zhao et. al., 2013) are used DPS control method.

(Bai et. al., 2008) used novel DPS control for eliminating reactive power and increasing system efficiency. (Zhao et. al., 2012) studied power characterization of DPS experimentally and lastly (Zhao et. al., 2013) includes current stress optimized switching strategy with mathematical equations experimentally. Consequently, all of these studies emphasize DPS control is more effective than traditional (conventional) phase shift control.

In DPS control method, four different phase shift angles are produced for switching strategy. In other words, groups of (Q_1-Q_2), (Q_3-Q_4), (S_1-S_2), (S_3-S_4) have different phase shift angles. PI parameters are same with extended and single phase shift controls. In this way, IGBTs are triggered with 1 or 0. Triggering signals are showed at part 4.4.1. and switching states (direction of current against minor time intervals) are demonstrated at part 4.4.2. Then simulation cases and Fortran codes of DPS are presented at part 4.4.3. and 4.4.4. respectively. Moreover, EPS simulation and its control block diagram are shown at Figure 4.73. and Figure 4.74 respectively.

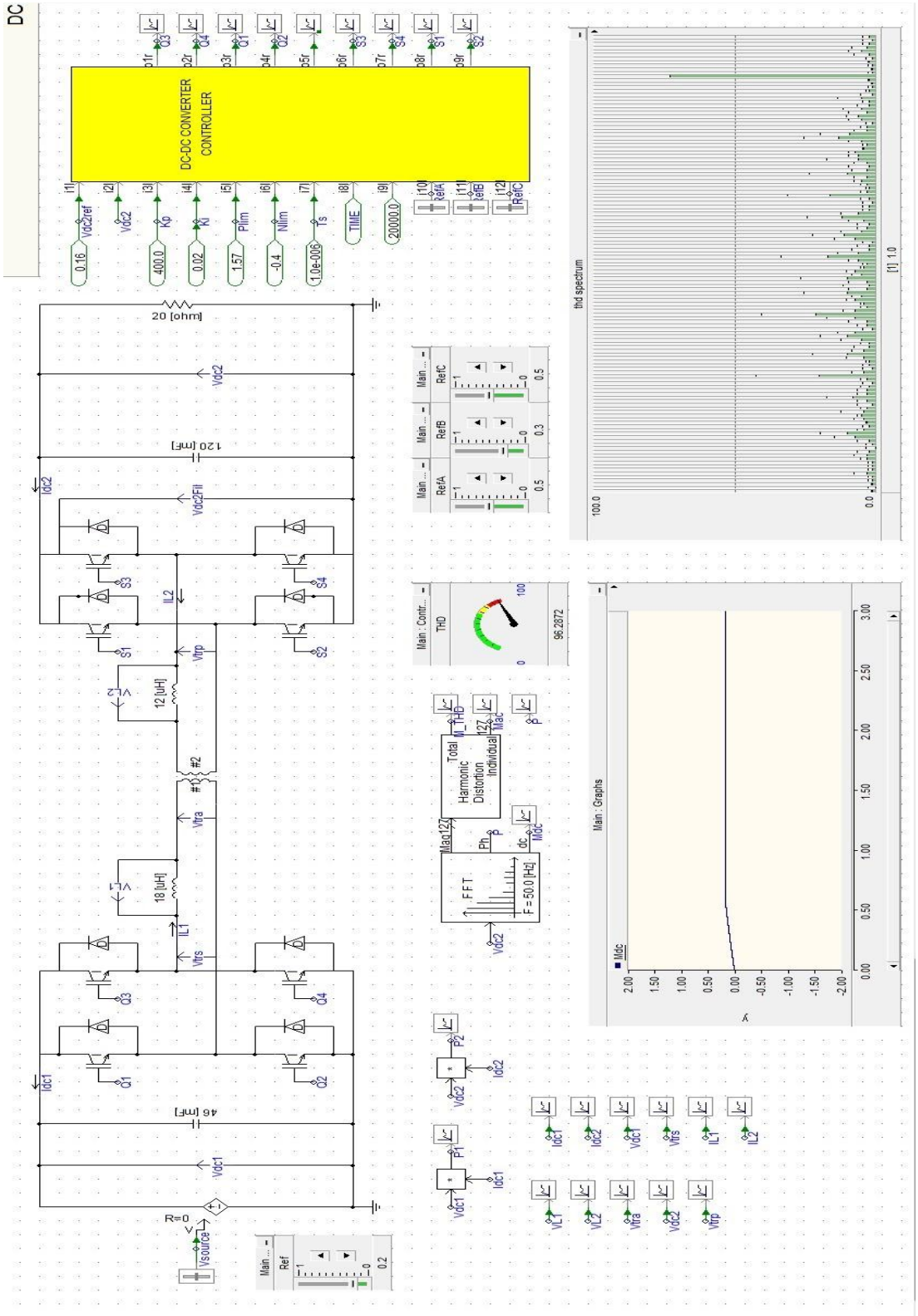

Figure 4.73. PSCAD Simulation of DPS Control

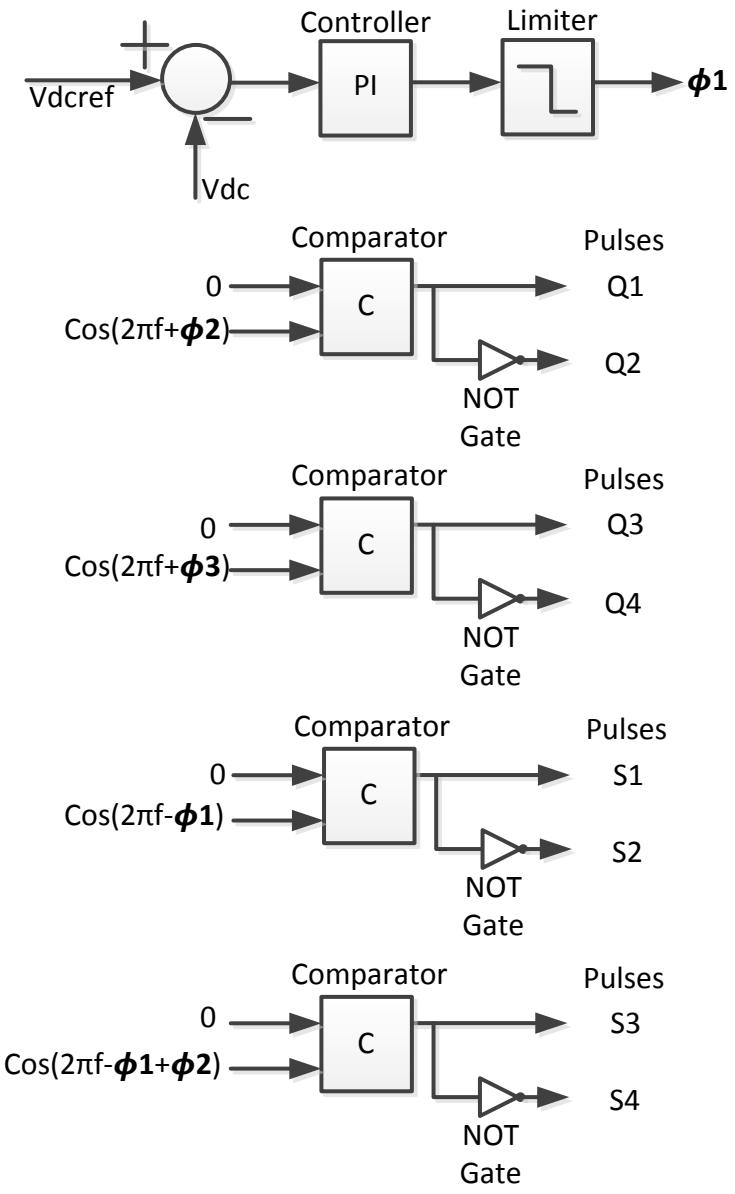

Figure 4.74. DPS Control Block Diagram

4.4.1. Triggering Signals

In DPS control method, IGBTs triggering signals can be showed at Table 4.6 and Figure 4.75.

Table 4.6. Triggering Signals of IGBTs at DPS Control

Stage A				**Stage B**			
Q_1	Q_2	Q_3	Q_4	S_1	S_2	S_3	S_4
1	0	1	0	1	0	1	0

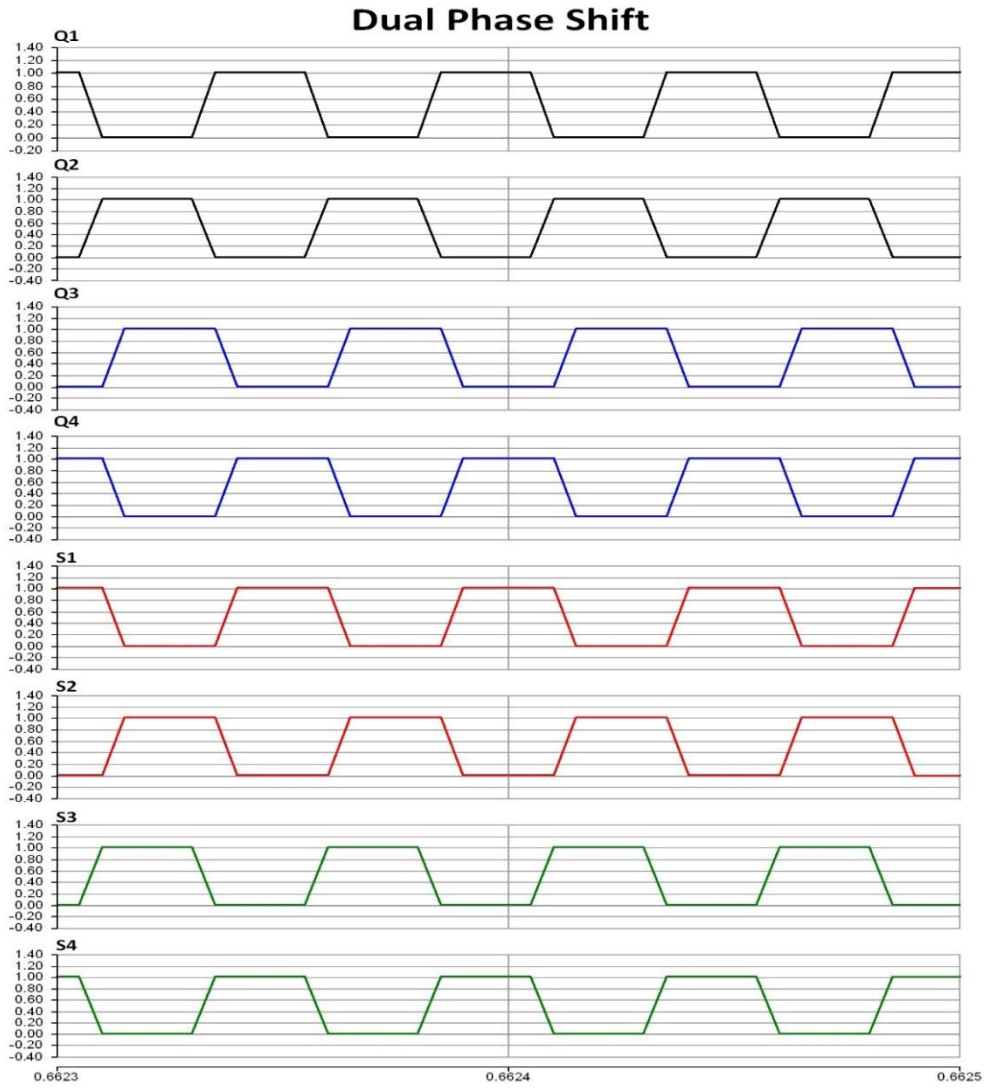

Figure 4.75. Triggering gate signals of DPS control method

4.4.2. Switching States for Buck-Boost Modes

In DPS control, the switching state issue is studied only in (Bai et. al., 2008) with soft switching strategy. Therefore, switching states are divided into 8 parts and

each part are explained by ZCS/ZVS are ON or OFF conditions. These time intervals are presented below without showing current flow in the converter circuit.

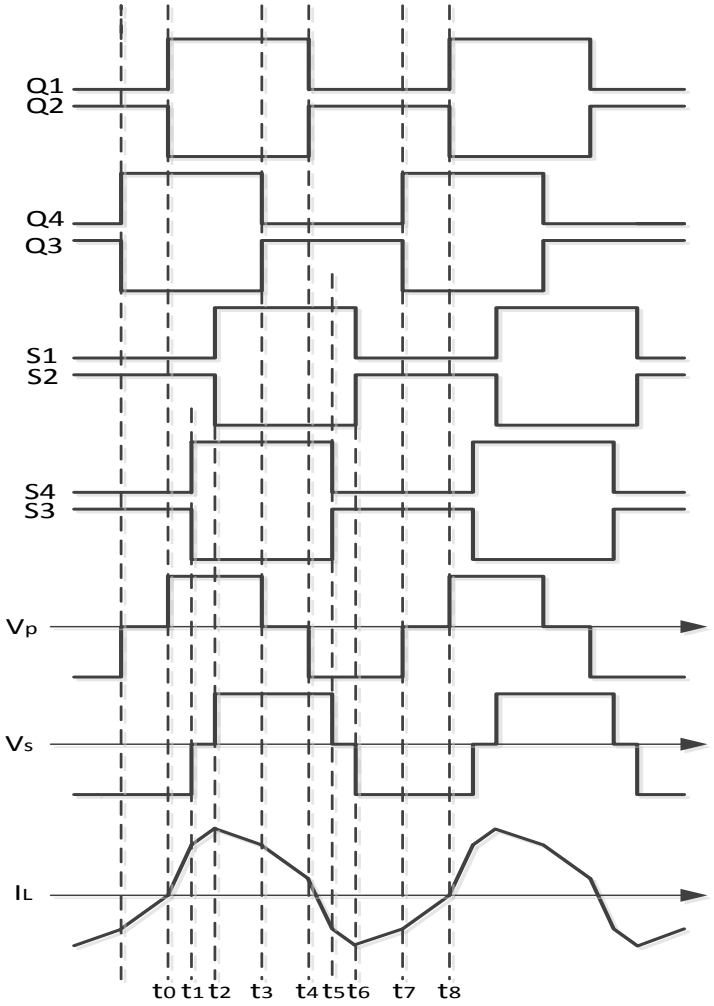

Figure 4.76. Voltage and current waveforms of DPS control (Bai et. al., 2008)

Figure 4.76. demonstrates time intervals for DPS control method and these time intervals are customized at 4.4.3. part, (Figure 4.78.)

These time intervals are represented ON-OFF conditions of switches and arrangement of hard and soft switchings.

1) $t = t_0$:

Q_1 turns ON and Q_2 turns OFF. Q_2 is hard switched OFF while Q_1 is switched ON at zero current (ZCS ON) since current flows through the anti-paralleled diode, not in Q_1.

2) t = t_1 :

S_4 turn ON and S_3 turn OFF. S_3 is hard switched OFF while S_4 is ZCS ON.

3) t = t_2 :

S_1 turn ON and S_2 turn OFF. S_2 is hard switched OFF while S_1 is ZCS ON.

4) t = t_3 :

Q_3 turn ON and Q_4 turn OFF. Q_4 is hard switched OFF while Q_3 is ZCS ON.

5) t = t_4 :

Q_2 turn ON and Q_1 turn OFF. Q_1 is hard switched OFF while Q_2 is ZCS ON.

6) t = t_5 :

S_3 turn ON and S_4 turn OFF. S_4 is hard switched OFF while S_3 is ZCS ON.

7) t = t_6 :

S_3 turn ON and S_4 turn OFF. S_4 is hard switched OFF while S_3 is ZCS ON.

8) t = t_7 :

Q_4 turn ON and Q_3 turn OFF. Q_3 is hard switched OFF while Q_4 is ZCS ON.

Therefore, all the turn-off actions are hard switching, while all the turn-on actions are ZCS.

4.4.3. Simulation Cases and Results

Simulations are carried out for the Table 4.7. Cases are changeable according to power flow way, buck-boost modes and parameters of circuit components.

Table 4.7. Cases of DPS Control Simulation; PF1: Power Flow1, PF2: Power Flow2

Converter Parameters			V_1	V_2	C_1	C_2	L_1	L_2	n	f
PF1	**Buck**	**Case1**	200V	160V	46mF	120mF	18µH	12µH	1:1	20kHz
		Case2	300V	100V	46mF	120mF	18µH	12µH	1:1	10kHz
	Boost	**Case3**	100V	160V	46mF	120mF	18µH	12µH	1:1	20kHz

PF2	**Buck**	**Case4**	160V	200V	46mF	120mF	18µH	12µH	1:1	20kHz
	Boost	**Case5**	160V	100V	46mF	120mF	18µH	12µH	1:1	20kHz
		Case6	300V	100V	46mF	120mF	18µH	12µH	1:1	10kHz

Simulation Results of Case 1:

V_1=200V, V_2=160V, C_1=46mF, C_2=120mF, L_1=18µH, L_2=12µH, n=1:1, f=20kHz

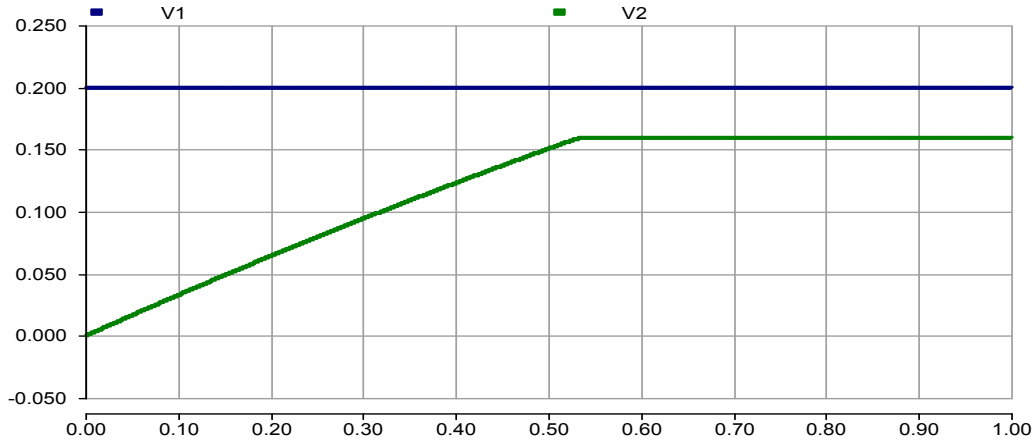

Figure 4.77. DC Link Voltages

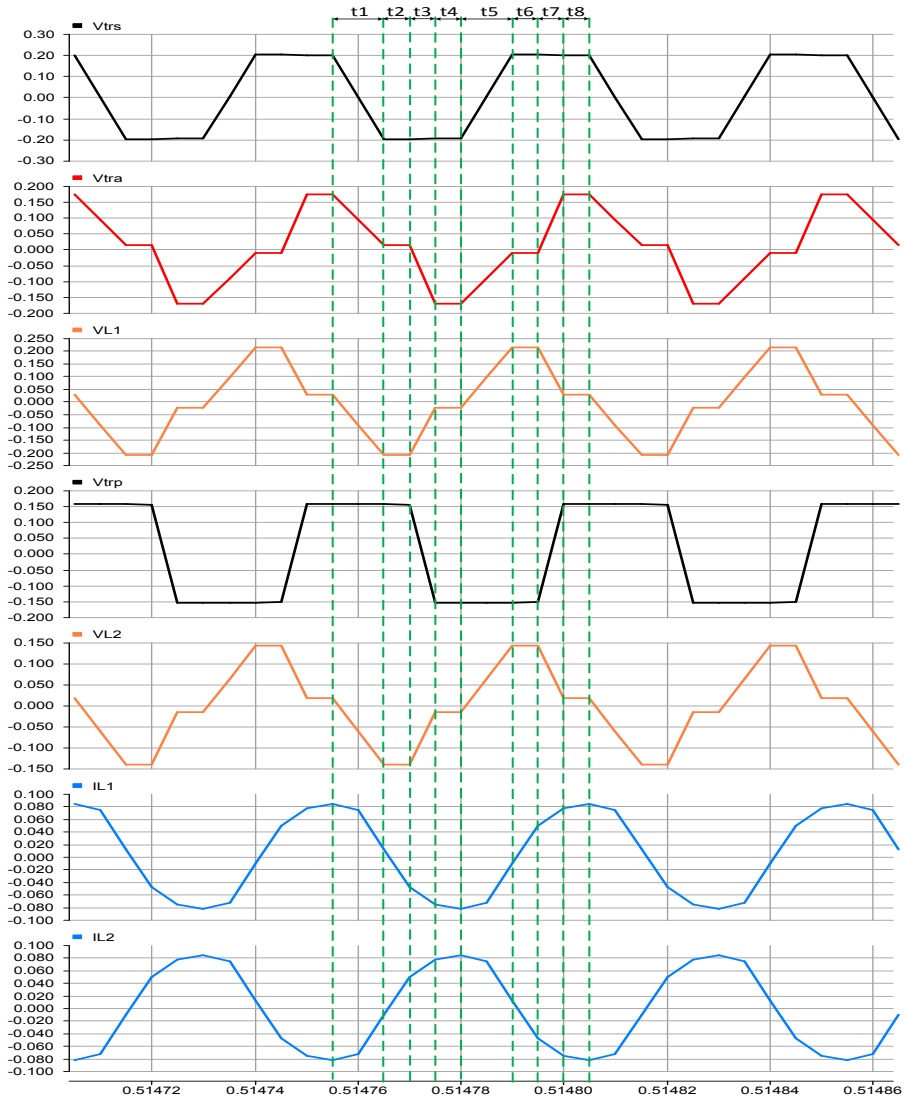

Figure 4.78. Voltage and Current Waveforms of Buck Mode at DPS Control

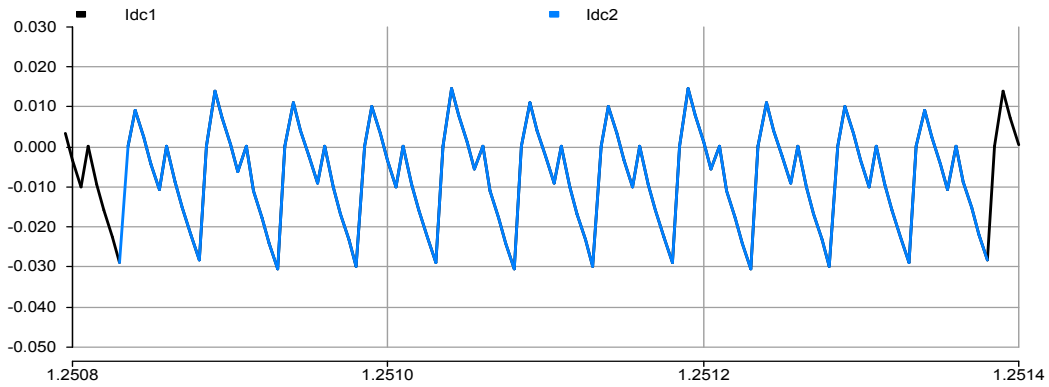

Figure 4.79. DC-Link Input and Output Currents

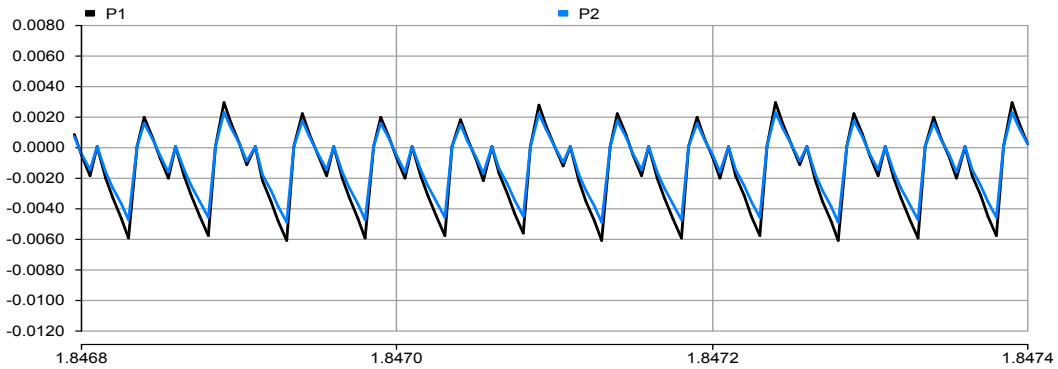

Figure 4.80. Input and Output Power Waveforms

Also, it is examined harmonics at primary side of the transformer and load side of the converter for this case.

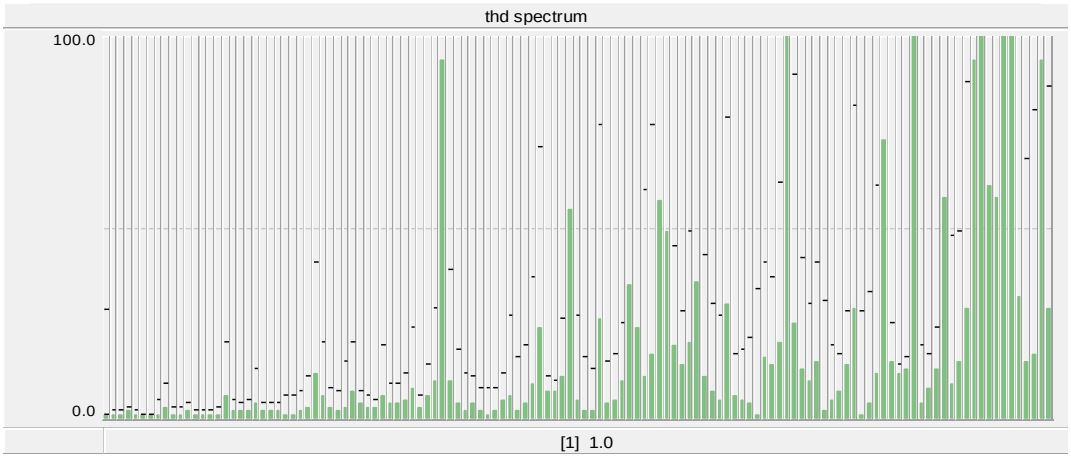

Figure 4.81. Harmonics Spectrum at Primary Side of Transformer

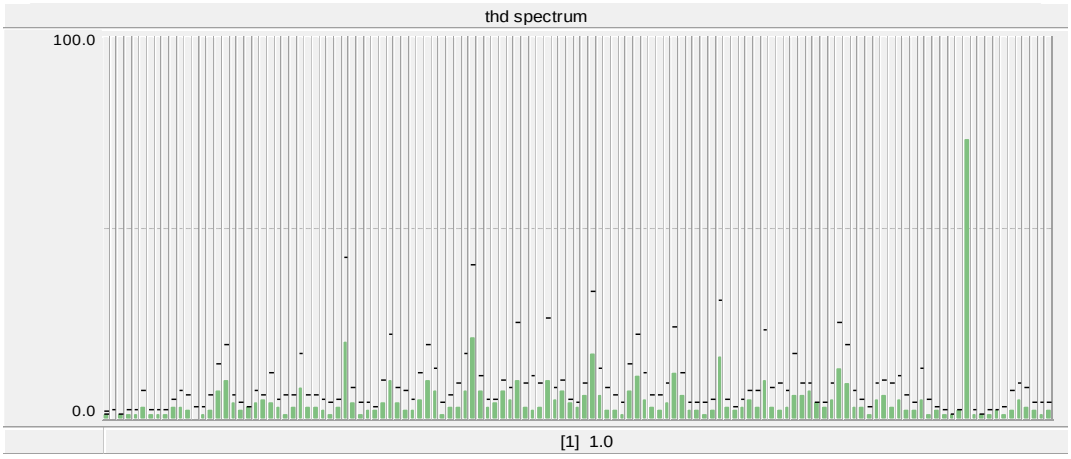

Figure 4.82. Harmonics Spectrum at Load Side

Simulation Results of Case 2:

V_1=200V, V_2=160V, C_1=46mF, C_2=120mF, L_1=18µH, L_2=12µH, n=1:1, f=10kHz

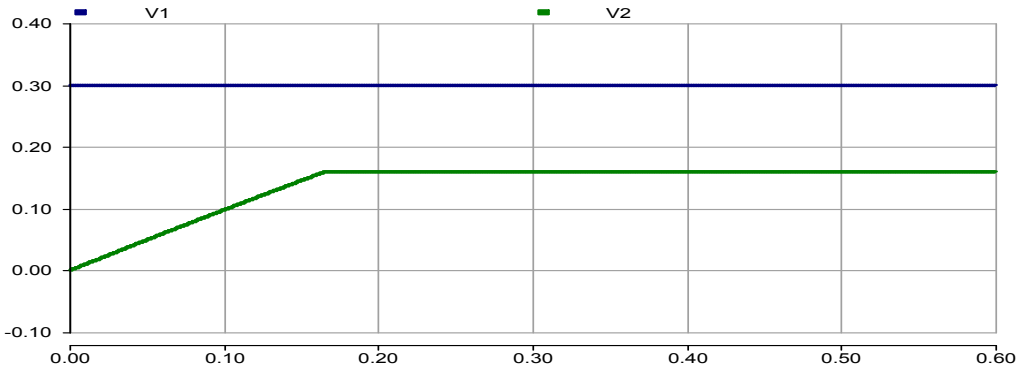

Figure 4.83. DC Link Voltages

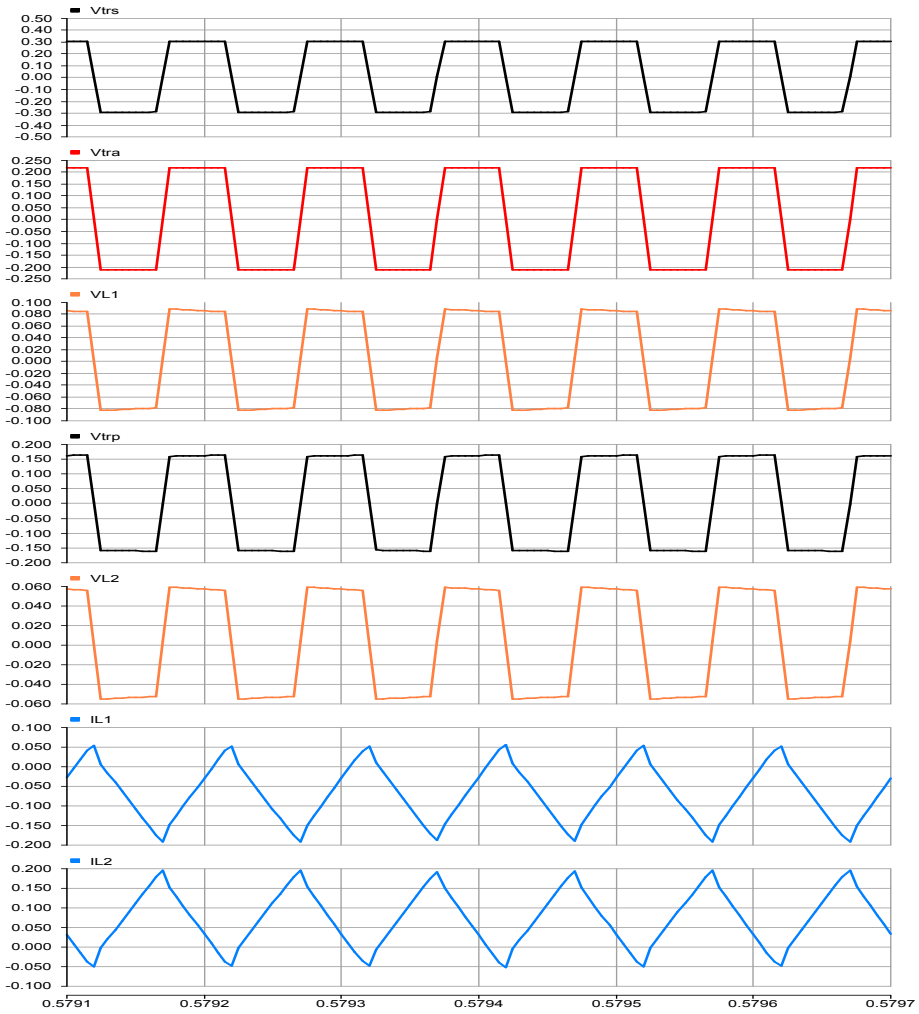

Figure 4.84. Voltage and Current Waveforms of Buck Mode at DPS Control

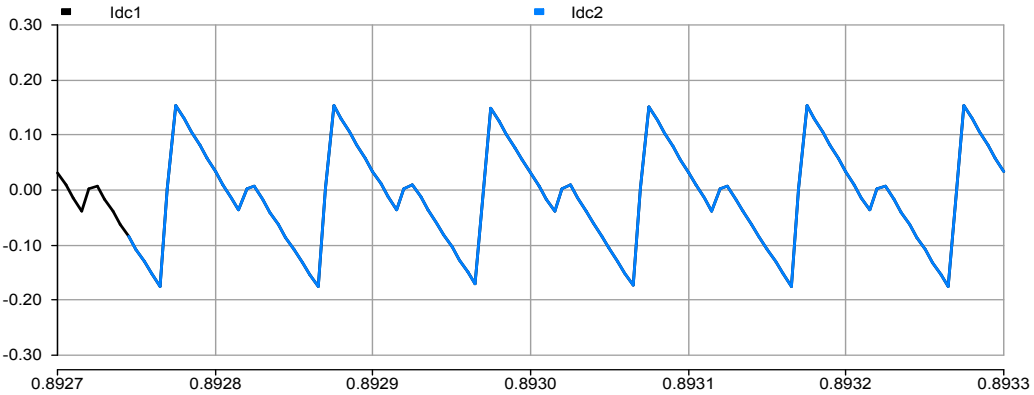

Figure 4.85. DC-Link Input and Output Currents

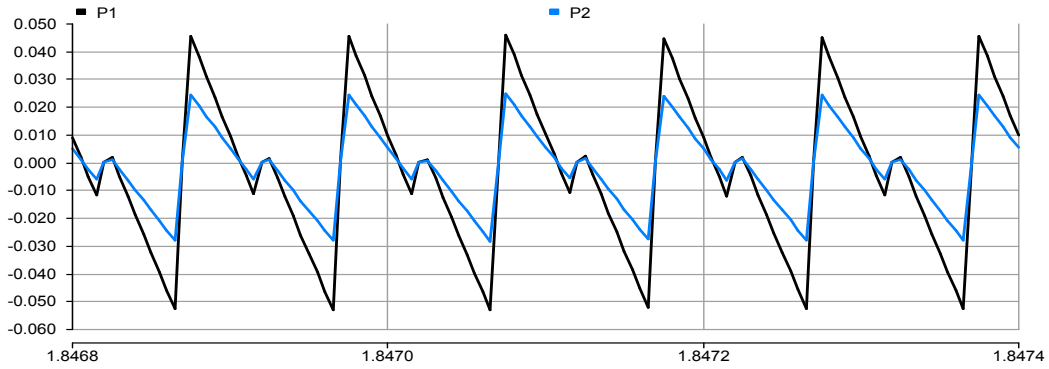

Figure 4.86. Input and Output Power Waveforms

Simulation Results of Case 3:

V_1=100V, V_2=160V, C_1=46mF, C_2=120mF, L_1=18µH, L_2=12µH, n=1:1, f=20kHz

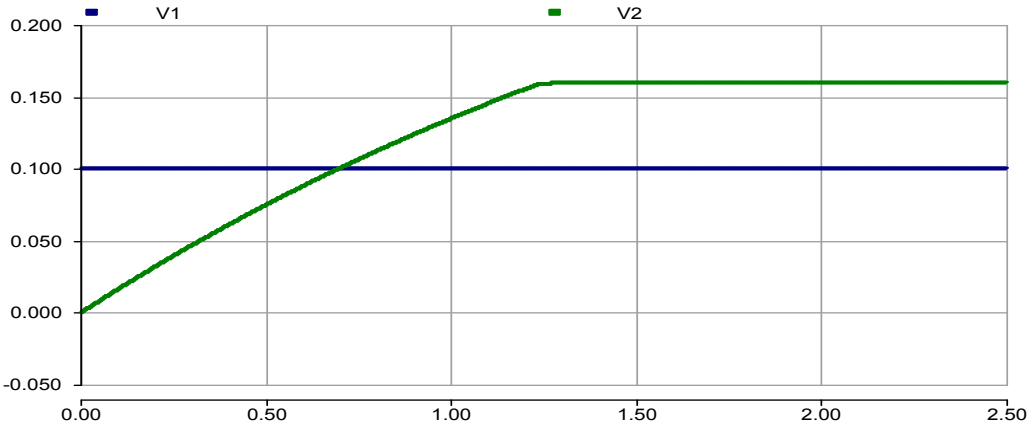

Figure 4.87. DC Link Voltages

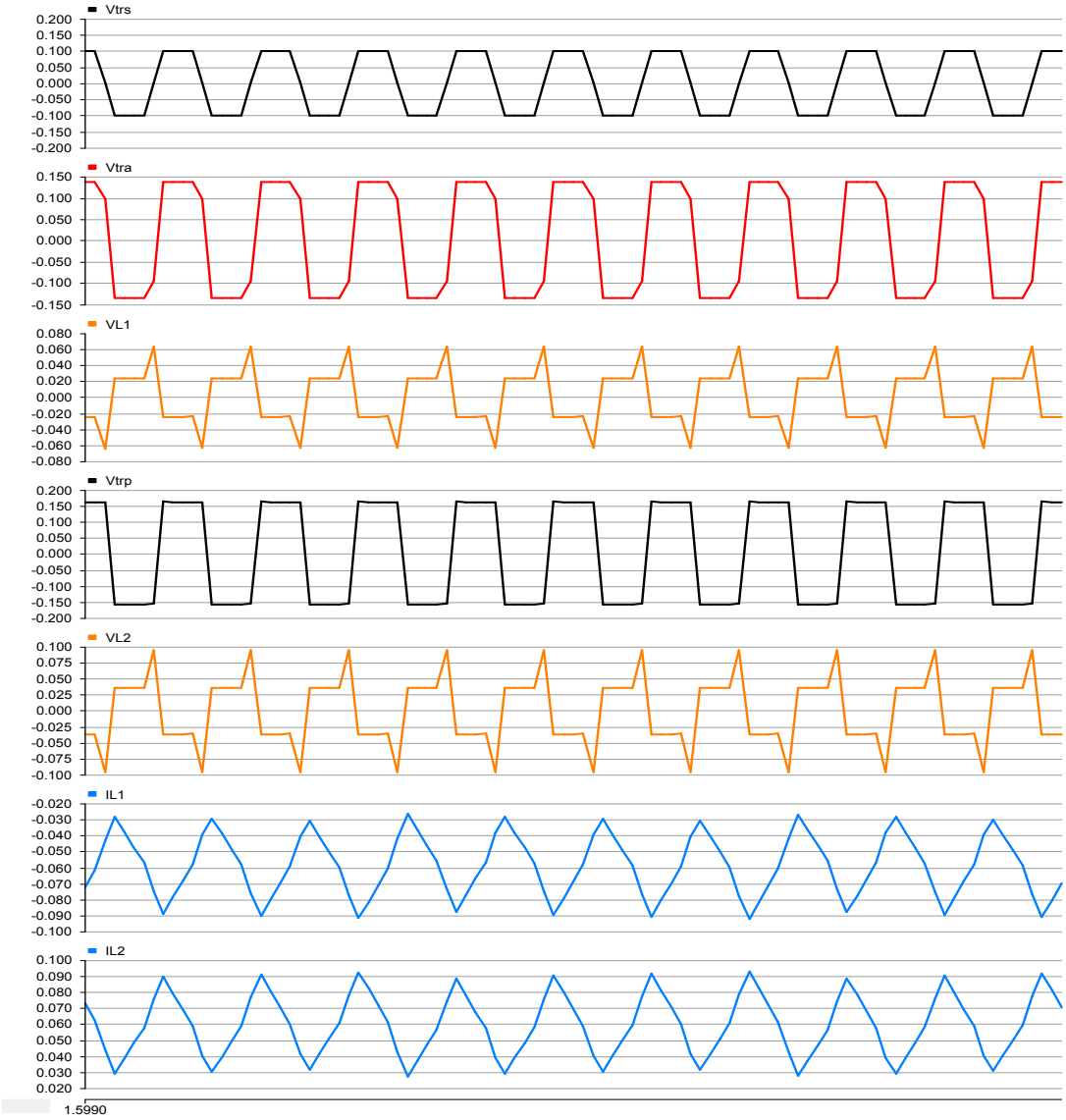

Figure 4.88. Voltage and Current Waveforms of Boost Mode at DPS Control

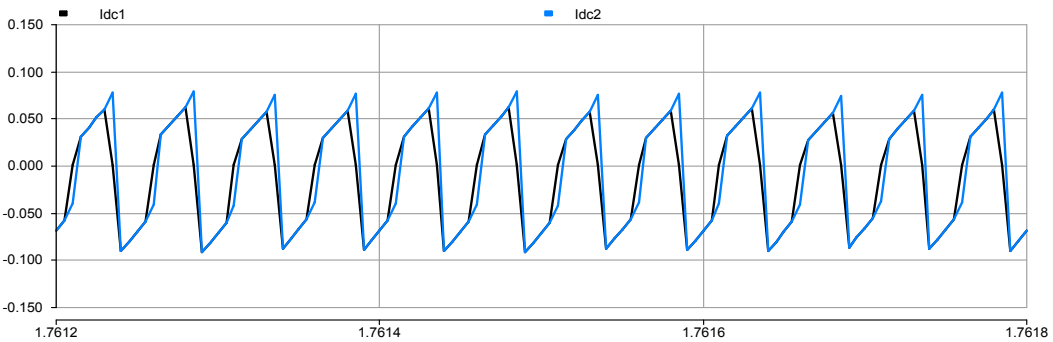

Figure 4.89. DC-Link Input and Output Currents

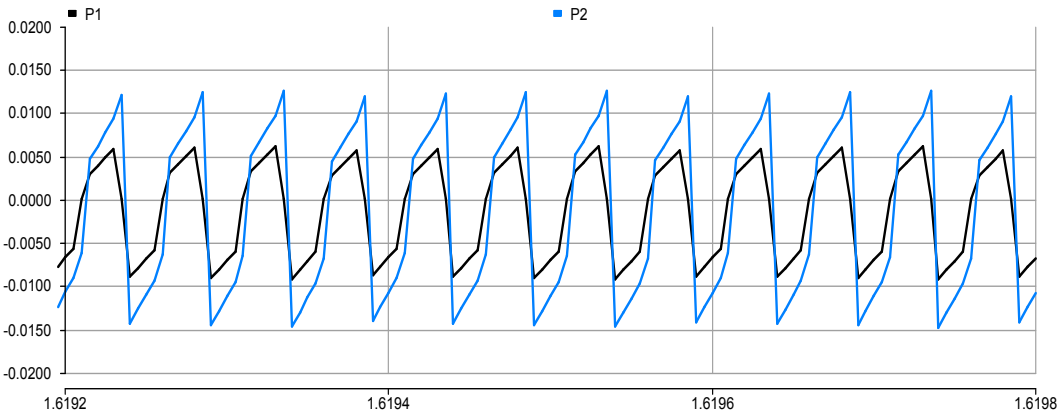

Figure 4.90. Input and Output Power Waveforms

Simulation Results of Case 4:

V_1=160V, V_2=200V, C_1=46mF, C_2=120mF, L_1=18µH, L_2=12µH, n=1:1, f=20kHz

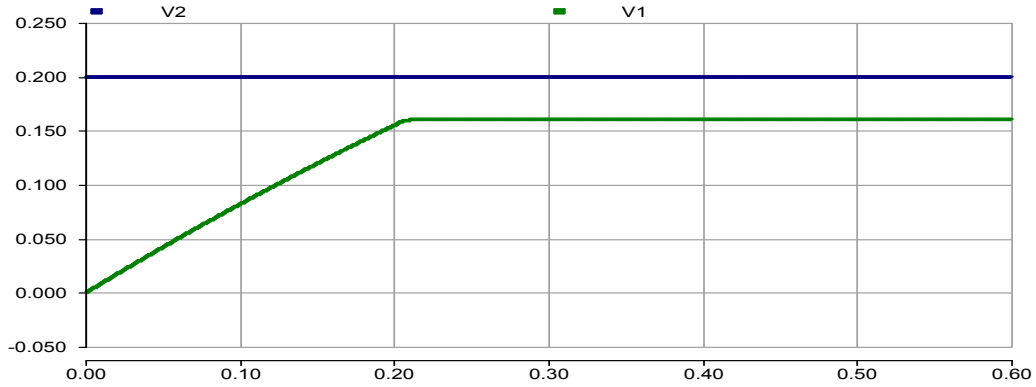

Figure 4.91. DC Link Voltages

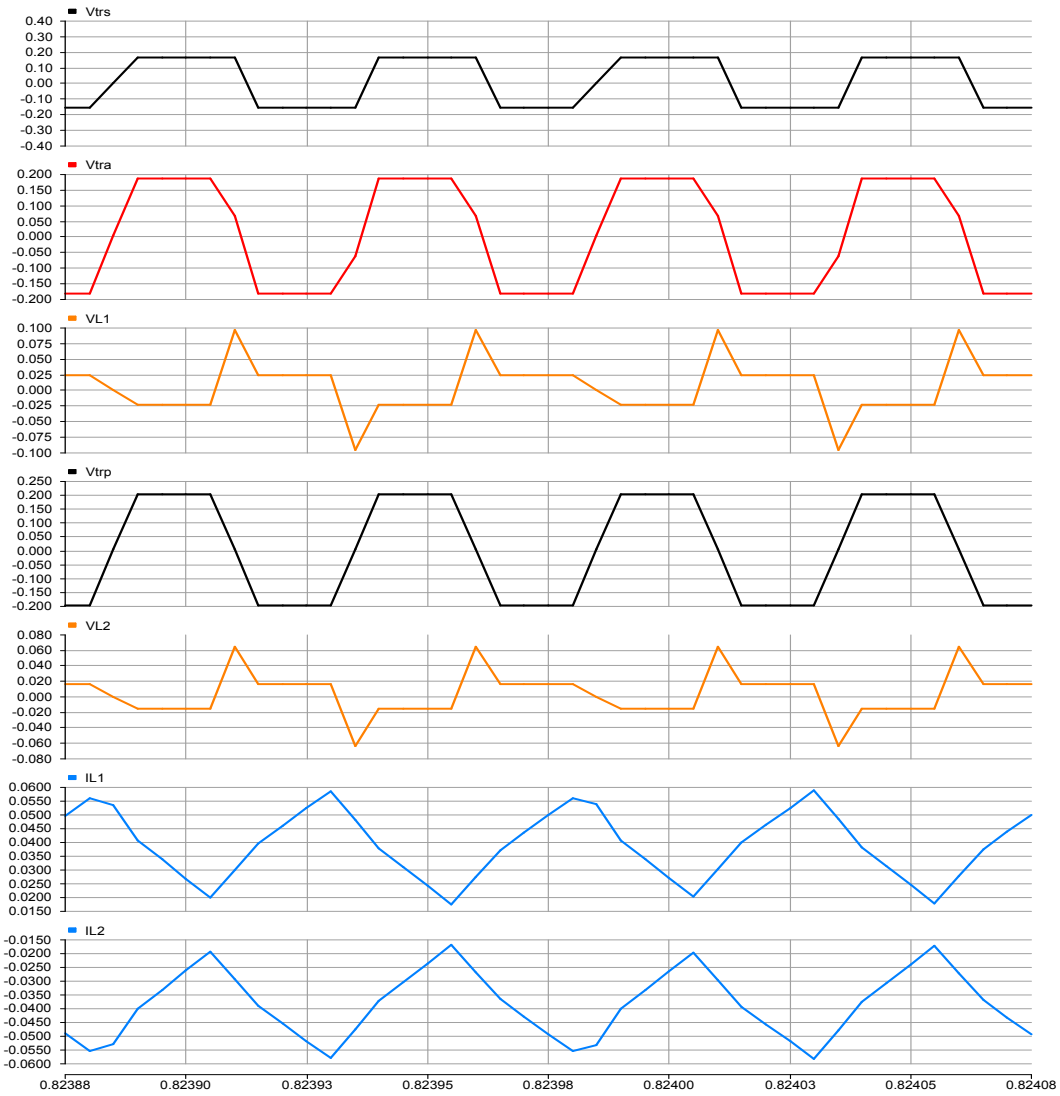

Figure 4.92. Voltage and Current Waveforms of Buck Mode at DPS Control

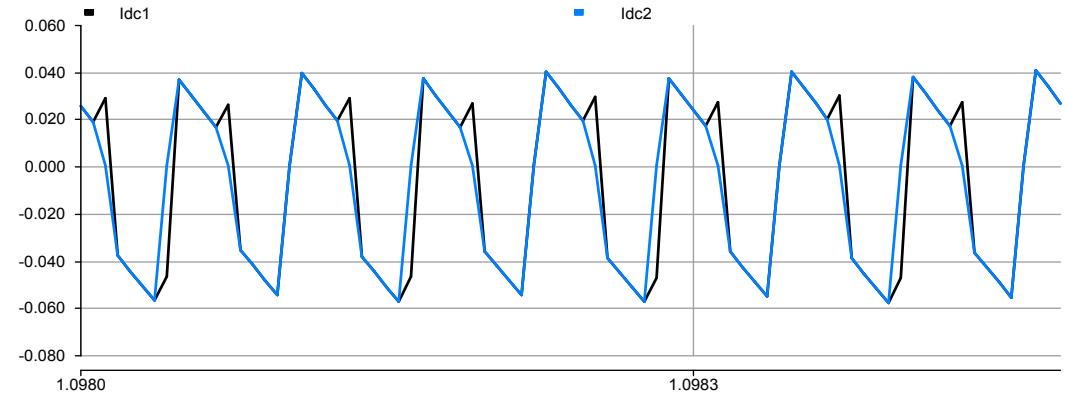

Figure 4.93. DC-Link Input and Output Currents

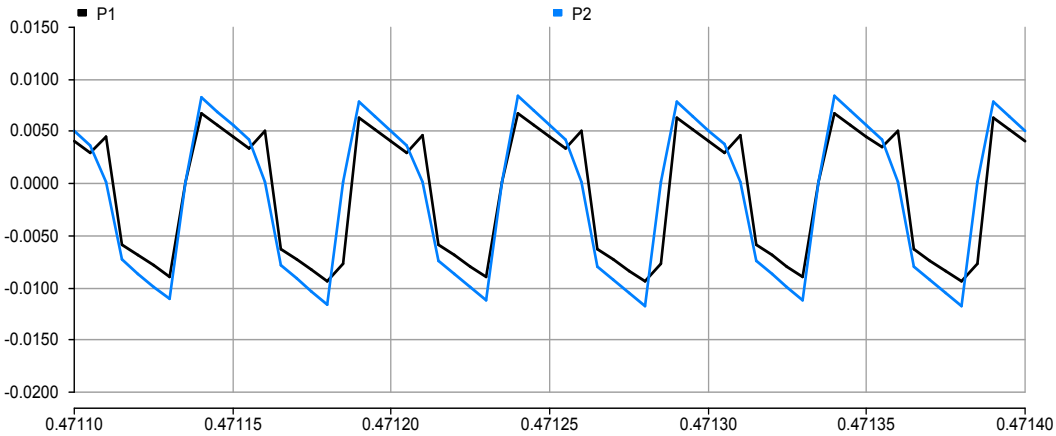

Figure 4.94. Input and Output Power Waveforms

Simulation Results of Case 5:

V_1=160V, V_2=100V, C_1=46mF, C_2=120mF, L_1=18µH, L_2=12µH, n=1:1, f=20kHz

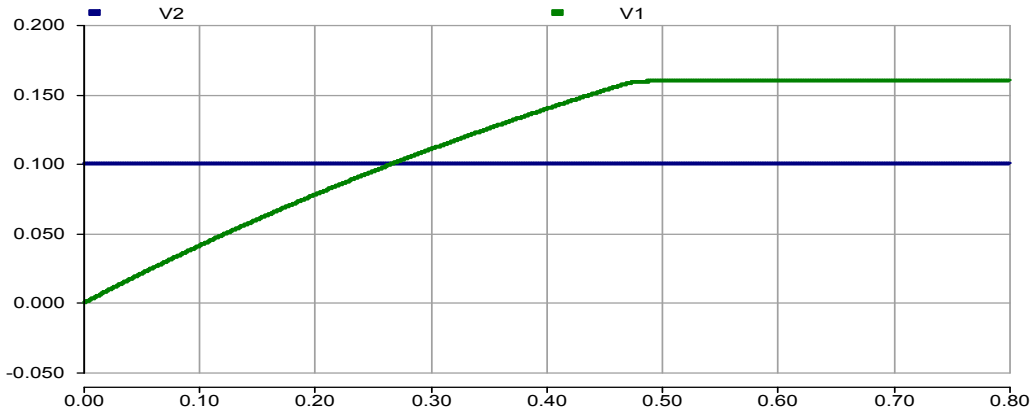

Figure 4.95. DC Link Voltages

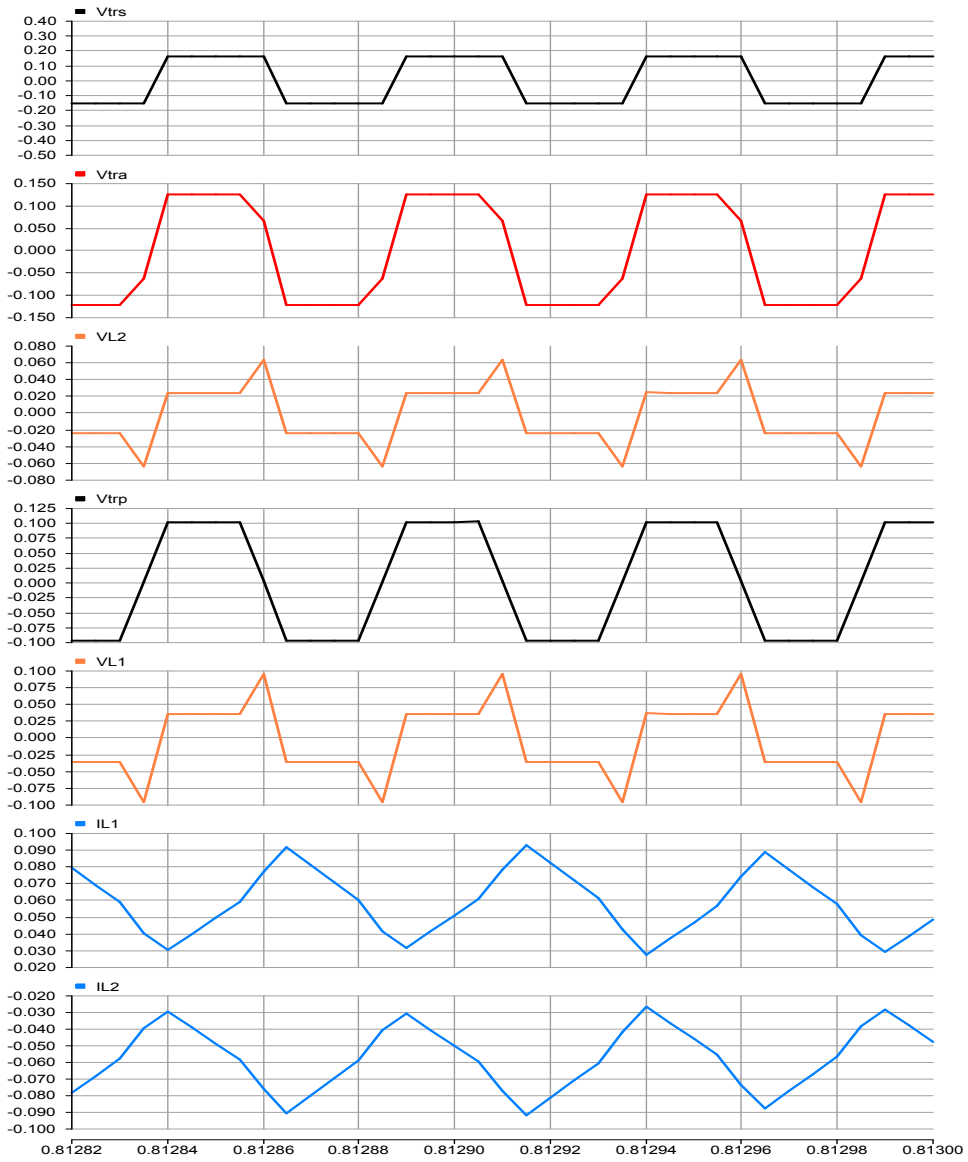

Figure 4.96. Voltage and Current Waveforms of Boost Mode at DPS Control

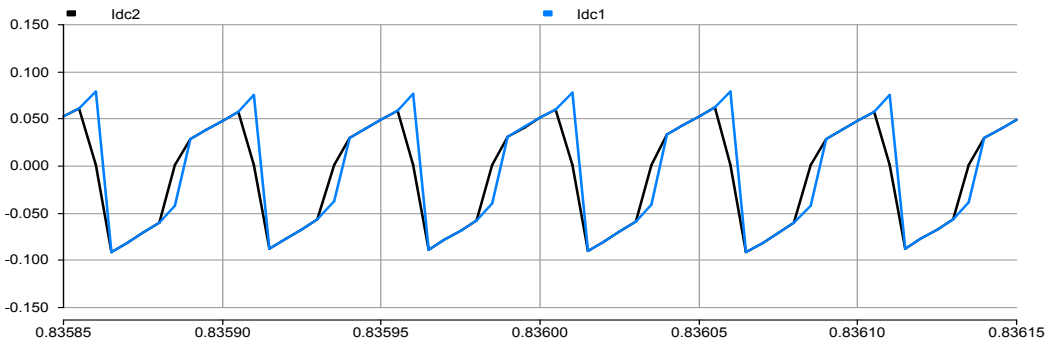

Figure 4.97. DC-Link Input and Output Currents

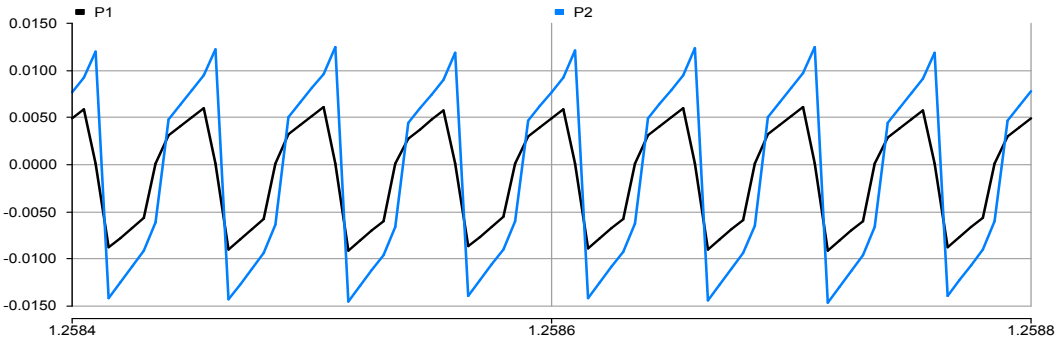

Figure 4.98. Input and Output Power Waveforms

Also, it is examined harmonics at primary side of the transformer and load side of the converter for this case.

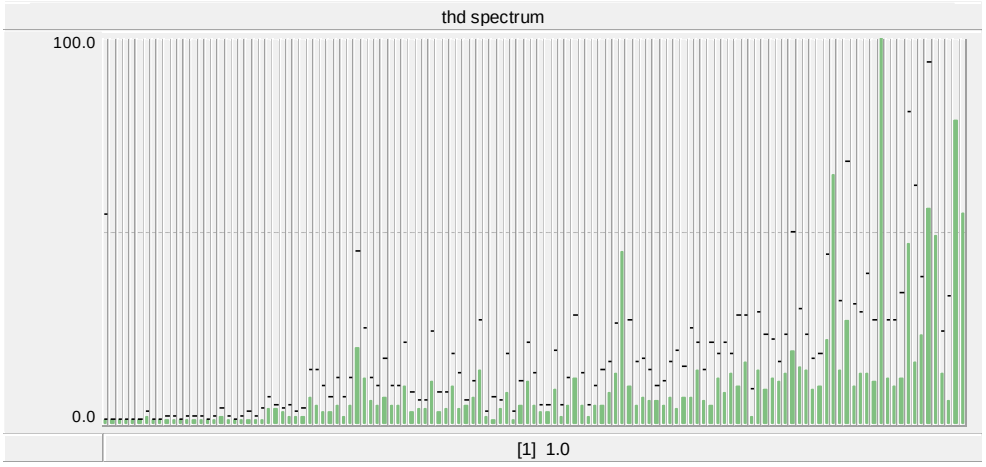

Figure 4.99. Harmonics Spectrum at Primary Side of Transformer

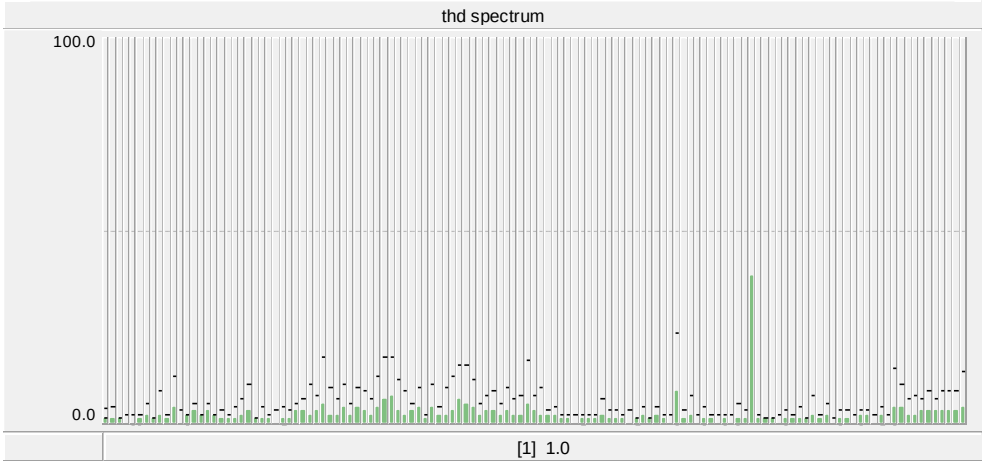

Figure 4.100. Harmonics Spectrum at Load Side

Simulation Results of Case 6:

V_1=300V, V_2=100V, C_1=46mF, C_2=120mF, L_1=18µH, L_2=12µH, n=1:1, f=10kHz

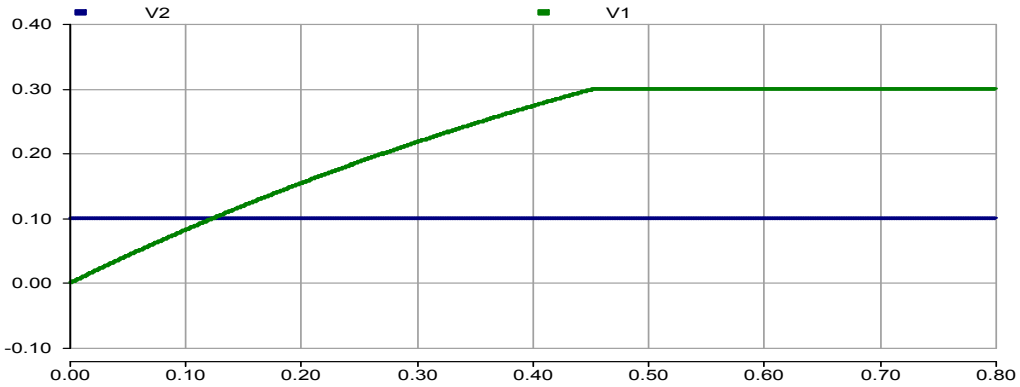

Figure 4.101. DC Link Voltages

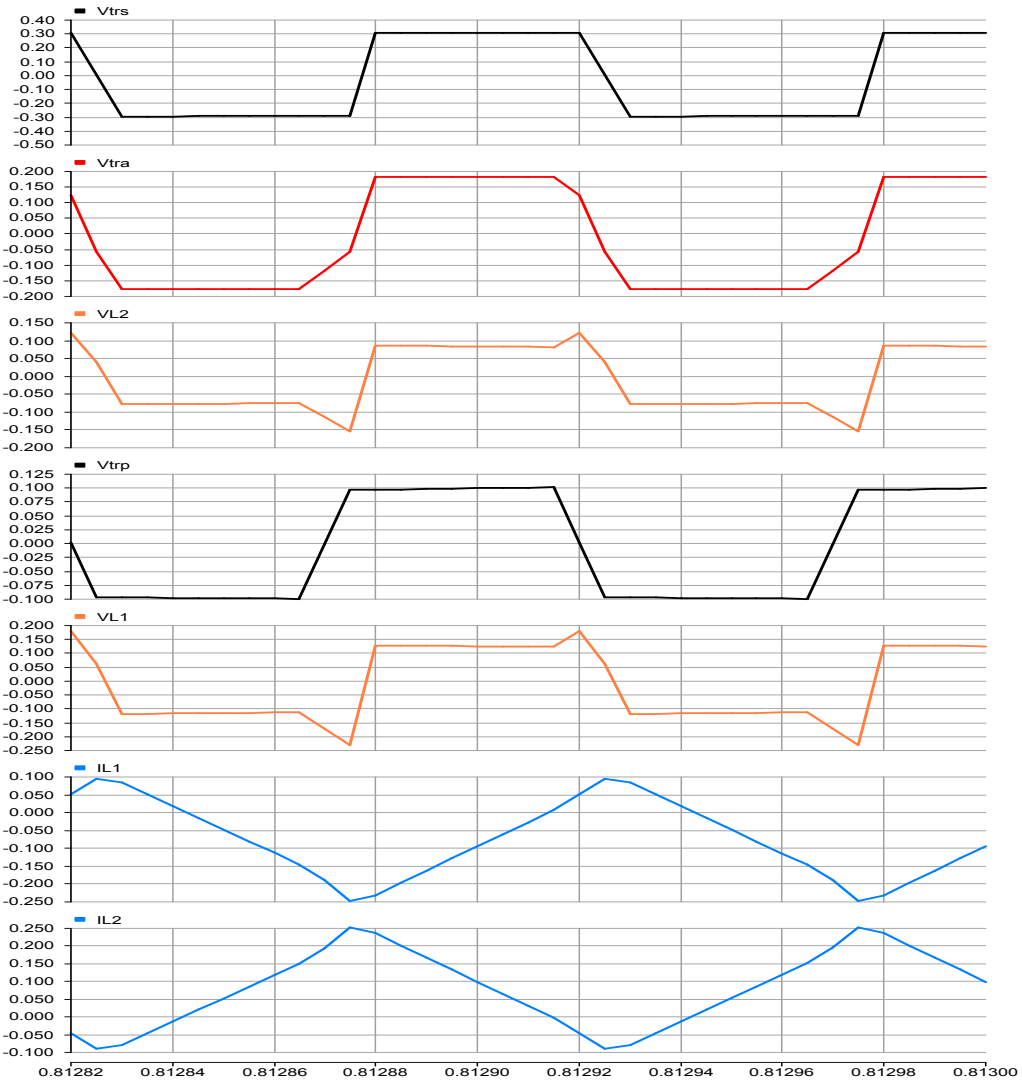

Figure 4.102. Voltage and Current Waveforms of Boost Mode at DPS Control

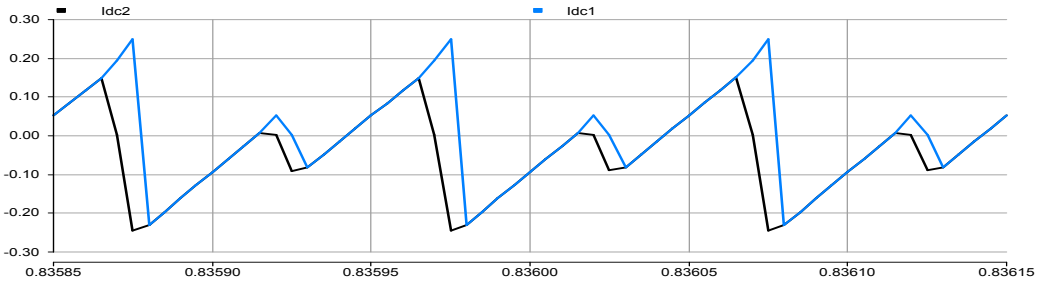

Figure 4.103. DC-Link Input and Output Currents

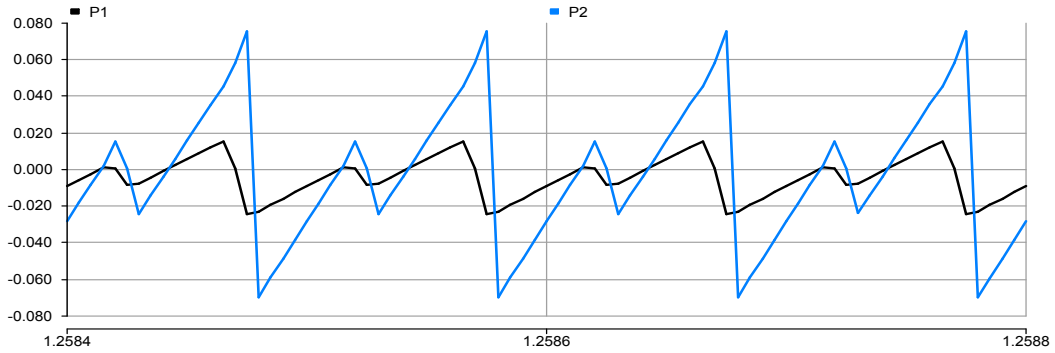

Figure 4.104. Input and Output Power Waveforms

4.4.4. Fortran Codes of DPS

```
#LOCAL REAL xVdc2_Err
#LOCAL REAL xP_dcdc
#LOCAL REAL xI_dcdc
#LOCAL REAL xRefdcdc

#LOCAL INTEGER xS1
#LOCAL INTEGER xS2
#LOCAL INTEGER xS3
#LOCAL INTEGER xS4
#LOCAL INTEGER xQ1
#LOCAL INTEGER xQ2
#LOCAL INTEGER xQ3
#LOCAL INTEGER xQ4

#LOCAL REAL xyA
#LOCAL REAL xyB
#LOCAL REAL xyC
#LOCAL REAL xyD
#LOCAL REAL xyphaseshift
#LOCAL REAL xfreq

! !!!!!!!!!!!!!!!! INPUTS !!!!!!!!!!!!!!!!
XVdc2ref=$i1l
XVdc2=$i2l
xKp_dcdc=$i3l
xKi_dcdc=$i4l
xLimP_dcdc=$i5l
xLimN_dcdc=$i6l
xTs=$i7l
xTime=$i8l
xfreq=$i9l
xRefA=$i10l
xRefB=$i11l
xRefC=$i12l

! !!! Taking Datas From Memory !!!!!!!
xI_dcdc = STORF(NSTORF)

xVdc2_Err = xVdc2ref - xVdc2Fil
xP_dcdc = xKp_dcdc * xVdc2_Err
xI_dcdc = xI_dcdc + xKi_dcdc * xTs * xVdc2_Err
xRefdcdc = xP_dcdc + xI_dcdc

IF (xRefdcdc > xLimP_dcdc) THEN
      xRefdcdc = xLimP_dcdc
ENDIF
```

```
IF (xRefdcdc < xLimN_dcdc) THEN
      xRefdcdc = xLimN_dcdc
ENDIF

xyA=COS(6.28318530717958647692528676655 9*xTime*xfreq + xRefA )
IF (xyA>=0) THEN
xS1=1
xS2=0
ELSE
xS1=0
xS2=1
ENDIF
xyC=COS(6.28318530717958647692528676655 9*xTime*xfreq + xRefB )
IF (xyC>=0) THEN
xS3=0
xS4=1
ELSE
xS3=1
xS4=0
ENDIF
xyB=COS(6.28318530717958647692528676655 9*xTime*xfreq - xRefdcdc )
IF (xyB>=0) THEN
xQ1=1
xQ2=0
ELSE
xQ1=0
xQ2=1
ENDIF
xyD=COS(6.28318530717958647692528676655 9*xTime*xfreq - xRefdcdc + xRefC )
IF (xyD>=0) THEN
xQ3=0
xQ4=1
ELSE
xQ3=1
xQ4=0
ENDIF
! !!!!!!!! Saving Datas !!!!!!!!!!!!!!!!!!
STORF(NSTORF) = xI_dcdc
! !!!!!!!! OUTPUT !!!!!!!!!!!!!!!!!!!!!!!!!!!!!!!!!!
$o1r= xS1
$o2r= xS2
$o3r= xS3
$o4r= xS4
$o5r= xRefdcdc
$o6r= xQ1
$o7r= xQ2
$o8r= xQ3
$o9r= xQ4

NSTORF = NSTORF+1
```

5. COMPARISON OF CONTROL METHODS

In this thesis, efficiency of different phase shift control methods is compared for bidirectional DC-DC dual active bridge converter topology. Main contribution of this thesis, which control method is better than the others by nonusing of snubber capacitors and reducing experimental cost. In this way, the bidirectional DC-DC converter is created by using different inductors and capacitor values for each control method and operated by different voltage levels with different frequencies for observing current-voltage-power waveforms, DC link settling times and calculating efficiencies. Moreover, effect of snubber capacitors on efficiencies will be explained at Table 5.1 and 5.2.

These results are obtained in simulations about comparing phase shift controller methods. (Kayaalp et. al., 2015)

- Generally, increasing of switching frequency has positive effect on system performance (increasing efficiency) at all of the controller methods. This condition is valid for all of the buck and boost modes.
- Basically, reducing switching frequency cause to reducing dc-link settling time. Also this is valid for all of the control methods and buck-boost modes.
- SPS has easy implementation than EPS and DPS. Thus, if the mathematical complexity is increase in a one control method, it can be reached that feasibility of this control method will be harder.
- On the other hand, if the mathematical complexity is increase in a control method, efficiency of this control method will be increase.
- Therefore, arrangement of mathematical complexity is SPS<EPS<DPS.
- Arrangement of feasibility cost is SPS<EPS<DPS.
- Arrangement of efficiencies is SPS<EPS=DPS.

The above arrangements are valid for general expressions. But in this thesis, only the last statement is differently obtained and it is summarized in Table 5.1. that shows the efficiency results with or without using snubber capacitors.

Table 5.1. Comparison of Efficiency Simulations on SPS, EPS and DPS. (Snubberless)

Power Flow	**Operating Modes**	**V_1-V_2**	**f_{sw}**	**SPS**	**EPS**	**DPS**	**Cases**
1	Buck	200V-160V	20kHz	25.9%	85.2%	78.5%	Case 1
1	Buck	300V-100V	10kHz	24.1%	33.3%	55.5%	Case 2
1	Boost	100V-160V	20kHz	25.8%	65.0%	50.0%	Case 3
2	Buck	200V-160V	20kHz	27.2%	73.5%	75.0%	Case 4
2	Boost	100V-160V	20kHz	22.8%	64.0%	61.2%	Case 5
2	Boost	100V-300V	10kHz	25.0%	33.3%	37.8%	Case 6

Note: High switching isolated transformer voltage ratio is n=1:1 and K_p=400, K_i=0.02 in all simulations. Also, resistance is 20Ω both power flows.

Efficiencies are calculated with (5.1).

$$\eta = \frac{P_{in} - (P_{in} - P_{out})}{P_{in}} \times 100 = \frac{P_{in} - P_{totalloss}}{P_{in}} \times 100 \tag{5.1}$$

It can be reached these statements using the Table 5.1.

- If the average efficiencies of control methods are calculated by using the above cases results, it is obtained n_{SPS}=25.13%, n_{EPS}=59.05% and n_{DPS}=59.67%.
- At these conditions, efficiencies of EPS and DPS almost equal. Thus, if we do not want to use snubber capacitors, EPS is enough for increasing the performance and it is not necessary doing extra calculations for DPS.
- On the other hand, if switching frequency is lower than 20kHz, positive effect of DPS against EPS and SPS can be seen gradually.
- Also, decreasing of switching frequencies has negative effect on system performance and it can be seen by comparing case1/case2 or case5/case6 for buck and boost modes.
- Changing of power flow ways are not suitable for increasing or decreasing efficiencies. Both directions give the similar results.

Moreover, Table 5.2. shows the efficiencies of control methods with using snubber capacitors.

Table 5.2. Comparison of Efficiencies on SPS, EPS and DPS with using snubber capacitors.

Power Flow	**Operating Modes**	**V_1-V_2**	**f_{sw}**	**SPS**	**EPS**	**DPS**	**Cases**
1	Buck	200V-160V	20kHz	92.4%	95.5%	97.9%	Case 1
1	Buck	300V-100V	10kHz	90.8%	94.7%	96.2%	Case 2
1	Boost	100V-160V	20kHz	90.3%	93.2%	96.6%	Case 3
2	Buck	200V-160V	20kHz	91.9%	96.2%	98.2%	Case 4
2	Boost	100V-160V	20kHz	90.5%	95.3%	97.6%	Case 5
2	Boost	100V-300V	10kHz	89.8%	93.8%	96.4%	Case 6

Note: $C_{snubber}$=0.068μF is connected to parallel with each IGBT and diode pairs in all simulations.

- Owing to snubber capacitors, system performance can be increased and arrangement of efficiencies is SPS<EPS<DPS. Because connection of snubber capacitors can decrease switching losses.
- Other statements (nonusing of snubber capacitors) are valid for the Table 5.2.

6. CONCLUSION

In this thesis, comparison of single phase shift, extended phase shift and dual phase shift control methods are operated in a single phase full bridge isolated bidirectional DC-DC converter topology. Innovative way of this thesis work is discovering of which control method is better than the others by examining efficiencies without using snubber capacitors. In the light of this aim, obtained results show that SPS has lower efficiency values than EPS and DPS and efficiencies of EPS and DPS occurred similar results. In addition, effect of snubber capacitors gives better performance results for all of the control methods and DPS effect is better than EPS and SPS effect.

Simulations are applied in PSCAD/EMTDC and voltage-current waveforms are validated with theoretical analysis. Firstly, this customization works began with finding of common used bidirectional dc-dc converter topology and control methods. Secondly, calculation of converter parameters (capacitors, inductors, transformer windings) and calculation of phase shift angles for control methods. Thirdly, simulations are operated and their results are compared with literature results. Therefore, simulation results are validated with theoretical and experimental analysis. Finally, power losses are calculated for each control methods by benefiting from simulation results and efficiencies are obtained by using or without using snubber capacitors.

In the thesis, control methods are compared without using snubber capacitors by decreasing costs, while the rate of input and output voltages are not high and it is found that EPS can be preferred instead of DPS. EPS has more advantage than DPS in both feasibility way and mathematical complexity. Thus, this condition emphasize the importance of this thesis.

In literature, some researches that took the high rate of input and output voltages, using of snubber capacitors became unavoidable to increase efficiency (Tan et. al., 2012), or it is possible to increase efficiencies by using different switching components even if the rate of input and output voltages is 1 (Akagi et. al., 2015). But snubber capacitors are not necessary for some conditions that efficiency is not as

important (Zhao et. al., 2012 , Bai et. al., 2008). These experimental studies are compared with the thesis results at Table 6.1.

Table 6.1. Comparison Table of Other Studies with This Thesis

Parameters	**Tan et. al., 2012**	**Akagi et. al., 2015**	**Zhao et. al., 2012**	**Bai et. al., 2008**	**This Thesis**	**This Thesis**
V_1	305V-355V	750V	140V-300V	205V	200V	100V
V_2	50V-59V	750V	0V-180V	270V	160V	300V
Transformer Turn Ratio	6:1	1:1	2:1	N:1	1:1	1:1
Switching Frequency	20kHz	20kHz	10kHz	10kHz	20kHz	10kHz
Power Ratings	6kW	42kW	5kW	5kW	15kW	15kW
Snubber Capacitors	Used	Used	Not used	Not Used	Not Used	Used
Control Method	SPS	SPS	EPS	DPS	EPS	EPS
Switching Components	IGBTs and MOSFETs	SiC MOSFET/SBD	IGBTs	IGBTs	Ideal IGBTs	Ideal IGBTs
Efficiency	96.5%	98.7%	90.2%	89.5%	85.2%	96.4%

Table 6.1. shows the below statements.

- Increment of the rate of input and output voltages cause to decrease of converter efficiency.
- Using of snubber capacitors or new switching components (SiC MOSFET/SBD) conduce to increase of system performance.
- If power rating of the system increase, the system efficiency can be decreased.
- Moreover, different type of transformer turn ratios are used to obtain maximum efficiency.
- Case1 and Case5 of control methods also include harmonic spectrum for primary side of the transformer and load side. Harmonics can be decreased at load side and this condition is valid for all control methods. If switching frequency is below the 20kHz, harmonics will reduce further.

- The thesis results demonstrate EPS control method can be preferred instead of DPS and SPS. Because literature generally created below of 15kW prototype in experimental studies.

Industrial Applications: There are different types of bidirectional DC-DC converters such as module type (0W-600W), open frame type (isolated or non-isolated), enclosed type and vehicle dc-dc power supplies in industrial applications. BRUSA which is the only industrial production company for EVs, made the most efficient bidirectional dc-dc converter in the world and its (BDC546) efficiency is 98.9% (BRUSA Web Page). It operates 150-750V at high voltage side and 50-600V at low voltage side. It uses CAN bus (Controller Area Network) controller system and has a water cooled cooling system. Its switching frequency is 41kHz, weight is 25.2kg, power rating is 180kW and its price is $35,715 (Metricmind Web Page).

Suggestions and Future Work: In the light of this thesis, a lot of researches can be studied for increasing converter efficiency by improving new control methods or changing material of switching components in the future. In short, application of phase-shift control methods can be used at converters of renewable energy sources such as photovoltaic systems, wind energy and electric vehicles at near future.

REFERENCES

AKAGI H., YAMAGISHI T., TAN N. M. L., KINOUCHI S., MIYAZAKI Y., KOYAMA M., 2015. Power Loss Breakdown of a 750-V 100-kW 20-kHz Bidirectional Isolated DC-DC Converter Using SiC-MOSFET/SBD Dual Modules, Industry Applications, IEEE Transactions on, Volume: 51, No: 1, Page(s): 420-428

BAI H., MI C. C., GARGIES S., 2008. The Short-Time-Scale Transient Processes in High-Voltage and High-Power Isolated Bidirectional DC-DC Converters, Power Electronics, IEEE Transactions on, Volume: 23, No: 6, Page(s): 2648-2656

BAI H., MI C., 2008. Eliminate Reactive Power and Increase System Efficiency of Isolated Bidirectional Dual-Active-Bridge DC-DC Converters using Novel Dual-Phase-Shift Control, Power Electronics, IEEE Transactions on, Volume: 23, No: 6, Page(s): 2905-2914

BAI H., MI C., 2008. Eliminate Reactive Power and Increase System Efficiency of Isolated Bidirectional Dual-Active-Bridge DC-DC Converters Using Novel Dual-Phase-Shift Control, Power Electronics, IEEE Transactions on, Volume: 23, No: 6, Page(s): 2905-2914

CHAN H. L., CHENG K. W. E., SUTANTO D., 2003. ZCS-ZVS bi-directional phase-shifted DC-DC converter with extended load range, Electric Power Applications, IEE Proceedings -, Volume: 150, No: 3, Page(s): 269-277

CHEN W., RONG P., LU Z., 2010. Snubberless Bidirectional DC-DC Converter With New CLLC Resonant Tank Featuring Minimized Switching Loss, Industrial Electronics, IEEE Transactions on, Volume: 57, No: 9, Page(s): 3075-3086

CHIU H. –J., LIN L. –W., 2006. A Bidirectional DC-DC Converter for Fuel Cell Electric Driving System, Power Electronics, IEEE Transactions on, Volume: 21, No: 4, Page(s): 950-958

DE DONCKER R. W., DIVAN D. M., KHERALUWALA M. H., 1991. A Three Phase Soft-Switched High-Power-Density DC-DC Converter for High Power Applications, Industrial Applications, IEEE Transactions on, Volume: 27, No: 1, Page(s): 63-73

DEHONG X., CHUANHONG Z., HAIFENG F., 2004. A PWM Plus Phase-Shift Control Bidirectional DC-DC Converter, Power Electronics, IEEE Transactions on, Volume: 19, No: 3, Page(s): 666-675

GREEN M., 2012. Design Calculations for Buck-Boost Converters, Texas Instruments, SLVA535A Application Report.

HUSSEIN M. M., SENJYU T., ORABI M., WAHAB M. A. A., HAMADA M. M., 2013. Control of a Stand-Alone Variable Speed Wind Energy Supply System, Applied Sciences, Volume: 3, No: 2, Page(s): 437-456

INOUE S., AKAGI H., 2007. A Bidirectional DC-DC Converter for an Energy Storage System With Galvanic Isolation, Power Electronics, IEEE Transactions on, Volume: 22, No: 6, Page(s): 2299-2306

KARSHENAS H. R., DANESHPAJOOH H., SAFAEE A., 2011. Bidirectional DC-DC Converters for Energy Storage Systems, Energy Storage in the Emerging Era of Smart Grid, InTech, Page(s): 161-178

KAYAALP R. İ., DEMİRDELEN T., KÖROĞLU T., CUMA M. U., BAYINDIR K. Ç., TÜMAY M., 2015. Comparison of Different Phase Shift Control Methods at Isolated Bidirectional DC-DC Converter, ICAT'15-Antalya, In Press

KHERALUWALA M. H., GASCOIGNE R. W., DIVAN D. M., BAUMANN E. D., 1992. Performance Characterization of a High-Power Dual Active Bridge DC-to-DC Converter, Industrial Applications, IEEE Transactions on, Volume: 28, No: 6, Page(s): 1294-1301

KHERALUWALA M. H., GASCOIGNE R. W., DIVAN D. M., BAUMANN E. D., 1992. Performance Characterization of a High-Power Dual Active Bridge dc-to-dc Converter, Industry Applications, IEEE Transactions on, Volume: 28, No: 6, Page(s): 1294-1301

KRISMER F., BIELA J., KOLAR J. W., 2005. A Comparative Evaluation of Isolated Bidirectional DC-DC Converters with Wide Input and Output Voltage, Industrial Applications Conference, IEEE Transactions on, Volume:1, Page(s): 599-606

LEE S. –W., LEE S. –R., JEON C. -H., 2006. A New High Efficient Bidirectional DC/DC Converter in the Dual Voltage System, Journal of Electrical Engineering & Technology, Volume: 1, No: 3, Page(s): 343-350

LI H., PENG F. Z., LAWLER J. S., 2003. A natural ZVS medium power bidirectional dc-dc converter with minumum number of devices, Industrial Applications, IEEE Transactions on, Volume: 39, No: 2, Page(s): 525-535

LINGYU X., DESHANG S., HONGYU C., 2014. A ZVS Bidirectional Three-Level DC-DC Converter with Direct Current Slew Rate Control of Leakage Inductance, Energy Conversion Congress and Exposition Conference, IEEE, Page(s): 4410-4415

MATSUO H., KUROKAWA F., 1984. New Solar Cell Power Supply System Using a Boost Type Bidirectional DC-DC Converter, Industrial Electronics, IEEE Transactions on, Vol. IE-31, No: 1, Page(s): 51-55

MERAL M. E., SARIBULUT L., TEKE A., TÜMAY M., 2009. A Novel Switching Signals Generation Method for Hybrid Multilevel Inverters, International Conference, ELECO 2009, Electrical and Electronics Engineering, IEEE, Page(s):428-431

MI C., BAI H., WANG C., GARGIES S., 2008. Operation, design and control of dual H-bridge-based isolated bidirectional DC-DC converter, IET Power Electronics, Volume: 1, No: 4, Page(s): 507-517

PENG F. Z., LI H., SU G. –J., LAWLER J. S., 2004. A new ZVS bidirectional dc-dc converter for fuel cell and battery application, Power Electronics, IEEE Transactions on, Volume: 19, No: 1, Page(s): 54-65

QIN H., KIMBALL J. W., 2012. Generalized Avarage Modeling of Dual Active Bridge DC-DC Converter, Power Electronics, IEEE Transactions on, Volume: 27, No: 4, Page(s): 2078-2084

RAFIQ M., UL HASAN M. F., 2012. Design and Analysis of 60kW DC-DC Converter for Hybrid Electric Vehicle Applications, MSc Thesis, Chalmers University of Technology, Göteborg

REDDY S. K. G., SWARUPA V., 2013. Extended Phase Shift Control of Isolated Bidirectional DC-DC Converter for Renewable Energy Sources Connected to Micro Grid, International Journal of Advanced Research in Electrical, Electronics and Instrumentation Engineering, Volume: 2, No: 8, Page(s): 3864-3872

RUFER A., BARRADE P., 2002. A supercapacitor-based energy-storage system elevators with soft commutated interface, Industrial Applications, IEEE Transactions on, Volume: 38, No: 5, Page(s): 1151-1159

SHEN J. -M., JOU H. -L., WU J. -C., 2012. Novel Transformerless Grid-Connected Power Converter with Negative Grounding for Photovoltaic Generation System, Power Electronics, IEEE Transactions on, Volume: 27, No: 4, Page(s): 1818-1829

SHI X., JIANG J., GUO X., 2013. An Efficiency-Optimized Isolated Bidirectional DC-DC Converter with Extended Power Range for Energy Storage Systems in Microgrids, Open Access, Energies, Volume: 6, Page(s): 27-44

TAN N. M. L., ABE T., AKAGI H, 2010. A 6-kW, 2-kWh Lithium-Ion Battery Energy Storage System Using a Bidirectional Isolated DC-DC Converter, International Power Electronics Conference, IEEE, Page(s): 46-52

TAN N. M. L., ABE T., AKAGI H., 2011. Topology and Application of Bidirectional Isolated DC-DC Converters, 8th International Conference on Power Electronics, IEEE Transactions on, Page(s): 1039-1046

TAN N. M. L., ABE T., AKAGI H., 2011. Topology and Application of Bidrectional Isolated DC-DC Converters, 8th International Conference on Power Electronics – ECCE Asia, The Shilla Jeju, Korea, Page(s): 1039-1046

TAN N. M. L., ABE T., AKAGI H., 2012. Design and Performance of a Bidirectional Isolated DC-DC Converter for a Battery Energy Storage System, Power Electronics, IEEE Transactions on, Volume: 27, No: 3, Page(s): 1237-1248

WANG J., LI S., YANG J., WU B., LI Q., 2015. Extended state observer-based sliding mode control for PWM based DC-DC buck power converter systems with mismatched disturbances, IET Control Theory Applications, Volume: 9, No: 4, Page(s): 579-586

WANG K., LIN C. Y., ZHU L., QU D., LEE F. C., LAI J., 1998. Bidirectional DC-to-DC Converters for Fuel Cell Systems, Transportation, IEEE Workshop Power Electronics, Page(s): 47-51

Web Page: http://electronics.stackexchange.com/questions/117520/dual-active-bridge-converter

Web Page: NPTEL Module 4: DC-DC Converters, Lecture 9: DC-DC Converters for EV and HEV Applications: http://www.nptel.ac.in/courses/108103009/9

Web Page: TDK Power Electronics World: http://www.global.tdk.com/news_center/publications/power_electronics_world/pdf/aaa60600.pdf

Web Page: http://www.brusa.eu/en/products/converter/power-dcdc-750-v/bdc546.html

Web Page: http://www.metricmind.com/price-list/

WEN H., XIAO W., SU B., 2014. Nonactive Power Loss Minimization in a Bidirectional Isolated DC-DC Converter for Distributed Power Systems, Industrial Electronics, IEEE Transactions on, Volume: 61, No: 12, Page(s): 6822-6831

WU K., W. DE SILVA C., DUNFORD W. G., 2012. Stability Analysis of Isolated Bidirectional Dual Active Full Bridge DC-DC Converter with Tripe Phase Shift Control, Power Electronics, IEEE Transactions on, Volume: 27, No: 4, Page(s): 2007-2017

XIE Y., SUN J., FREUDENBERG J. S., 2010. Power Flow Characterization of a Bidirectional Galvanically Isolated High Power DC/DC Converter Over a Wide Operating Range, Power Electronics, IEEE Transactions on, Volume: 25, No: 1, Page(s): 54-66

ZHANG J., 2008. Bidirectional DC-DC Power Converter Design Optimization, Modeling and Control, Doctor of Philosophy Thesis, Blacksburg-Virginia

ZHAO B., SONG Q., LIU W., 2012. Power Characterization of Isolated Bidirectional Dual-Active-Bridge DC-DC Converter With Dual-Phase-Shift Control, Power Electronics, IEEE Transactions on, Volume: 27, No: 9, Page(s): 4172-4176

ZHAO B., SONG Q., LIU W., SUN W., 2013. Current-Stressed-Optimized Switching Strategy of Isolated Bidirectional DC-DC Converter With Dual-Phase-Shift Control, Industrial Electronics, IEEE Transactions on, Volume: 60, No: 10, Page(s): 4458-4467

ZHAO B., SONG Q., LIU W., SUN Y., 2014. Dead-Time Effect of the High-Frequency Isolated Bidirectional Full-Bridge DC-DC Converter: Comprehensive Theoretical Analysis and Experimental Verification, Power Electronics, IEEE Transactions on, Volume: 29, No: 4, Page(s): 1667-1680

ZHAO B., YU Q., LENG Z., CHEN X., 2012. Switched Z-Source Isolated Bidirectional DC-DC Converter and Its Phase-Shifting Shoot –Through Bivariate Coordinated Control Strategy, Industrial Electronics, IEEE Transactions on, Volume: 59, No: 12, Page(s): 4657-4670

ZHAO B., YU Q., SUN W., 2012. Extended-Phase-Shift Control of Isolated Bidirectional DC-DC Converter for Power Distribution in Microgrid, Power Electronics, IEEE Transactions on, Volume: 27, No: 11, Page(s): 4667-4680

ZHAO C., ROUND S. D., KOLAR J. W., 2010. Full Order Averaging Modelling of Zero-Voltage-Switching-Phase-Shift Bidirectional DC-DC Converters, IET Power Electronics, Volume: 3, No: 3, Page(s): 400-410

ZHU L., 2006. A Novel Soft-Commutating Isolated Boost Full-Bridge ZVS-PWM DC-DC Converter for Bidirectional High Power Applications, Power Electronics, IEEE Transactions on, Volume: 21, No: 2, Page(s): 422-429

BIOGRAPHY

Rahmi İlker KAYAALP was born in Ankara, Turkey in 1989. He graduated from Adana Seyhan ÇEAŞ Anatolian High School in 2007. He received his B.S. degree in Electrical and Electronics Engineering Department from Çukurova University in 2013. After completion his B.S. education, he started MSc education in Electrical and Electronics Engineering Department in Çukurova University. He has been working as a Research Assistant in Electrical and Electronics Engineering Department of the Çukurova University since 2013. His research areas are Power Quality, Power Electronics and Energy Efficiency.

APPENDIX

Publication Arose Form This Thesis Work

1.International Conference Papers:

- KAYAALP R. İ., DEMİRDELEN T., KÖROĞLU T., CUMA M. U., BAYINDIR K. Ç., TÜMAY M., 2015. Comparison of Different Phase-Shift Control Methods at Isolated Bidirectional DC-DC Converter, International Conference on Advanced Technology & Sciences, Advanced Technology & Science